

Centre Eau Terre Environnement

GEOTHERMAL ENERGY POTENTIAL OF ACTIVE MINES IN NORTHERN REGIONS: THE ÉLÉONORE MINE CASE-STUDY

Par

Edgardo Jose Alvarado

Mémoire présenté pour l'obtention du grade de

Maître ès Sciences (M.Sc.)

en sciences de la Terre

Jury d'évaluation

Président du jury et
examinateur interne

Geneviève Bordeleau
INRS – Eau Terre et Environnement

Examinateur externe

Philippe Pasquier
Département des génies civil,
géologique et des mines
École Polytechnique de Montréal

Directeur de recherche

Jasmin Raymond
INRS – Eau Terre Environnement

Codirecteur de recherche

René Therrien
Université Laval

REMERCIEMENTS

D'abord, je veux exprimer ma gratitude à mon directeur de recherche, Jasmin Raymond, d'avoir cru en moi et de m'avoir confié un projet aussi innovant et intéressant. Merci de m'avoir laissé travailler de manière autonome, avec juste la bonne dose de supervision. Merci également de m'avoir donné la chance de participer à des conférences, une école d'été et de réaliser un stage international. Ces expériences m'ont permis de partager nos travaux de recherche ainsi que d'approfondir mes connaissances, sur mon projet et le monde. Enfin, merci pour ta disponibilité, ton support constant, tes commentaires et tes idées. Je suis très reconnaissant pour cette opportunité.

À mon codirecteur, René Therrien, merci pour ta disponibilité et d'avoir consacré amplement de temps pour m'assister dans le développement du modèle numérique. Ta patience, tes connaissances, tes commentaires et ta minutieuse révision du modèle ont été essentiels pour mener à terme cette étude.

À Félix-Antoine Comeau, merci pour ta participation depuis le tout début. Ta collaboration, ton souci du détail, tes commentaires et recommandations ont été indispensables dans la production d'un travail de qualité.

Je tiens à remercier tous les partenaires impliqués dans le projet sur le potentiel des ressources et technologies géothermiques pour l'approvisionnement énergétique des mines du Nord. Particulièrement, Goldcorp Inc. - Mine Éléonore (maintenant Newmont-Goldcorp Corporation) pour leur participation et leur intérêt dans le projet. Merci à David Labrecque, ancien coordonnateur d'énergie, Martin Perron, surintendant à la géologie et Luc St-Arnaud, directeur de stratégie et amélioration continue. De même, merci à Maxime Boivin de la compagnie TRANE pour sa disponibilité et assistance.

Un grand merci à mes amis et collègues de l'INRS et l'Université Laval. Finalement, à ma famille, je vous remercie infiniment pour l'encouragement et le soutien constant.

À vous tous, merci.

RÉSUMÉ

Plusieurs mines situées dans les régions nordiques doivent chauffer les galeries souterraines en raison des conditions climatiques très froides. L'appel de puissance requis pour chauffer les galeries avec un système électrique est élevé et entraîne des coûts énergétiques importants. Les minières emploient donc des hydrocarbures pour suffire à leur besoin calorifique, mais l'impact environnemental demeure un enjeu de taille. L'une des alternatives de chauffage, reposant sur des ressources locales et ayant une faible consommation électrique, est l'énergie géothermique issue de l'eau de dénoyage d'une mine. L'objectif principal de ce projet est d'évaluer le potentiel géothermique de la mine Éléonore de Newmont-Goldcorp, une mine en opération située à Eeyou Istchee Baie-James dans le Nord-du-Québec. Plus précisément, ce projet vise à caractériser la ressource géothermique afin de concevoir un système de pompe à chaleur géothermique (PACG), adapté aux opérations minières, qui permettra de réduire les coûts, la consommation d'hydrocarbures et les émissions de gaz à effet de serre (GES). D'abord, un bilan énergétique a été réalisé pour établir la quantité d'énergie nécessaire pour chauffer les galeries. Ensuite, les propriétés physico-chimiques de l'eau ont été analysées afin d'estimer le risque de corrosion et d'entartrage. À l'aide de toutes ces informations, un système de PACG préliminaire a été conçu pour calculer la quantité d'énergie géothermique qui peut être extraite de l'eau de dénoyage de la mine. Les résultats montrent qu'un système de PACG muni d'un échangeur de chaleur intermédiaire installé à la sortie de la mine permettrait de produire en moyenne 39 % des 26,6 GWh/année nécessaires pour chauffer les galeries souterraines, de diminuer les coûts de chauffage de 33 %, en plus de réduire les émissions de GES d'environ 1993 tonnes/année. Le modèle hydrogéologique développé pour la mine Éléonore suggère qu'un système de pompe à chaleur géothermique adapté au système de dénoyage de la mine pourrait fournir un maximum de 45 % de la demande en chauffage des galeries souterraines de façon durable au cours des prochaines années. Ce projet de recherche indique qu'avec une évaluation adéquate, les systèmes de PACG peuvent être adaptés aux mines en exploitation situées dans un contexte nordique et peuvent combler une partie de leurs besoins énergétiques de manière écologique, abordable et constante.

Mots-clés : Géothermie; énergie géothermique; pompe à chaleur; dénoyage; eau de mine; mine active; énergie durable; énergie renouvelable; modèle numérique; Québec; galeries souterraines

ABSTRACT

Several mines in northern regions must heat underground workings, surface buildings or process water due to frigid weather conditions. The power demand for electrical heating is high and entails significant energy expenses. Mining companies, therefore, use fossil fuels for heating, which creates environmental challenges. An eco-conscious alternative, based on local resources and low electricity consumption, is the use of geothermal energy from the mine dewatering system. The Newmont - Goldcorp Éléonore mine, an active mine located on the Eeyou Istchee territory of James Bay in Northern Quebec, was selected as a case study. The geothermal resource was characterized to design a geothermal heat pump system (GHPs) adapted to mining operations. The energy balance was calculated to establish the heating energy requirements of the mine. Subsequently, the physicochemical properties of the water from four different sampling points along the dewatering system were analyzed. Finally, a preliminary GHPs was designed to assess the amount of geothermal energy that can be extracted from the dewatering system of the mine. Under current conditions, a system equipped with an intermediate heat exchanger installed at the exit of the dewatering system could provide 39% of the 26.6 GWh/year needed to heat the underground workings, reducing heating costs by 33% and greenhouse gas emissions by 1993 tons/year. A hydrogeological numerical model developed for the Éléonore mine suggests that a geothermal heat pump system adapted for the dewatering system of the mine is sustainable throughout the life of the mine and could supply up to 45% of the underground workings heating demands in the upcoming years. Thus, this research indicates that with adequate assessment, geothermal heat pump systems can be adapted to active mining operations in a northern context and can contribute to their energy needs in an environmental, affordable, and constant manner.

Keywords: Geothermal; geothermal energy; heat pump; dewatering; mine water; active mine; sustainable energy; renewable energy; numerical model; Québec; underground workings

AVANT-PROPOS

Ce mémoire comporte six chapitres. Le premier chapitre présente le contexte de la recherche, ainsi que la problématique générale des mines localisées en milieu nordique, marqué par le manque d'infrastructures dû à l'éloignement, ce qui entraîne une augmentation des coûts de production, et un besoin en chauffage accru, en raison des conditions climatiques plus froides. Une problématique spécifique apparaît ainsi : ce besoin énergétique en chauffage plus élevé des mines en milieu nordique est ainsi la plupart du temps comblé par des sources d'énergie fossiles. Le chapitre expose également les motivations et les objectifs du projet. Le deuxième chapitre aborde le contexte géologique, hydrogéologique, hydrologique, structural et énergétique du site à l'étude, soit la mine Éléonore de Newmont-Goldcorp. Le troisième chapitre décrit la méthodologie utilisée pour concevoir un système géothermique adapté aux opérations de la mine, ainsi que la création du modèle numérique hydrogéologique pour évaluer la durabilité de la ressource. Le quatrième chapitre contient les résultats et le chapitre cinq discute de ceux-ci. Le dernier chapitre comprend finalement les conclusions, les recommandations et les perspectives.

Les chapitres de ce mémoire constituent une ébauche d'un article à soumettre dans une revue scientifique et pour cette raison, la rédaction a été réalisée en anglais. Un sommaire récapitulatif donne un aperçu des principaux points abordés dans cette étude.

SOMMAIRE RÉCAPITULATIF

INTRODUCTION

L'industrie minière est une source importante d'emplois et de revenu. Au Canada, les compagnies minières contribuent approximativement 72,0 G\$ au produit intérieur brut (PIB), dont 2,2 G\$ sont versés aux gouvernements fédéral et provincial sous forme d'impôts. Il s'agit de la quatrième plus grosse industrie du pays, dépassée seulement par les industries de services, manufacturière et immobilière. Cependant, au Québec, environ 50 % des mines en exploitation sont localisées sur le territoire défini par le Plan Nord, soit au nord du 49e parallèle, là où les infrastructures y sont très limitées, voire inexistantes, le réseau électrique y est la plupart du temps inaccessible et les conditions climatiques y sont difficiles (Ministère de l'Énergie et des Ressources naturelles, 2015). Ainsi, la demande énergétique des opérations minières situées dans ce contexte nordique augmente de manière exponentielle. Par conséquent, une partie supplémentaire des dépenses est tributaire de la consommation électrique et de carburant pour le chauffage, puisqu'il est parfois nécessaire de chauffer les galeries souterraines en période hivernale. En effet, les coûts de production d'une mine en contexte nordique peuvent être entre 2 et 2,5 fois supérieures à une mine semblable localisée à une latitude plus basse (Marshall, 2016). Par ailleurs, il n'est pas rentable d'utiliser l'énergie électrique pour le chauffage, car l'appel de puissance des systèmes électriques est élevé et entraîne des coûts financiers importants. D'autre part, les sources d'énergie renouvelable les plus couramment utilisées, telles que l'éolien et le solaire, sont intermittentes et ne peuvent pas garantir le chauffage continu nécessaire pour assurer le confort et la sécurité des travailleurs d'une mine. Les entreprises minières emploient alors des combustibles fossiles pour satisfaire leurs besoins calorifiques, mais avec un impact environnemental conséquent.

Le futur de l'industrie minière du Canada se situe dans des régions éloignées et nordiques. Dans l'intention d'établir des opérations minières durables, tout en augmentant la rentabilité, il est pertinent d'entreprendre des démarches afin de mettre en place des alternatives d'énergie locale pour un chauffage constant, écologique et abordable. L'extraction de l'énergie géothermique de faible enthalpie disponible dans les mines est une alternative digne d'intérêt. Une mine s'avère un emplacement favorable pour l'implantation d'un système géothermique, puisque des débits d'eau importants se doivent en premier lieu d'être captés pour dénoyer le site et mettre à bien les opérations, mais également parce que les profondeurs impliquées sont de l'ordre du kilomètre et les températures sont supérieures par rapport à la surface. D'autre part, les puits et les systèmes

de pompage déjà en place pour le dénoyage peuvent être couplés à un système de pompes à chaleur géothermique (PACG). Un système géothermique adapté aux opérations minières permettrait d'extraire l'énergie de l'eau souterraine et de surface ou des résidus miniers dans l'optique de chauffer les infrastructures des sites miniers ou des communautés dans une perspective de développement durable (Raymond et al., 2008).

Motivation et Objectifs

La source d'énergie disponible au sein des grands volumes d'eau qui inondent maintenant les mines inactives (fermées) a déjà été étudié (Raymond et Therrien, 2014; Bailey et al., 2016; Loredo et al., 2016; Banks et al., 2017; Al-Habaibeh et al., 2018), ce qui n'est cependant pas le cas à l'heure actuelle dans les mines en opération (actives). Néanmoins, l'utilisation de systèmes géothermiques couplés à ceux de dénoyage déjà en place sur les sites miniers en activité se pose comme une alternative intéressante et innovante afin de combler les demandes énergétiques élevées des opérations minières situées dans les milieux nordiques, tels que dans le nord du Québec (Raymond, 2010). L'objectif principal de cette étude est ainsi d'évaluer le potentiel géothermique d'une mine en exploitation dans un environnement nordique dans le but de dresser un portrait techno-économique des systèmes de pompes à chaleur géothermique comme solution aux besoins en chauffage des sites miniers. La mine Éléonore de Newmont-Goldcorp, située sur le territoire d'Eeyou Istchee en Jamésie dans le nord du Québec, est le sujet d'étude. Il s'agit d'une mine en opération qui utilise actuellement un système de brûleurs au propane afin de chauffer les galeries souterraines pour améliorer les conditions de travail sous terre lors des mois les plus froids de l'année (communication personnelle, Goldcorp, 2017). Plus précisément, ce projet vise à caractériser la ressource géothermique issue de l'eau de dénoyage de la mine en effectuant la conception d'un système de pompes à chaleur couplé au système de pompage des eaux déjà en place dans les mines. Dans un tel système, l'eau issue du dénoyage de la mine serait redirigée vers les pompes à chaleur pour en extraire l'énergie thermique. L'hypothèse mise de l'avant est qu'un tel système ne nécessitant aucun forage offrirait une période de retour sur l'investissement plus courte qu'un système de PACG conventionnel dont l'installation requiert des coûts importants liés aux forages et l'aménagement des échangeurs de chaleur (Grasby et al., 2011). De cette façon, un système géothermique couplé aux opérations de dénoyage permettrait de diversifier les sources d'énergie de la mine, ainsi que de combler une partie des besoins énergétiques en chauffage. Cela s'inscrit dans une perspective de développement durable, puisqu'un tel système permettrait de minimiser non seulement les coûts de production, mais également la consommation d'hydrocarbures et les émissions de gaz à effets

de serre (GES). D'autre part, ce projet a pour but d'évaluer la pérennité des ressources géothermiques d'une mine active dans le temps en développant un modèle numérique hydrogéologique permettant de préciser la quantité d'énergie disponible au cours de l'exploitation de la mine selon des conditions variables de l'eau de dénoyage, telles que la température et le débit de pompage.

REVUE DE LITTÉRATURE – ÉNERGIE GÉOTHERMIQUE POUR LES MINES EN CONTEXTE NORDIQUE

La revue de littérature porte *a priori* sur les enjeux rencontrés par les opérations minières situées en milieu nordique, ainsi que sur le potentiel géothermique du nord du Québec. Subséquemment, la revue aborde le fonctionnement des pompes à chaleur géothermique et les diverses configurations existantes. Postérieurement, les différentes catégories de réservoirs géothermiques retrouvées dans les sites miniers sont présentées. La dernière section passe en revue des projets géothermiques qui ont été réalisés en couplant un système de pompes à chaleur géothermique avec le système de dénoyage d'une mine.

Enjeux des sites miniers situés en milieu nordique

Avec une demande croissante des minéraux et des métaux, les entreprises minières réalisent de plus en plus de projets d'exploitation minérale dans des régions nordiques et éloignées. Au Canada et au Québec, la plupart des projets miniers sont situés au nord du 49^e parallèle (Ministère de l'Énergie et des Ressources naturelles, 2015; Natural Resources Canada, 2018b). Malgré que ce territoire soit riche en ressources naturelles, le climat est beaucoup plus froid qu'au sud et l'accès aux infrastructures est limité. Dans ces conditions, les coûts de production y sont beaucoup plus élevés. Une des sources de dépenses les plus importantes est l'approvisionnement énergétique. Plus précisément, en raison des conditions climatiques particulièrement froides, le chauffage des galeries souterraines devient une réalité des mines situées dans un contexte nordique. Le chauffage des galeries souterraines est un besoin de chauffage supplémentaire qui devient un contributeur important à l'augmentation des dépenses. Par exemple, dans un contexte nordique, le coût énergétique total d'extraction par tonne de minerai est de 5,07 \$ et le coût du chauffage des galeries souterraines varie de 0,06 à 0,29 \$ par tonne de minerai extrait (Natural Resources Canada, 2005). Le chauffage des ouvrages miniers est un défi important à aborder.

La construction des lignes de transmission électrique à partir d'une centrale hydroélectrique se présente souvent comme une première option en vertu de son abondance. Néanmoins, les mines

se situent loin des lignes de transport électrique, ce qui ne rend pas rentable la réalisation d'un projet de raccordement au réseau. Le projet diamantifère Renard de Stornoway Diamonds, situé à Baie-James dans le centre-nord du Québec, a évalué la possibilité de se raccorder au réseau d'Hydro-Québec avec une ligne de transmission de 161 kV et d'environ 160 km. La mine a considéré le projet comme non rentable, en conséquence d'un coût total estimé de 175 M\$, soit approximativement 1,1 M\$ par kilomètre (Perron, 2016). Dans les cas où le réseau électrique est accessible, chauffer avec un système électrique n'est pas lucratif en raison de l'appel de puissance élevé.

Ainsi, les entreprises minières utilisent souvent des combustibles fossiles pour satisfaire leurs besoins énergétiques. En 2016, 50 % de la consommation d'énergie totale du secteur minier au Québec provenait de combustibles fossiles (Natural Resources Canada, 2016). À titre d'exemple, durant la phase d'exploration et développement, la mine Renard consommait 27,5 M de litres de diesel annuellement pour combler les 21,6 MW de puissance requis pour les opérations souterraines et en surface (Belzile et al., 2017). Dans le nord du Québec, la mine Casa Berardi de Hecla Mining consommait 1,9 M de litres de propane pour le chauffage de galeries souterraines (Vision Biomasse Québec, 2015). La mine Raglan, située au Nunavik, consomme de 50 à 60 M de litres de diesel par an (SNC - Lavalin, 2016). Dans les Territoires du Nord-Ouest, la mine Diavik de Rio Tinto consomme environ 65 M de litres de diesel par an (Bertoli, 2015).

Les entreprises minières cherchent des alternatives afin de réduire les coûts de production, tout en minimisant l'impact environnemental. Récemment, plusieurs compagnies se sont tournées vers le gaz naturel liquide (GNL), compte tenu de son faible prix. En 2016, juste avant le début de l'entrée en production, la mine Renard a remplacé les fournaises au diesel par un système de gaz naturel liquide (Perron, 2016). Bien que le GNL soit une option économique attrayante, il demeure un combustible fossile et sa rentabilité fluctue en fonction du prix. Par exemple, au Québec, les coûts énergétiques des mines sont passés de 235,5 M\$ à 685,9 M\$ entre 2000 et 2014 en raison de la hausse du prix du pétrole (Natural Resources Canada, 2016). Cependant, le prix du pétrole est en baisse depuis 2015, témoignant de la volatilité des prix des hydrocarbures. Par ailleurs, la mine Casa Berardi a installé un système de biomasse forestière résiduelle à la place des brûleurs de propane pour le chauffage des galeries souterraines. Ce système a entraîné une réduction des émissions de gaz à effet de serre (GES) de 2 732 tonnes annuelles (Vision Biomasse Québec, 2015). L'énergie éolienne devient également une alternative employée par plusieurs mines dans le Nord. Au Nunavik, deux éoliennes de 3 MW avec un système de stockage par batterie bidirectionnel installées à la mine Raglan permettent

d'économiser 4,2 M de litres de diesel et d'empêcher l'émission de 6 800 T de GES (Tugliq, 2019). En outre, la mine Diavik a aussi mis en œuvre quatre éoliennes avec une puissance de 2,3 MW. La concrétisation de ce projet a permis de réduire la consommation de diesel de 4,3 M de litres par an, ainsi que de limiter l'émission de 12 000 tonnes de CO₂ équivalent. Le coût total du projet était de 30 M\$ avec une période de retour sur investissement d'environ 7 ans (Bertoli, 2015).

La recherche et l'établissement des sources énergétiques rentables et écologiques pour les entreprises minières sont un enjeu crucial. Les systèmes de PACG couplés aux systèmes de dénoyage, comme d'autres sources d'énergie renouvelable, tel que l'énergie solaire ou éolienne, peuvent fournir une énergie locale, abordable et écoresponsable. Cependant, l'un des principaux avantages de l'énergie géothermique relativement à d'autres sources d'énergie renouvelables est sa faible fluctuation due à des facteurs externes, tels que le climat. Par exemple, l'énergie solaire et éolienne possèdent en moyenne une capacité intermittente variant entre 20 % et 40 % (Ren et al., 2017; Miller et Keith, 2018). En comparaison, les systèmes géothermiques possèdent un facteur de capacité compris entre 90 % et 97 %, permettant la production d'énergie d'une façon presque constante (Shortall et al., 2015). Cette option permettrait de combler une proportion du besoin énergétique en chauffage des mines dans un contexte nordique et constitue une option qui mérite d'être évaluée.

Potentiel géothermique du nord du Québec

La température du milieu souterrain détermine le type de réservoir géothermique (Ghoreishi-Madiseh et al., 2015). Par exemple, lorsque le milieu souterrain atteint des températures supérieures à 150 °C, le réservoir géothermique se définit alors de type « haute température ». L'eau ou la vapeur d'eau dans ce type de réservoir peuvent être utilisées pour produire de l'électricité. Un réservoir géothermique est de type « température moyenne » lorsque la température du milieu souterrain varie entre 80 et 150 °C (Grasby et al., 2011). Dans ce cas, les fluides extraits du réservoir peuvent être utilisés pour produire de l'électricité avec une centrale binaire. Finalement, lorsque l'eau se retrouve à une température inférieure à 80 °C, le réservoir est de « basse température ». Si la température de l'eau est suffisamment élevée, l'eau dans le sous-sol peut être utilisée directement par un système énergétique de quartier ou pour d'autres activités industrielles. Néanmoins, lorsque la température ne dépasse pas les 30 °C, l'énergie peut être extraite par l'entremise d'un système de pompes à chaleur géothermique (PACG), typiquement pour des fins de chauffage ou climatisation. Même lorsque les températures sont relativement basses, seulement un faible écart de température est nécessaire entre la source

d'énergie et l'endroit de consommation d'énergie en raison de l'efficacité des pompes à chaleur géothermiques. Par exemple, à faible profondeur dans le sol, la température est basse, mais relativement stable. Cela entraîne une différence moyenne de 3 à 5 °C entre la température du sol et la température moyenne de l'air durant toute l'année.

Tel est le cas dans le nord du Québec, où, malgré les fortes variations de température saisonnières, la température moyenne annuelle en surface varie entre -9 et 2 °C (Comeau, 2017). Toutefois, la température du sol non perturbé, soit la profondeur à laquelle le sol conserve une température constante au long de l'année, retrouvée normalement à une profondeur supérieure à huit mètres, se maintient entre -4 et 7 °C selon la latitude. L'écart entre la température moyenne annuelle en surface et la température du sol non perturbé est en moyenne de 5 °C (Ouzzane et al., 2015). Ainsi, durant la période froide, la chaleur renfermée dans ce réservoir de basse température peut être extraite et amplifiée avec un système PACG. D'autre part, durant la période estivale, le milieu souterrain peut agir comme dissipateur de la chaleur ambiante.

Un facteur déterminant du potentiel géothermique du nord du Québec est qu'il est contenu au sein du Bouclier canadien, composé de roches ignées et métamorphiques anciennes (2,85 Ga à 970 Ma). Ces roches ont subi une décomposition radiogénique pendant une longue période. En conséquence, celles-ci produisent très peu de chaleur (Grasby et al., 2011). En effet, le flux de chaleur dans le nord du Québec est un des plus faibles au Canada. Les trois principales provinces géologiques qui se trouvent dans le nord du Québec, la Province de Grenville, la Province du Supérieur, la Province de Churchill montrent un flux de chaleur moyen de 30,8, 32,1 et 34,4 mW m⁻², respectivement (Comeau, 2017). Malgré le faible flux de chaleur, les roches du Bouclier canadien possèdent une conductivité thermique souvent supérieure à 3,0 W m⁻¹ K⁻¹. Leur excellente capacité de transfert de chaleur facilite l'extraction de la chaleur renfermée dans ce réservoir de faible enthalpie avec un système de PACG (Grasby et al., 2011). Les types de pompes à chaleur géothermique et les mécanismes qui leur permettent d'extraire et rehausser l'énergie disponible dans les réservoirs géothermiques de basse température pour de fins de chauffage ou climatisation sont abordés dans la prochaine section.

Pompes à chaleur géothermique (PACG)

Mécanique

L'utilisation des PACG est idéale pour extraire et rehausser l'énergie disponible dans les réservoirs géothermiques de basse température ($< 30^{\circ}\text{C}$) pour de fins de chauffage ou climatisation. L'ensemble des pompes à chaleur sont basées sur un cycle de Carnot inverse, dans lequel la chaleur est transmise d'une source de chaleur, telle que l'eau ou le sol, vers un endroit de consommation de chaleur (Sarbu et Sebarchievici, 2014). Ces systèmes permettent de cette façon le transfert de la chaleur du milieu souterrain vers les bâtiments durant l'été et des bâties vers la terre pendant la période hivernale.

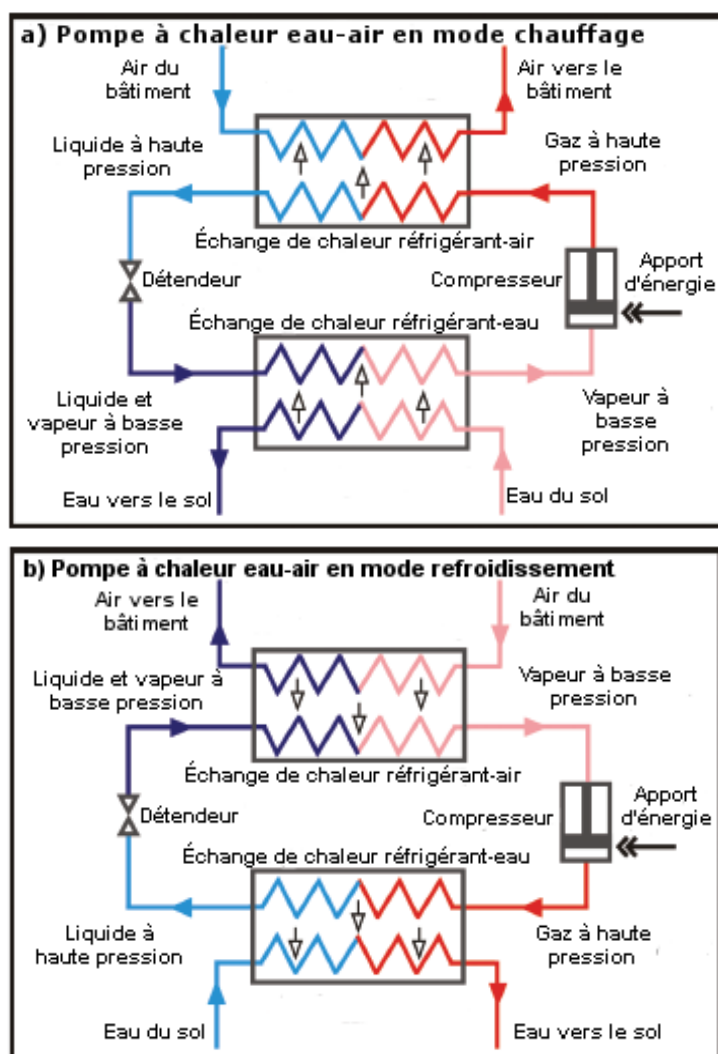


Figure 1 : Fonctionnement d'une pompe à chaleur eau-air en mode a) chauffage et b) climatisation (Raymond et al., 2010).

En mode chauffage (Figure 1 a), l'eau ou le fluide caloporteur circule vers l'évaporateur afin d'accroître la température d'un réfrigérant avec un très faible point d'ébullition. Par la suite, le réfrigérant, maintenant sous forme de gaz, est compressé pour augmenter la pression et conséquemment la température. Le réfrigérant est ensuite acheminé vers un échangeur de chaleur réfrigérant-air pour chauffer l'air du bâtiment. Finalement, le réfrigérant se déplace vers un condenseur, en plus de passer par un détendeur pour diminuer la pression et la température du gaz. Le cycle est inversé en mode climatisation (Figure 1 b).

Néanmoins, le processus de compression consomme une quantité d'énergie variant selon l'efficacité de la pompe à chaleur. Les relations suivantes permettent de calculer l'efficacité d'une thermopompe (Sarbu et Sebarchievici, 2014) :

$$COP_{ch} = \frac{Q_{ch}}{Q_{comp}} \quad \text{et} \quad COP_{clim} = \frac{Q_{clim}}{Q_{comp}} \quad (1.0)$$

Où:

COP_{ch} = coefficient de performance en mode chauffage

COP_{clim} = coefficient de performance en mode climatisation

Q_{ch} = puissance de chauffage de la pompe à chaleur [W]

Q_{clim} = puissance de climatisation de la pompe à chaleur [W]

Q_{comp} = puissance consommée par le compresseur [W]

Le coefficient de performance (COP) représente le rapport entre le taux d'extraction de chaleur total de la PACG et la quantité d'énergie requise par le compresseur. Le coefficient de performance diffère selon le système de PACG, mais varie typiquement entre 2 et 3, pouvant atteindre 6 dans certains systèmes. En comparaison, un système de chauffage électrique possède un COP de 1.

Types de PACG

De nombreuses configurations de PACG existent en fonction du réservoir géothermique, ainsi que de la façon dont le transfert de chaleur se produit (Figure 2). Les trois principaux types d'arrangements sont présentés dans les sections subséquentes.

Pompe à chaleur d'aquifère

Dans un système géothermique dit de « boucle ouverte », l'eau d'un aquifère, qui constitue la source de chaleur, est pompée vers la surface par un puits de production. Un échangeur de chaleur intermédiaire doit par conséquent précéder la PACG afin de prévenir la corrosion et

l'entartrage. Après avoir passé par la PACG, l'eau peut être évacuée dans un plan d'eau ou retournée à l'aquifère par un puits d'injection (Figure 2 a et b; Kavanaugh & Rafferty, 2014; Raymond et al., 2010). Les PACG de ce type sont abordables et largement disponibles, mais la présence d'un aquifère, un débit suffisant, la qualité de l'eau, le pompage excessif, en plus du déversement des eaux peut poser des problèmes (Kavanaugh et Rafferty, 2014). Au Québec, le règlement sur le prélèvement des eaux et leur protection stipule que l'eau captée par un système géothermique à boucle ouverte doit être retournée dans l'aquifère d'origine (Gouvernement du Québec, 2014).

Pompe à chaleur d'eau de surface

Les PACG d'eau de surface permettent de réaliser l'échange thermique à partir de plans d'eau, tels que les lacs ou les rivières, en utilisant un système géothermique de type « boucle ouverte » ou « boucle fermée » (Figure 2 c et d; Kavanaugh & Rafferty, 2014). Dans une boucle ouverte, l'eau est captée dans le plan d'eau et acheminée vers la PACG en passant par un échangeur intermédiaire. Par la suite, l'eau est déversée dans le même plan d'eau (Raymond et al., 2010). Dans une telle configuration, l'installation d'un échangeur intermédiaire est requise afin de protéger le système contre la corrosion et l'incrustation. Les avantages des pompes à chaleur d'eau de surface à boucle ouverte sont leur faible besoin en énergie pour le pompage grâce aux débits d'eau élevés, ainsi que le faible coût de maintenance et d'exploitation. Cependant, dans ces systèmes la température est inférieure à celle de l'eau dans les aquifères, et la température est sujette à des variations qui peuvent influencer la performance du système de pompes à chaleur.

Quant à la boucle fermée, il s'agit d'un réseau de tuyaux dans lequel un fluide caloporteur circule afin d'effectuer l'échange énergétique. Un échangeur de chaleur intermédiaire n'est donc pas requis. Ce type de configuration peut subir des fluctuations de température en raison des changements de température dans les plans d'eau en surface (Raymond et Therrien, 2008; Raymond et al., 2010).

Pompe à chaleur couplée au sol

L'échange de chaleur dans un système de pompes à chaleur couplé au sol a lieu par l'entremise d'une boucle fermée, installée de façon verticale ou horizontale, par lequel un fluide caloporteur circule (Figure 2 e et f; (Kavanaugh et Rafferty, 2014). Dans ce genre de système, le fluide caloporteur n'entre pas en contact avec les matériaux souterrains ou l'eau souterraine, diminuant

ainsi les risques environnementaux. De même, du fait que le fluide caloporeur est conçu pour ne pas constituer un risque de corrosion et d'entartrage pour la thermopompe, l'utilisation d'un échangeur de chaleur intermédiaire n'est pas requise.

Les PACG couplés au sol offrent plusieurs avantages. D'abord, les réseaux verticaux peuvent être mis en place avec une aire réduite, la quantité de tuyaux nécessaire est inférieure comparativement à d'autres configurations et les fluctuations de température sont moins importantes, car la température du sol est stable en profondeur. Par contre, les coûts d'installation sont supérieurs par rapport aux autres types de PACG en raison de la nécessité de réaliser des forages variant typiquement entre 100 et 180 m de profondeur. Les réseaux horizontaux sont plus abordables, mais occupent des superficies étendues et subissent des variations de température, car l'ensemble des installations sont localisées à une profondeur variante généralement entre 1.5 et 1.8 m (Kavanaugh et Rafferty, 2014).

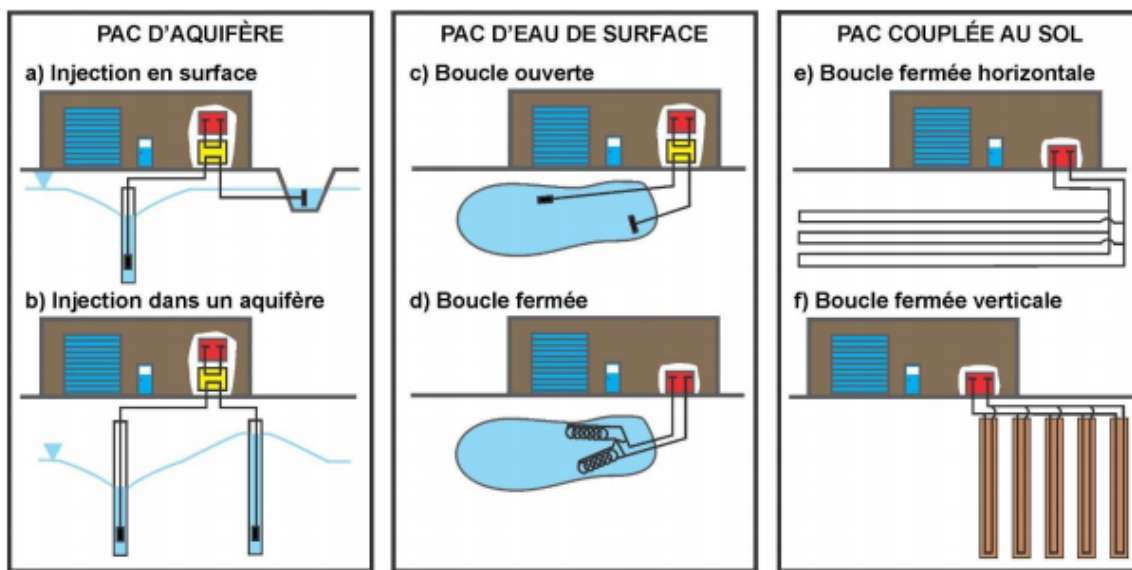


Figure 2 : Configuration des pompes à chaleur géothermique. Le rectangle rouge représente la pompe à chaleur, tandis que le jaune montre un échangeur de chaleur intermédiaire (tiré de Raymond et al., 2010).

Géothermie de basse température sur les sites miniers

L'énergie géothermique associée aux activités minières s'avère une alternative fort attrayante dans le but de contribuer aux besoins énergétiques des opérations. D'abord, la température est plus élevée et stable en profondeur en raison du gradient géothermique et de l'effet isolant du sol. Également, d'un point de vue du potentiel géothermique, une mine et le socle rocheux qui l'entoure forment un système d'une conductivité hydraulique globale plus élevée comme conséquence du réseau de galeries souterraines, permettant ainsi d'atteindre des débits de

pompage élevés. Il existe plusieurs emplacements dans une mine avec un potentiel géothermique intéressant, tels que les haldes à résidus et les réservoirs d'eau de surface. Par exemple, dans certaines mines, l'oxydation des minéraux dans les haldes à résidus miniers entraîne des réactions chimiques exothermiques offrant une source de chaleur propice à l'extraction de l'énergie géothermique (Ghomshai et Meech, 2005; Raymond et al., 2010).

L'énergie disponible dans les mines peut combler une proportion du besoin énergétique en chauffage et climatisation des bâtiments ou des galeries souterraines (Preene et Younger, 2014). Selon Ghomshai et Meech (2005) et Ordóñez Alonso et al. (2010), l'énergie générée par un système de PACG associé aux mines peut varier entre 1 et 14 MW. Malgré ce potentiel, les systèmes géothermiques sont peu utilisés en raison du coût élevé des forages (Bailey et al., 2016). Cependant, sur un site minier une fraction substantielle de l'investissement initial est couvert, car une partie de l'infrastructure nécessaire pour extraire l'énergie géothermique, telle que les puits, le système de dénoyage et les plans d'eau artificiels sont déjà en place (Preene et Younger, 2014). Dans le cas d'une mine en exploitation, un système de PACG permettrait d'extraire l'énergie de l'eau de dénoyage. L'énergie générée pourrait fournir une partie du besoin supplémentaire nécessaire pour le chauffage des galeries souterraines dans les mines en opération dans un contexte nordique. Pour ce faire, les opérations de dénoyage doivent être coordonnées avec les opérations de chauffage de la mine. L'évaluation de chaque site minier est donc essentielle afin de concevoir un système géothermique adapté au contexte de la mine.

Systèmes géothermiques dans les sites miniers

Le système de pompes à chaleur est conçu en fonction du type de réservoir géothermique disponible dans la mine. Les prochaines sections sont consacrées aux réservoirs géothermiques couramment retrouvés dans les mines et les systèmes PACG correspondants.

Aquifère

Dans le cas des mines souterraines abandonnées, les eaux d'infiltration remplissent les galeries souterraines de la mine, puisque le système de dénoyage de la mine est inactif et la conductivité hydraulique globale du système est élevée (Hall et al., 2011). Le milieu souterrain de la mine devient alors un « aquifère anthropique » (Adams et Younger, 2001). Dans ces conditions, une pompe submersible peut être utilisée afin de capter l'eau vers le système de PACG en surface et de réinjecter l'eau dans les galeries souterraines ou dans un plan d'eau en surface (Raymond et Therrien, 2008). D'une manière semblable, les pompes du système de dénoyage dans une mine

active permettent de pomper l'eau vers le système PACG en surface et de réinjecter l'eau dans l'aquifère via un puits d'injection ou, si l'eau a été traitée, dans un plan d'eau situé à proximité. Dans les deux cas, il s'agit des systèmes géothermiques ouverts tels que ceux présentés à la Figure 2 *a et b*. Par exemple, à la mine Gaspé, localisée près de la ville de Murdochville, le gradient mesuré est de $0,011 \text{ }^{\circ}\text{C m}^{-1}$ et les galeries souterraines atteignent 700 m de profondeur. Selon Raymond et Therrien (2014), l'installation d'un système de PACG avec un débit de $0,019 \text{ m}^3 \text{ s}^{-1}$ et une température moyenne de sortie de la pompe de $6 \text{ }^{\circ}\text{C}$ permettrait de fournir la totalité des 1 488 MWh nécessaires pour chauffer le parc industriel de la ville de Murdochville, Québec.

Eau de surface

Les plans d'eau artificiels des mines sont un endroit propice à l'installation de systèmes de PACG (Grasby et al., 2011). Après la fermeture d'une mine, de multiples plans d'eau artificiels, tels que les bassins de polissage, demeurent sans utilisation. Dans le cas des mines à ciel ouvert, la plupart deviennent inondées en fin de vie (Raymond et Therrien, 2014). Les mines en exploitation contiennent également de nombreux réservoirs d'eau. De plus, comme les opérations minières sont des propriétés privées, les sites miniers possèdent moins de restrictions concernant la mise en place des systèmes géothermiques couplés aux eaux de surface (Raymond et al., 2010). Dans le milieu minier, l'installation d'un système de PACG d'eau de surface comme présenté à la Figure 2 *c et d* est donc une possibilité. Un tel système a d'ailleurs été mis en œuvre à la carrière Goyer afin de chauffer et climatiser un complexe d'appartements à Saint-Bruno-De-Montarville, Québec (Raymond et al., 2008; Raymond et al., 2010; Grasby et al., 2011). Par contre, l'emploi d'un échangeur de chaleur intermédiaire est essentiel, puisque l'eau chargée en éléments chimiques provenant du lessivage des roches circule à l'intérieur du système.

Résidus miniers

Les résidus de l'extraction minière sont conservés sous la forme de fragments de roches ou sédiments non consolidés dans des parcs à résidus ou des haldes à stérile. Lorsque les résidus sont exposés aux éléments, certains minéraux, tels que la pyrite, s'oxydent, ce qui produit des quantités considérables de chaleur. La température des résidus peut atteindre entre $55 \text{ }^{\circ}\text{C}$ et $65 \text{ }^{\circ}\text{C}$ (Lefebvre et al., 2001; Raymond et al., 2010). À la mine Doyon, à Rouyn-Noranda, la température dans les haldes à stérile dépassait $40 \text{ }^{\circ}\text{C}$, 20 ans après leur mise en place (Raymond et al., 2008). Au Québec, plus de 55 haldes à stérile avec un bon potentiel géothermique

pourraient être exploités avec un système de pompes à chaleur à boucle fermée, tel que celui présenté à la Figure 2 e et f (Raymond et al., 2008).

Études précédentes

Plusieurs projets ont été réalisés à travers le monde en utilisant des systèmes de PACG pour extraire l'énergie des mines. Au Canada, un système de PACG a été installé à la mine fermée et inondée Ropak Can Am à Springhill, en Nouvelle-Écosse, pour chauffer et climatiser un quartier résidentiel de 16 700 m². Ce système, couplé au système de dénoyage de la mine, permet de produire environ 45 kW en extrayant l'énergie de l'eau à 18 °C contenue dans les galeries souterraines situées à une profondeur de 1 350 m (Jessop et al., 1995). En Écosse, des systèmes de PACG ont été implémentés dans une mine de charbon inondée à Shettleston et Lumphinnans. L'eau provenant d'une profondeur variant de 100 à 170 m entre dans les PACG à une température oscillant entre 12 à 14,5 °C, tandis que l'eau sort du système à 3 °C, ce qui permet le chauffage d'un quartier résidentiel de 18 maisons (Watzlaf et Ackman, 2006). En Allemagne, l'utilisation des systèmes géothermiques pour extraire l'énergie de l'eau de dénoyage des mines est une pratique courante depuis les années 1980. Les projets existants, d'une puissance installée de 80 à 350 kW, sont employés pour usage direct dans des zones résidentielles, scolaires et à des fins récréatives (Wieber et Pohl, 2008). En 2018, la ville d'Alsdorf en Allemagne a débuté un projet d'énergie géothermique visant à combler la croissante demande énergétique de la ville (Aachener-Zeitung, 2018). Ce projet permettra d'utiliser l'eau d'une mine abandonnée qui atteint 900 m de profondeur et contient de l'eau à 26 °C (Stratego, 2016). En outre, un des plus grands projets géothermiques impliquant un système de PACG a été mis en œuvre dans une mine inondée et inactive à Heerlen, Pays-Bas. Le système, capable de produire 700 kW, fournit 80 % du besoin énergétique en chauffage et climatisation d'un quartier résidentiel de 350 maisons et 20 000 m² de surface commerciale. Durant l'hiver, l'eau est pompée à une profondeur de 700 m, où sa température varie entre 30 et 35 °C. Pendant l'été, le système sert à climatiser et l'eau est pompée à partir du niveau 250 m à une température entre 16 et 19 °C (Hall et al., 2011). D'autres projets ont également été réalisés en Norvège ainsi qu'aux États-Unis. Le Tableau 1 montre l'ensemble des projets géothermiques. Tous ces projets sont constitués d'un système de PACG ouvert installé dans des mines abandonnées et inondées. Au Canada, cette filière énergétique mérite d'être développée, puisqu'il existe approximativement 2 262 mines abandonnées et répertoriées contenant un potentiel énergétique d'environ 18 642 TJ (Raymond et al., 2010).

D'autre part, l'étude des systèmes de PACG couplés aux opérations de dénoyage des mines actives demeure marginale (Patsa et al., 2015; Amiri et al., 2016), et la mise en œuvre inexiste. Selon Raymond et al. (2010), au Canada, environ 200 mines sont en opération et, parmi ces dernières, 50 possèdent un bon potentiel géothermique. D'après les travaux effectués par Koufos (2012), l'incorporation de systèmes de PACG dans 12 mines en opération au Manitoba, en Ontario et au Québec permettrait à l'industrie minière d'économiser 1,5 M\$ CAD et de réduire les émissions de GES de 18 850 tonnes de CO₂ annuellement.

Tableau 1: Systèmes géothermiques mis en œuvre dans des projets miniers abandonnés (modifié de Hall et al., 2011; Koufos, 2012).

Mine		Profondeur (m)	Débit (L/s)	¹ ΔT (°C)	Économie annuelle (\$/année)	Puissance (kW)	État du projet
Springhill, Nouvelle-Écosse		140	4	7	45 000	45	Opérationnel
Heerlen, Pays-bas		700	22	5	n/d	700	Opérationnel
Shuttleston, Écosse		122	3	9	n/d	16 maisons	Opérationnel
Lumphinnans, Écosse		170	n/d	9	n/d	18 maisons	Opérationnel
Park Hills, États-Unis		122	5	11	30 844	113	Opérationnel
Folldal, Norvège		600	n/d	n/d	n/d	18	Opérationnel
Henrich, Allemagne		n/d	n/d	n/d	n/d	350	Opérationnel
Sachsen, Allemagne		n/d	n/d	n/d	n/d	82	Opérationnel
Zollverein, Allemagne		n/d	n/d	n/d	n/d	n/d	Opérationnel
Alsdorf, Allemagne		900	n/d	Température du réservoir 26 °C	n/d	n/d	Conception

¹Difference de température entre l'eau souterraine entrant et sortant du système géothermique

D'après la revue bibliographique, les recherches sur l'utilisation des systèmes géothermiques dans les mines actives sont marginales, d'où l'intérêt d'effectuer une étude de faisabilité en partenariat avec Newmont-Goldcorp sur le site de la mine Éléonore.

MÉTHODOLOGIE

L'évaluation du potentiel géothermique de la mine Éléonore comporte deux volets. Le premier est la conception d'un système de pompe à chaleur géothermique (PACG) adapté au système de dénoyage de la mine. Cette étape consiste à déterminer la quantité d'énergie nécessaire pour chauffer les galeries souterraines, ainsi que le coût et l'impact environnemental du système actuel de brûleurs au propane. Ensuite, les données de température et de débit de l'eau des quatre sites potentiels, soit à la sortie de la mine, à l'entrée et à la sortie de l'usine de traitement des eaux industrielles (UTEI), ainsi qu'à la sortie de l'émissaire ont été collectées et analysées pour évaluer le risque de corrosion et d'entartrage. À l'aide de toutes ces informations, un système de PACG préliminaire a été conçu pour calculer la quantité d'énergie géothermique qui peut être extraite de l'eau de dénoyage de la mine. Le deuxième volet du projet comprend le développement d'un modèle numérique hydrogéologique pour simuler le débit dénoyage, le rabattement et la température de sortie de l'eau afin de déterminer la durabilité de la ressource géothermique et préciser la quantité d'énergie générée par le système géothermique au cours de la vie de la mine.

RÉSULTATS

Bilan initial

La première étape de la conception du système de PACG a été de déterminer la charge calorifique actuelle des chantiers souterrains, les coûts de chauffage encourus ainsi que l'impact environnemental. Selon les calculs effectués avec les données de l'année 2016, le chauffage de galeries souterraines nécessite 26 664 MWh ou 37 MW thermiques, ce qui représente 22,5% des besoins énergétiques totaux de la mine. Le système de chauffage au propane est requis d'octobre à avril. Celui-ci consomme 3,4 millions de litres par an, générant des dépenses de 1,5 million de dollars canadiens par an tout en libérant 5 600 tonnes de dioxyde de carbone (Figure 4.1).

Évaluation du site

D'après la comparaison pour la période 2015-2017, le débit le plus élevé est celui à la sortie de la mine, avec un débit moyen de $299 \text{ m}^3\text{h}^{-1}$. Le débit vers l'émissaire présente un débit légèrement plus faible, avec $278 \text{ m}^3\text{h}^{-1}$. Le débit moyen à l'entrée de l'UTEI est de $230 \text{ m}^3\text{h}^{-1}$, tandis qu'à la sortie de l'usine de traitement des eaux le débit moyen est de $167 \text{ m}^3\text{h}^{-1}$. Le débit à la sortie de l'UTEI est inférieur comparativement à celui à la sortie de la mine, car une proportion de l'eau de l'usine de traitement des eaux est utilisée par l'usine de gestion de résidus. Le débit vers

l'émissaire est aussi légèrement inférieur, car une proportion de l'eau est utilisée pour le contrôle de la poussière, pour le garage et pour remplir le réservoir d'eau douce.

D'après la comparaison pour la période 2016-2017, l'eau avec la température moyenne la plus élevée se retrouve à la sortie de la mine, avec une température moyenne annuelle de 12,1 °C. Cela s'explique notamment par le fait que l'eau de la mine provient d'un réservoir d'eau localisé au niveau 400 où les eaux de plusieurs procédés, tels que le nettoyage du remblai à pâte (*paste flush water*) en plus de l'eau d'infiltration, se réunissent. Les eaux provenant du puits d'exploration et de production, ainsi que de la rampe sont aussi dirigées vers ce réservoir. L'eau de la mine préserve alors une température plus élevée comparativement aux autres endroits, puisque l'eau souterraine a une température constante qui augmente avec le gradient géothermique. En plus, le sol agit comme isolant en protégeant l'eau contre les conditions météorologiques. D'ailleurs, la température à l'entrée de l'UTEI est légèrement plus faible, avec une température moyenne de 10,9 °C. Toutefois, durant l'hiver, l'eau entrant dans l'UTEI a une température moyenne de 8 °C. Ceci indique une perte variant de 1,2 à 4,1 °C entre la zone de sortie de l'eau de dénoyage de la mine et l'entrée de l'UTEI. La perte de chaleur est le résultat de l'exposition de l'eau aux conditions atmosphériques lorsque l'eau passe par le bassin de polissage et sédimentation précédant l'UTEI. Finalement, la température moyenne vers l'émissaire est de 9,0 °C. Il s'avère important de noter que la température moyenne à la sortie de la mine est considérablement plus élevée par rapport aux autres sites durant l'hiver et le printemps, en plus d'être légèrement moins élevée pendant l'été. Ces conditions sont idéales pour le chauffage des galeries pendant la saison froide et la climatisation au cours de l'été.

Qualité de l'eau

Dans la zone de sortie de l'eau de dénoyage, l'indice de saturation de Langelier (ISL) dénote un léger risque d'entartrage, et l'indice de stabilité Ryznar (ISR) suggère que l'eau ne présente pas un potentiel d'entartrage ou de corrosion. Selon l'indice de saturation Puckorius (ISP), qui minimise l'effet tampon de l'eau, il existe un potentiel de corrosion important. L'indice de corrosion Larson-Skold (ICLS) prévoit également un taux de corrosion élevé. À l'émissaire, aucun risque d'entartrage n'est présent, mais le potentiel de corrosion est plus élevé par rapport à la zone de sortie d'eau de la mine. La diminution du pH, de la concentration en calcium et en bicarbonate et l'augmentation de la teneur en chlorure, sulfate et matières solides dissoutes totales vers l'émissaire contribuent au risque accru de corrosion. Globalement, la zone de sortie de l'eau de

dénoyage présente la température et le débit les plus élevés, ainsi qu'un plus faible risque de corrosion.

Évaluation de la performance

La performance du système a été évaluée du point de vue énergétique, économique et environnemental. Le système de pompe à chaleur géothermique conçu pour les conditions du site est constitué de trois pompes à chaleur Multistack TRANE capables de gérer le débit moyen du système de dénoyage. De plus, en raison du risque potentiel de corrosion, un échangeur de chaleur à plaques a été inclus pour empêcher l'eau de circuler directement dans le système de pompe à chaleur. Les composants de l'échangeur de chaleur à plaques sont fabriqués en acier inoxydable de type 304 et 316 pour protéger le système contre la corrosion (Kavanaugh et Rafferty, 2014). Le système coûte 325 000 CAD. Ce prix comprend l'échangeur à plaques, le compresseur et l'évaporateur ainsi qu'un échangeur d'air. Il n'inclut pas les coûts de fonctionnement et d'entretien, d'installation et l'inflation.

Des calculs ont été effectués pour chaque site avec les valeurs mensuelles du débit et de la température de l'eau de dénoyage pour les années 2015 et 2016. Les résultats suggèrent que le système de PACG situé à la zone de sortie de l'eau de dénoyage pourrait générer entre 9 471 et 10 283 MWh par an, ce qui correspond à un niveau de pénétration énergétique qui varie entre 35 et 39% (Tableau 4.4). Pendant l'hiver, le niveau de pénétration diminue en raison de l'augmentation de la demande énergétique générée par la baisse de la température ambiante. En février, le mois le plus froid de 2015 et 2016, le niveau de pénétration énergétique est respectivement de 18% et 17%.

En termes de coûts de production d'énergie, les dépenses encourues par le système PACG correspondent uniquement à l'électricité consommée par le compresseur. Selon l'énergie consommée par le système PACG conçu pour cette étude et le prix de l'électricité à la mine, le coût de fonctionnement d'un tel système oscillerait entre 56 000 \$ et 60 000 \$ par an. Ensuite, la quantité d'énergie générée par le système de pompe à chaleur est soustraite de la demande totale de chauffage de galeries souterraines pour obtenir la quantité d'énergie fournie par le système de brûleur au propane. Les économies annuelles nettes sont ensuite déterminées en comparant les coûts générés par le système hybride à ceux du système de chauffage au propane. En 2015, le chauffage des galeries souterraines avec un système de chauffage hybride aurait coûté 1,4 million de dollars - une diminution de 30% des coûts de chauffage, ce qui représente 600 000 \$ d'économies nettes. En 2016, un tel système aurait coûté 1,04 million de dollars, ce

qui représente une diminution de 33% des coûts de chauffage ou 514 000 \$ d'économies nettes (Tableau 4.5). De plus, l'incorporation de ce système réduirait la consommation de propane de 1,24 à 1,36 million de litres par an, tout en réduisant les émissions de CO₂ de 1 825 à 1 993 tonnes par an (Tableau 4.6).

Modélisation numérique

Charge hydraulique, rabattement et température

Selon les plans de la mine, le pic de production serait atteint en 2019 et devrait rester à ce niveau pendant plusieurs années. Une régression linéaire effectuée avec les valeurs de débit observées pendant la période de calage a été utilisée pour prédire les débits (Figure 4.4). Le débit de dénoyage prévu atteint 656,8 m³h⁻¹ en 2019 et augmente progressivement jusqu'à ce qu'il atteigne le débit de dénoyage maximal de 718 m³h⁻¹ en 2024 (Tableau 4.8; Beausoleil et al. (2014)). Une fois que le débit de dénoyage maximal est atteint, le débit de dénoyage reste constant jusqu'à la fermeture de la mine en 2026 plus cinq années supplémentaires en cas d'agrandissement de la mine. L'augmentation du débit de dénoyage jusqu'à ce que la mine atteigne sa production maximale, suivie d'un palier jusqu'à la fermeture de la mine, est un comportement observé précédemment dans le cycle de vie des mines (Ugorets et Pereira, 2018).

De 2013 au début de 2019, le dénoyage de la mine a généré un rabattement de 790 m, soit environ 131 m par an. Le niveau d'eau actuel estimé à partir de la profondeur des galeries souterraines est de 1190 m. Avec la poursuite du développement souterrain et l'augmentation prévue du débit de dénoyage qui s'ensuit, les résultats suggèrent que le niveau 1370 sera atteint au début de 2024. En 2027, le modèle atteint un régime quasi permanent, avec un rabattement final de 1383 m et un rayon d'influence de 2,26 km.

L'augmentation du débit et du rabattement a une influence considérable sur la température de sortie de l'eau de dénoyage. Au cours de la première année de dénoyage, la température moyenne de l'eau sortant du système est plus faible, car l'eau est pompée exclusivement à partir du niveau 400. La température moyenne de l'eau durant la première année est de 7,3 °C. Avec le développement progressif de la mine, l'eau est pompée à une plus grande profondeur, où la température est plus élevée en raison du gradient géothermique et de l'effet isolant du sol. Une fois que la station de pompage de niveau 650 commence à pomper, la température moyenne durant la deuxième année augmente à 11,8 °C. Cependant, les débits des stations en profondeur sont inférieurs aux débits des principales stations de pompage situées à proximité de la surface.

Ainsi, la température augmente initialement, mais atteint une valeur quasi constante s'écartant peu de la moyenne observée de 12,1 °C, avec seulement une augmentation de 0,3 °C de 2019 à 2031 (Figure 4.6 et Tableau 4.9).

Production d'énergie maximale et potentielle

Un maximum de 26 664 MWh pourrait être produit annuellement, une quantité d'énergie qui représente 45% de la demande totale de chauffage des galeries souterraines, en supposant que la charge de chauffage reste au niveau de l'année 2016. Les coûts de chauffage diminueraient de 36% tout en réduisant les émissions de gaz à effet de serre de 2 067 tonnes/an. Cela permettrait de réduire la consommation de 1,6 million de litres de propane annuellement (Tableau 4.10). Indépendamment de l'année auquel le débit opérationnel maximal du système est atteint; ces valeurs constituent la quantité d'énergie maximale pouvant être générée par le système proposé.

Néanmoins, le système PACG sélectionné est un système modulaire qui peut être facilement modifié pour gérer des débits plus élevés et extraire de plus grandes quantités d'énergie. À partir de 2018, la quantité d'énergie disponible augmente considérablement, car le débit et la température augmentent progressivement. Les résultats indiquent que la quantité d'énergie produite annuellement augmente de 29 215 MWh en 2018 à 39 183 MWh en 2031 (Tableau 4.11). La puissance passe de 40 MW en 2018 à 53,9 MW en 2031. Au final, un total cumulé de 33 933 MWh serait généré jusqu'à la fin de vie prévue de la mine en 2026 et un total de 53 479 MWh d'ici 2031.

CONCLUSIONS

Un système de pompe à chaleur géothermique adapté au système de dénoyage d'une mine active semble techniquement faisable et durable tout au long de la vie de la mine. La qualité de l'eau constitue le principal défi technique, mais elle peut être gérée en suivante des mesures de prévention et d'atténuation adéquates. Par ailleurs, l'eau saline retrouvée à la mine Éléonore est présente à travers le Bouclier canadien et se retrouve possiblement dans d'autres mines ce qui servira comme point de comparaison dans le cadre des études futures. Néanmoins, les mines actives devraient être étudiées cas par cas, car les facteurs critiques influençant le potentiel géothermique, notamment le flux de chaleur local, le gradient géothermique, la profondeur de la mine, la qualité de l'eau de mine, la configuration du système de pompage et le débit de dénoyage peuvent tous varier selon l'emplacement. Globalement, le système de pompe à chaleur géothermique proposé peut contribuer de façon importante aux besoins en chauffage de la mine

Éléonore d'une manière écologique, abordable, constante et durable. Ce projet de recherche peut servir comme guide et comme point de comparaison pour l'évaluation du potentiel géothermique de l'eau de dénoyage d'autres mines en opération situées dans un contexte nordique. Enfin, la mise en œuvre de ce projet pilote à la mine Éléonore, qui pourrait être appuyé par divers intervenants, permettrait de fournir les données opérationnelles nécessaires à la validation des résultats, contribuant ainsi à l'intégration de sources d'énergie alternatives dans l'industrie minière.

Des recherches futures sont nécessaires pour établir la viabilité économique du système de pompe à chaleur géothermique comme source d'énergie alternative pour la mine Éléonore. De plus, il est nécessaire d'étudier le potentiel de climatisation de la PACG pendant les mois les plus chauds de l'année. De même, de nouvelles études pourraient être réalisées pour évaluer la performance opérationnelle du système de surveillance de la qualité de l'eau et des deux échangeurs de chaleur intermédiaires fonctionnant en parallèle pour gérer les risques de corrosion et d'entartrage de l'eau. La recherche pourrait étudier plus en détail la qualité de l'eau sur d'autres sites miniers en opération pour créer une base de données de l'eau de mine qui pourrait être analysée et comparée par rapport aux conditions réelles observées pour développer un outil mieux adapté pour quantifier le risque d'entartrage et de corrosion de l'eau. Enfin, les mines actives, et préféablement les projets miniers en développement, devraient être identifiés pour évaluer la faisabilité d'implémenter un système de pompes à chaleur géothermique en tant que contributeur aux besoins énergétiques des opérations minières et stimuler la transition énergétique.

CONTENTS

REMERCIEMENTS.....	III
RÉSUMÉ.....	V
ABSTRACT.....	VII
AVANT-PROPOS	IX
SOMMAIRE RÉCAPITULATIF.....	XI
CONTENTS.....	XXXI
LIST OF FIGURES	XXXV
LIST OF TABLES	XXXVII
LIST OF ABBREVIATIONS.....	XXXIX
1 INTRODUCTION	1
2 SITE BACKGROUND	3
2.1 LOCATION AND CLIMATE	3
2.2 GEOLOGY	4
2.2.1 <i>Regional Geology</i>	4
2.2.2 <i>Local Geology</i>	6
2.2.3 <i>Structural Features</i>	7
2.3 HYDROGEOLOGICAL CONTEXT	8
2.4 ENERGY CONTEXT.....	9
2.5 MINE PLAN AND FUTURE WORKS	10
2.6 GEOTHERMAL SETTING.....	12
3 METHODOLOGY	15
3.1 DESIGN OF THE GEOTHERMAL HEAT PUMP SYSTEM.....	15
3.1.1 <i>Initial energy balance</i>	15
3.1.2 <i>Site survey and selection</i>	16
3.1.3 <i>Flow and temperature</i>	17
3.1.4 <i>Water Quality</i>	18
3.1.5 <i>Geothermal Heat Pump System Design and Performance Assessment</i>	19
3.2 NUMERICAL MODEL DEVELOPMENT	25
3.2.1 <i>Theoretical Approach and Governing Equations</i>	25
3.2.2 <i>Modelling Strategy</i>	26
3.2.3 <i>Conceptual Model</i>	27
3.2.4 <i>Model Calibration</i>	34
3.2.5 <i>Model Predictions</i>	37
3.2.6 <i>Sensitivity Analysis</i>	38

4 RESULTS	39
4.1 DESIGN OF THE GEOTHERMAL HEAT PUMP SYSTEM.....	39
4.1.1 <i>Initial energy balance</i>	39
4.1.2 <i>Site assessment</i>	41
4.1.3 <i>Water Quality</i>	43
4.1.4 <i>Geothermal Heat Pump System Design and Performance Assessment</i>	46
4.2 NUMERICAL MODEL DEVELOPMENT	51
4.2.1 <i>Physical and Thermal Properties</i>	51
4.2.2 <i>Model Results</i>	53
4.2.3 <i>Uncertainty Analysis</i>	59
5 DISCUSSION	61
6 CONCLUSIONS	77
7 BIBLIOGRAPHY	79
8 APPENDIX I SCALING AND CORROSION INDICES	87
<i>Langelier and Ryznar Saturation Indices</i>	87
<i>Puckorius Scaling Index</i>	87
<i>Larson-Skold Corrosion Index</i>	88
9 APPENDIX II PLATE HEAT EXCHANGER EFFICIENCY CALCULATION.....	89
<i>Plate Heat Exchanger Efficiency Calculation</i>	89
10 APPENDIX III WATER QUALITY	91
<i>Table III.1: Site 1 - Mine Water Outlet Zone</i>	91
<i>Table III.2: Site 2 - Water Treatment Plant Entrance</i>	92
<i>Table III.3: Site 3 - Water Treatment Plant Exit</i>	93
<i>Table III.4: Site 4 - Emissary</i>	94
<i>Table III.5: Evolution of water pH and conductivity</i>	95
11 APPENDIX IV SCALING AND CORROSION INDICES CALCULATOR FILE AND RESULTS	97
<i>Scaling and Corrosion indices calculator file</i>	97
<i>Scaling and Corrosion indices results</i>	98
12 APPENDIX V GEOTHERMAL HEAT PUMP PERFORMANCE ASSESSMENT SITE 2 - 4	99
<i>Table V.1: Site 2 – Water Treatment Plant Entrance</i>	99
<i>Table V.2: Site 3 – Water Treatment Plant Exit</i>	102
<i>Table V.3: Site 4 – Emissary</i>	105
13 APPENDIX VI GROK, MPROP, AND FPROP HGS FILES	109
14 APPENDIX VII ROCK SAMPLES THERMAL PROPERTIES.....	111
<i>Table VII.1: Rock sampling locations and depths</i>	111

<i>Statistical distribution of the thermal properties of rock samples from the Éléonore mine according to location</i>	112
<i>Statistical distribution of the thermal properties of rocks samples from the Éléonore mine according to geological unit.....</i>	118
15 APPENDIX VIII DEWATERING GEOTHERMAL POTENTIAL OF THE ÉLÉONORE MINE RESEARCH REPORT (R1869).....	121

LIST OF FIGURES

FIGURE 2.1: MAP OF MINES IN OPERATION AND ELECTRICITY PRODUCTION IN THE PLAN NORD TERRITORY WITH THE LOCATION OF THE ÉLÉONORE MINE.....	4
FIGURE 2.2: MAP OF THE GEOLOGICAL PROVINCES OF QUEBEC SHOWING ACTIVE AND FUTURE MINING PROJECTS, IN ADDITION TO THE LOCATION OF THE ÉLÉONORE MINE.....	5
FIGURE 2.3: LITHOTECTONIC MAP OF THE JAMES BAY REGION.....	6
FIGURE 2.4: GEOLOGICAL MAP OF THE ÉLÉONORE PROPERTY	7
FIGURE 2.5: MAJOR GEOLOGICAL STRUCTURES FOUND AT THE ÉLÉONORE MINING SITE (DOMINGUE, 2017).	8
FIGURE 2.6: SURFACE AND UNDERGROUND INFRASTRUCTURE AT THE ÉLÉONORE SITE	11
FIGURE 2.7: MAP OF THE ÉLÉONORE SITE AND THE ROBERTO GOLD DEPOSIT.....	12
FIGURE 3.1: POTENTIAL GHPS SITES AT THE ÉLÉONORE MINE.....	17
FIGURE 3.2: PHYSICO-CHEMICAL AND MICROBIOLOGICAL ANALYSES CARRIED OUT WITH SAMPLES FROM THE ÉLÉONORE MINE.....	18
FIGURE 3.3: GEOTHERMAL HEAT PUMP SYSTEM DESIGNED FOR THE DEWATERING OUTLET AREA OF THE ÉLÉONORE MINE.	20
FIGURE 3.4: COEFFICIENT OF PERFORMANCE OF THE SELECTED HEAT PUMP.	23
FIGURE 3.5: THREE-DIMENSIONAL REPRESENTATION OF THE ÉLÉONORE MINE MODEL.....	28
FIGURE 3.6: HYDROSTRATIGRAPHIC UNITS INCLUDED IN THE HYDROGEOLOGICAL MODEL	30
FIGURE 3.7: TWO-DIMENSIONAL REPRESENTATION OF THE ÉLÉONORE MINE MODEL AND THE DEWATERING FLOW RATE FROM 2013 TO 2019	31
FIGURE 3.8: THREE-DIMENSIONAL REPRESENTATION OF THE MINE MODEL SHOWING THE INITIAL AND BOUNDARY CONDITIONS	33
FIGURE 3.9: OBSERVED AND SIMULATED TEMPERATURE OF WATER AT THE DEWATERING OUTLET ZONE.....	36
FIGURE 3.10: OBSERVED AND SIMULATED WATER LEVEL DRAWDOWN AT THE ÉLÉONORE MINE.....	36
FIGURE 3.11: OBSERVED VS SIMULATED HEADS.....	37
FIGURE 4.1: INITIAL ECONOMIC, ENVIRONMENTAL AND ENERGY BALANCE OF THE PROPANE BURNER SYSTEM USED TO HEAT THE UNDERGROUND WORKING OF THE ÉLÉONORE MINE.	40
FIGURE 4.2: ASSESSMENT OF INITIAL CONDITIONS AT THE ÉLÉONORE MINE.....	42
FIGURE 4.3: MAJOR ION CONCENTRATION.....	45

FIGURE 4.4: CALIBRATED AND PREDICTED DEWATERING FLOW RATES	54
FIGURE 4.5: PREDICTED HYDRAULIC HEADS AT THE ÉLÉONORE MINE IN 2031.....	55
FIGURE 4.6: PREDICTED WATER TEMPERATURE AT THE DEWATERING OUTLET ZONE.	56
FIGURE 4.7: SENSITIVITY OF THE CALIBRATED AND PREDICTIVE NUMERICAL MODEL OF THE ÉLÉONORE MINE.....	60
FIGURE 5.1: PIPER DIAGRAM OF THE ÉLÉONORE MINE WATER.....	64
FIGURE 5.2: SCHEMATIC DEPICTION OF THE GEOTHERMAL SYSTEM CONFIGURATION PROPOSED FOR THE ÉLÉONORE MINE.....	66
FIGURE 5.3: SIMULATED TEMPERATURE IN THE UNDERGROUND WORKINGS	71

LIST OF TABLES

TABLE 2.1: HYDROSTRATIGRAPHIC UNITS AT THE MINE SITE (GOLDER ASSOCIATES, 2009; DOMINGUE, 2017).....	9
TABLE 3.1: PHYSICAL AND THERMAL PROPERTIES OF THE ÉLÉONORE MINE MODEL.....	29
TABLE 3.2: MEAN ANNUAL DEWATERING FLOW RATE	32
TABLE 3.3: PHYSICAL AND THERMAL PROPERTIES OF THE ÉLÉONORE MINE AFTER MODEL CALIBRATION.....	35
TABLE 3.4: SENSITIVITY ANALYSIS SCENARIOS PERFORMED WITH THE ÉLÉONORE MINE MODEL.....	38
TABLE 4.1: EVOLUTION OF MINE WATER CHEMISTRY FROM THE DEWATERING OUTLET ZONE TO THE EMISSARY...	43
TABLE 4.2: SCALE AND CORROSION INDICES RESULTS.....	45
TABLE 4.3: SCALE AND CORROSION INDICES INTERPRETATION.....	46
TABLE 4.4: MONTHLY ENERGY PRODUCTION RATE AND PENETRATION LEVEL OF THE GHPs DESIGNED FOR THE DEWATERING OUTLET ZONE.....	48
TABLE 4.5: MONTHLY ENERGY PRODUCTION COSTS COMPARISON BETWEEN THE PROPANE-BASED SYSTEM AND A HYBRID (GEOTHERMAL-PROPANE) HEATING SYSTEM.....	49
TABLE 4.6: MONTHLY PROPANE CONSUMPTION AND CO ₂ EMISSIONS COMPARISON BETWEEN THE PRESENT PROPANE-BASED SYSTEM AND A HYBRID (GEOTHERMAL-PROPANE) HEATING SYSTEM.....	50
TABLE 4.7: THERMAL PROPERTIES OF ROCKS FROM THE ÉLÉONORE MINE.....	52
TABLE 4.8: MEAN ANNUAL DEWATERING FLOW RATE AT THE ÉLÉONORE MINE.....	54
TABLE 4.9: SIMULATED MEAN ANNUAL DEWATERING TEMPERATURES AT THE DEWATERING OUTLET ZONE OF THE ÉLÉONORE MINE.....	56
TABLE 4.10: MAXIMUM ENERGY OUTPUT OF THE PROPOSED GEOTHERMAL HEAT PUMP SYSTEM.....	58
TABLE 4.11: HEATING ENERGY AND POWER POTENTIAL	58
TABLE 5.1: STRENGTHS, WEAKNESSES, OPPORTUNITIES, AND THREATS (SWOT) ANALYSIS OF IMPLEMENTING A GEOTHERMAL HEAT PUMP SYSTEM AT THE ÉLÉONORE MINE.....	75

LIST OF ABBREVIATIONS

Nomenclature

$\Delta_c H^\circ$	enthalpy of combustion [L^2T^2]
A	active transfer surface in the intermediate heat exchanger [L^2]
a	distance between plates [L]
C	heat capacity rate [$L^2Mt^{-3}T^{-1}$]
c_p	specific heat capacity [$L^2T^{-1}t^{-2}$]
D	thermal dispersion term [L^2t^{-1}]
E	energy [L^2Mt^{-2}]
e	carbon footprint [ML^2Mt^{-2}]
E_{CO_2}	CO_2 emissions [M]
$f_{gas-liquid}$	gas to liquid propane conversion factor [-]
h	heat transfer coefficient [$Mt^{-3}T^{-1}$]
h_h	hydraulic head [L]
K	Hydraulic conductivity [Lt^{-1}]
k	thermal conductivity [$MLt^{-3}T^{-1}$]
L	plate length [L]
\dot{m}	mass flow rate [Mt^{-1}]
Pr	Prandlt number [-]
Q	power or heat extraction rate [ML^2t^{-3}]
q	Darcy flux in the subsurface [Lt^{-1}]
Q'	flow rate [L^3t^{-1}]
Re	Reynolds number [-]
Ss	specific storage [L^{-1}]
t	time [t]
T	temperature [T]
U	overall heat transfer coefficient [$Mt^{-3}T^{-1}$]
um	average fluid velocity [Lt^{-1}]

Symbols and Greek letters

Γ	Volumetric flux in the porous medium [$L^3L^{-2}t^{-1}$]
∇	Divergence [-]

ϵ	heat exchanger efficiency [%]
μ	dynamic viscosity [MLt^{-1}]
ρ	density [ML^{-3}]

Subscripts and Superscripts

air	air
b	bulk
ch	heating
clim	cooling
comp	compressor
eq	equilibrium
glycol	-
gw	groundwater
in	-
initial	-
k	Temperature in Kelvin
max	maximum
mes	measured
min	minimum
out	-
r	ratio
sat	saturated
setpoint	desired temperature
th	thermal
w	water or aqueous phase

Abbreviations

ASHRAE	American Society of Heating, Refrigeration and Air-Conditioning Engineers
CAD	Canadian dollars
CAPEX	Capital expenditure
COP	Coefficient of performance
EWT	Entering water temperature
GES	Gaz à effet de serre
GHPS	Geothermal Heat Pump System

GUSPM	Gallons U.S per minute
HGS	HydroGeoSphere
INRS	Institut national de la recherche scientifique
LSCI	Larson-Skold Corrosion Index
LSI	Langelier Saturation Index
MBBR	Moving Bed Biofilm Reactor
NSE	Nash-Sutcliffe Efficiency
NTU	Number of Transfer Units
OPEX	Operating expenses
PACG	Pompe à chaleur géothermique
PHX	Plate Heat Exchanger
PSI	Puckorius Scaling Index
RSI	Ryznar Stability Index
SWOT	Strengths, Weaknesses, Opportunities and Threats
TCS	Thermal Conductivity Scanner
WTP	Water Treatment Plant

1 INTRODUCTION

The mining industry is an important source of jobs and revenue. Mining companies in Canada contribute approximately \$ 72.0 billion to the gross domestic product (GDP) and \$ 2.2 billion is paid to the federal and provincial governments in taxes. It is the fourth largest industry in the country, surpassed only by the service, manufacturing and real estate industries. However, in Quebec, approximately 50% of the mines in operation are located in the territory defined by the Plan Nord, which is north of the 49th parallel, where infrastructure is limited or even non-existent. The electrical grid is often inaccessible and the climate is harsh (Ministry of Energy and Natural Resources, 2015). Consequently, additional expenses are incurred due to the consumption of electricity and fuel for heating, since it is sometimes necessary to heat the underground galleries in winter. In a northern context, the production costs of a mine can be between 2 and 2.5 times higher than a similar mine located at a lower latitude (Marshall, 2016). Nevertheless, it is not profitable to use electricity for heating, because the power demand of electrical systems is high and entails significant financial costs. On the other hand, the most commonly used renewable energy sources, such as wind and solar, are intermittent and cannot guarantee the continuous heating necessary to ensure the comfort and safety of miners. Mining companies must then use fossil fuels to meet their heating needs, but this involves a significant environmental impact.

The future of Canada's mining industry lies in remote and northern regions. It is relevant to take steps to introduce constant, ecological and affordable local energy alternatives to establish sustainable mining operations while increasing profitability. Extracting low enthalpy geothermal energy available from mines is a worthwhile alternative. A mine proves to be a favourable location for the installation of a geothermal system since significant water flows must be extracted to dewater the site and secure the operations. Additionally, wells and pumping systems that are already in place for the dewatering operations can be coupled to a geothermal heat pump system (GHPS). Furthermore, the depths involved are in the order of kilometres and temperatures are higher than at the surface. A geothermal system adapted to mining operations would extract energy from the groundwater or mining residues to heat the infrastructure of mining sites or nearby communities from a sustainable perspective (Raymond et al., 2008).

The source of energy available in the large volumes of water contained in flooded inactive mines has already been studied (Raymond and Therrien, 2014; Bailey et al., 2016; Loredo et al., 2016; Banks and al., 2017; Al-Habaibeh et al., 2018). This is presently not the case with active mines. Thus, the use of geothermal systems coupled to the dewatering systems already in place in active

mining operations is an interesting and innovative alternative to meet the high energy demands of mining operations located in northern environments, such as in northern Quebec (Raymond, 2010). The main objective of this study is, therefore, to assess the geothermal potential of an active mine located in a northern context in order to provide a techno-economic portrait of geothermal heat pump systems as a sustainable alternative to the heating needs of mining sites. The Eleonore mine of Newmont-Goldcorp, located in the Eeyou Istchee James Bay territory in northern Québec, is the subject of study. It is an active mine that currently uses a propane burner system to heat the underground workings during the coldest months of the year (personal communication, Goldcorp, 2017). Specifically, this project aims to assess the dewatering geothermal potential of an active mine by designing a heat pump system adapted to the dewatering system that is already in place. In such a system, the water exiting the dewatering system could be redirected to the heat pump to extract the thermal energy. The hypothesis put forward is that such a system requiring no drilling would offer a shorter payback period than a conventional GHPS, the installation of which requires significant costs related to drilling and the installation of the heat exchangers (Grasby et al., 2011). In this way, a geothermal system coupled with the dewatering operations would diversify the mine's energy sources and contribute to the heating energy needs. Such a system would minimize not only production costs but also the consumption of fossil fuels and greenhouse gas (GHG) emissions. The project also aims to assess the long-term sustainability of the geothermal resource in active mine by developing a hydrogeological numerical model that can estimate the amount of energy available throughout the life of the mine under varying dewatering flow rates and temperature conditions.

2 SITE BACKGROUND

2.1 Location and Climate

The Éléonore mine is a gold-mining project owned by Newmont Goldcorp, situated in Cree lands on the Eeyou Istchee James Bay Territory in Northern Québec. The mining site is located 825 km north of Montréal, 175 km east of James Bay's coast and 600 km west of Fermont (Figure 2.1). Matagami and Chibougamau are the nearest towns. These cities provide access to community, transportation and health services for many mine workers. Matagami can be reached by ground transportation, but flights from Montréal, Chibougamau and Val d'Or to the Éléonore airstrip are the primary means of conveyance for personnel (Charland, 2018).

In this region, the topography varies between 215 m and 300 m above sea level. The area is characterized by an abundance of lakes, swamps, rivers, and vegetation typical of taiga with sparse forests (Charland, 2018). A subarctic climate prevails throughout the sector, with a mean temperature reaching -18.5 °C during the winter and 13 °C through the summer — meanwhile, precipitation averages 710 mm annually (Natural Resources Canada, 2019a).

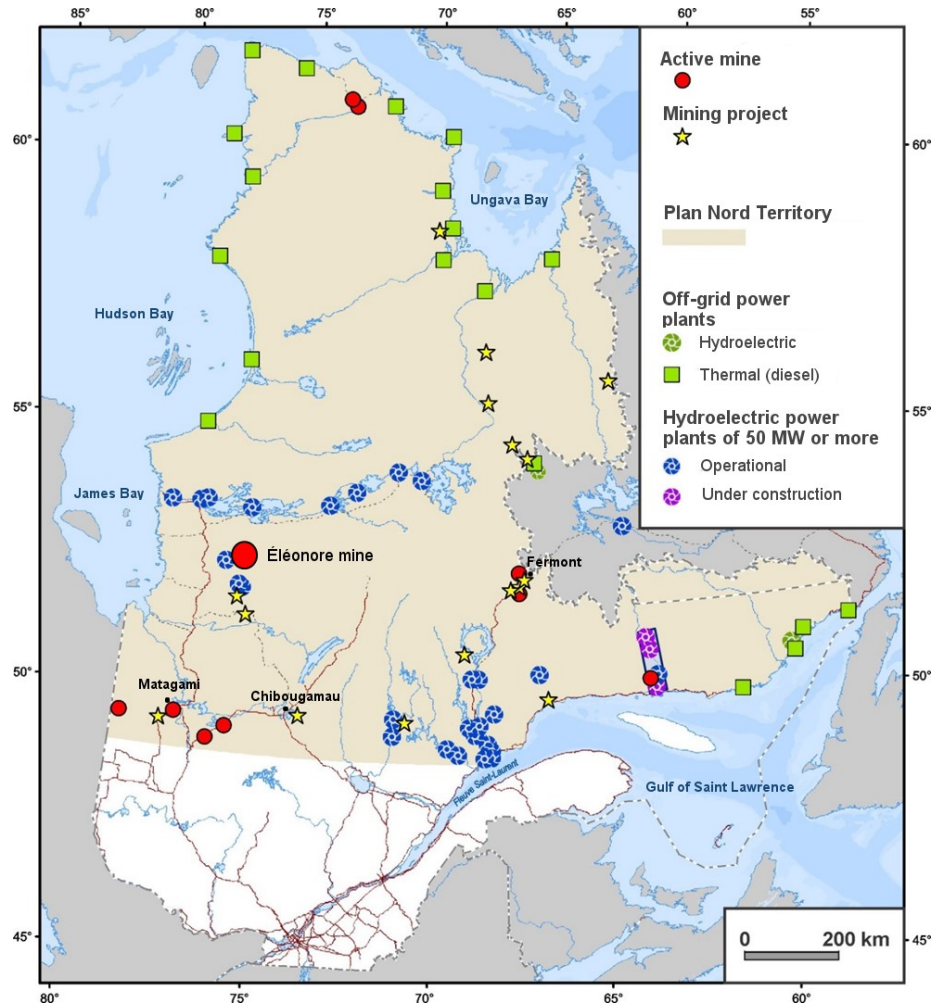


Figure 2.1: Map of mines in operation and electricity production in the Plan Nord territory with the location of the Éléonore mine (Modified from Ministère de l'Énergie et des Ressources naturelles (2015).

2.2 Geology

2.2.1 Regional Geology

The Éléonore mine is located in the Superior geological province of the Canadian Shield. The Superior Province is bordered to the south and southeast by the Grenville Province and to the north and east by the Churchill Province (Figure 2.2). It consists of Neo-Archaean rocks containing inclusions of Meso and Paleo-Archaean weathered rocks with an increasing regional metamorphic gradient. These rocks range from the greenschist to the granulite facies (Ravenelle, 2010; Fontaine et al., 2015).

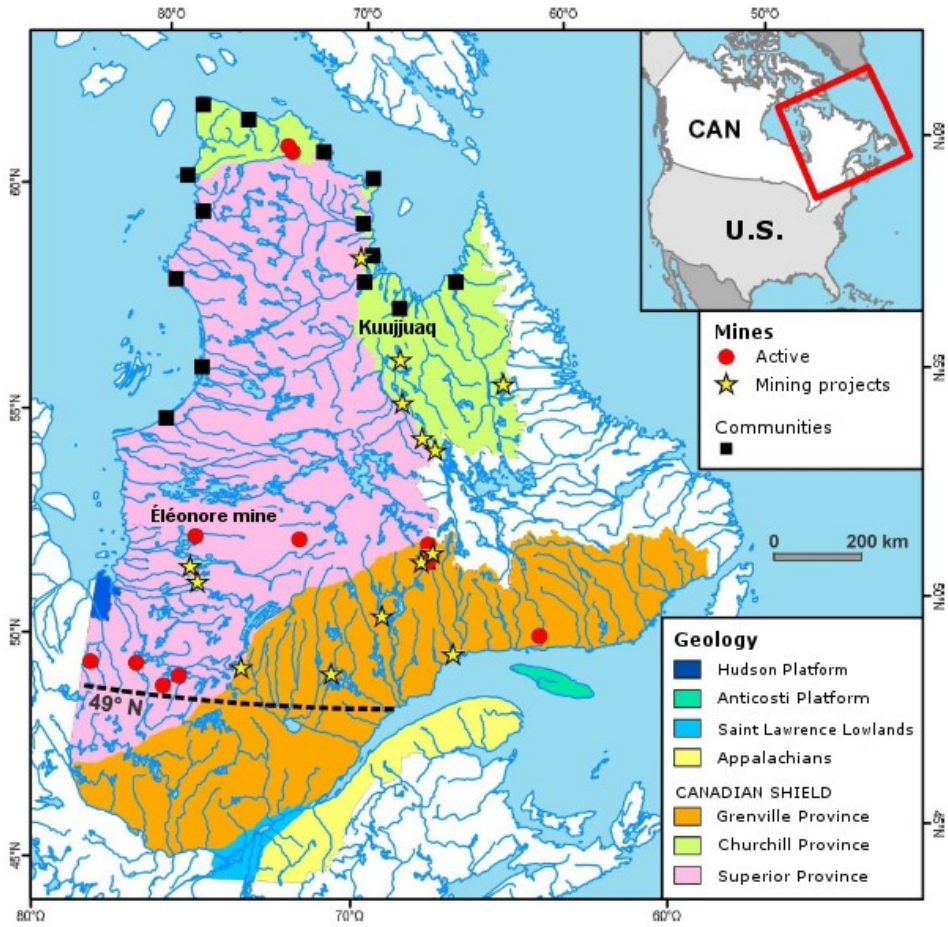


Figure 2.2: Map of the geological provinces of Quebec showing active and future mining projects, in addition to the location of the Éléonore mine (modified from Comeau (2017) and based on Ministère de l'Énergie et des Ressources naturelles (2012).

Specifically, the mine lies along the boundary between the La Grande and the Opinaca geological subprovince (Figure 2.3). The Opinaca subprovince is composed of migmatized metasedimentary granulitic rocks of approximately 2.663 and 2.637 Ga, in addition to several pegmatitic intrusions. The La Grande Subprovince, consisting of volcanic and metasedimentary rocks ranging from green shale to amphibolite, border the site to the north and the west. The La Grande province also exhibits numerous synvolcanic to late-tectonic tonalitic, granodioritic, pegmatitic and dioritic intrusions. The Roberto gold deposit is found between the contact of these two subprovinces (Ravenelle, 2010; Fontaine et al., 2015).

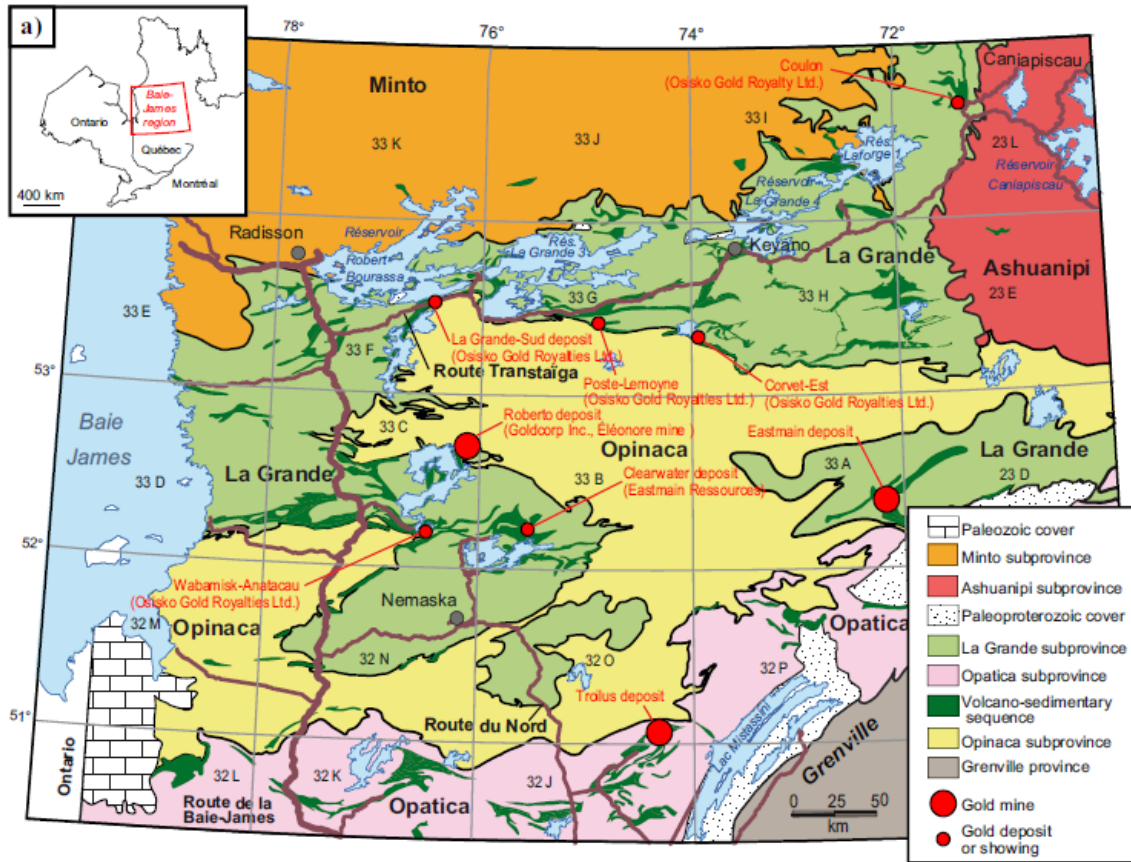


Figure 2.3: Lithotectonic map of the James Bay region (maps by Fontaine et al. (2015) based on Système d'information géominière of Québec (SIGEOM) data).

2.2.2 Local Geology

The Éléonore mine property is bounded to the south by the Opinaca intrusion and to the west by the Ell Lake intrusion, which contains several Au-Ag-Cu-Mo mineralizations (Fontaine et al., 2015). The Opinaca pluton is bordered to the east by a pillow-shaped lava flow and lapilli tuff covered by a polymictic conglomerate. The conglomerate layer forms the base of the Low formation. The upper and oldest section of the Low Formation is composed of massive greywacke (< 2.714 Ga) interbedded with aluminosilicate-bearing greywacke (< 2.697 Ga). The latter superposes a younger layer of finely bedded greywacke (2.675 Ga), interbedded with massive greywacke (Fontaine et al., 2015).

Goldcorp's gold mineralization at the Éléonore mine is hosted in the youngest layer of the Low Formation (Figure 2.4). The mineralization, reaching up to 1500 m in depth, originated from a hydrothermal system that produced a metasomatic replacement halo rich in potassium and magnesium. The mineralized area was also influenced by a distal replacement halo rich in calcium

(Ravenelle, 2010; Fontaine et al., 2015). The mineralized zones exist in the following forms: quartz-dravite-microcline-phlogopite vein stockwork, replacement zones containing microcline, phlogopite or dravite and quartz-diopside-schorl-arsenopyrite veins. Towards 2.616 Ga, numerous pegmatitic intrusions deformed and intersected the mineralized zone (Fontaine et al., 2015).

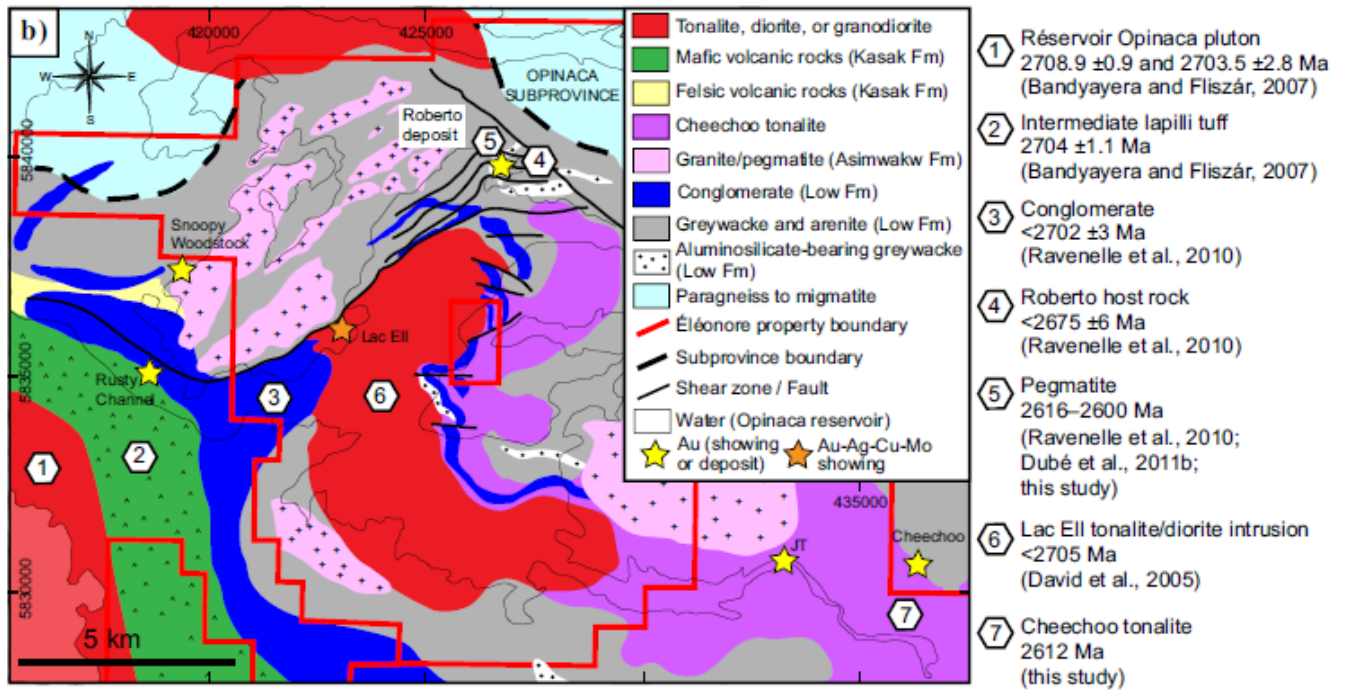


Figure 2.4: Geological map of the Éléonore property showing the location of the Roberto deposit, as well as the geochronological data illustrating the tectonometamorphic context and the magmatic events associated with the mineralization (Ravenelle, 2010; Bandyayera et al., 2010; Ravenelle, 2013; Fontaine et al., 2015). Fm = formation. Geographical coordinates: NAD83, UTM zone 18N.

2.2.3 Structural Features

Geotechnical studies carried out at the Éléonore mine point out the occurrence of several major structures. First, a set of highly permeable subhorizontal joints (*Shaft*) formed by isostatic rebound penetrates the primary lithologies. These structures slip slightly to the north and intersect the mine's vertical shafts. A significant NE sloping chloritic fault (*Rmp_fx01*) intersects the family of sub-horizontal joints to a depth of 650 m (Domingue, 2017; Charland, 2018). Furthermore, two NE-SW (*dx*) subvertical structures formed of diabase dykes, as well as five major subvertical (*Nw_fx*) NW-SE quartz-epidote breccia occur in the property. The width of some of these subvertical structures can reach up to one metre. Various minor subvertical and subhorizontal E-

O, NO-SE, and NE-SO oriented faults ($m0$) also intercept the underground workings. Figure 2.5 shows the entirety of the main geological structures present at the Éléonore mine.

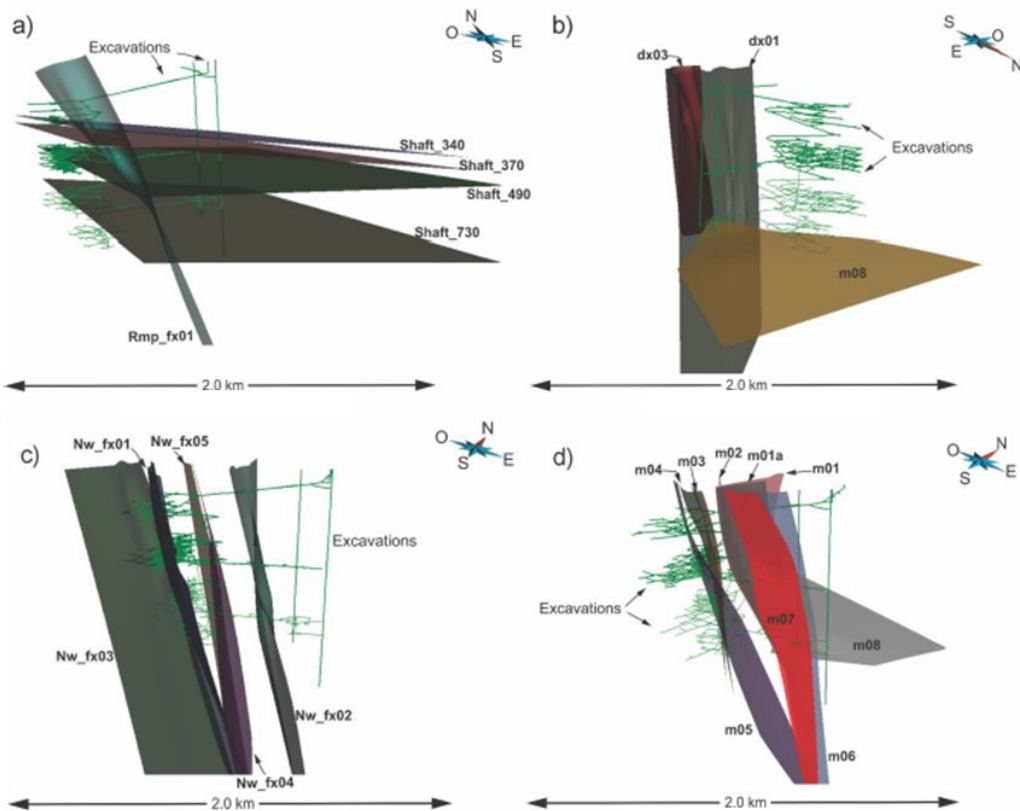


Figure 2.5: Major geological structures found at the Éléonore mining site (Domingue, 2017). Underground workings are shown in green. A) Rmp_fx01: NE sloping chloritic fault and Shaft: highly permeable sub horizontal structures intersecting the underground shafts. B) dx: NE-SW oriented subvertical structures formed of diabase dykes. C) Nw_fx: subvertical NW-SE oriented quartz-epidote breccia structures. D) m0: minor subvertical and subhorizontal E-O, NO-SE, and NE-SO oriented faults.

2.3 Hydrogeological Context

The underground workings of the Éléonore mine are located under part of the Opinaca Reservoir, which is a 1000 km² hydroelectric reservoir that contributes to the La Grande hydroelectric complex and acts as a focal point for the waters in the region (Domingue, 2017). In this area, the piezometric level is near the ground surface, which varies from 211 m to 247 m above sea level. A preliminary hydrogeological assessment of the site indicates a mean water level of 215 m above sea level and an annual groundwater recharge that varies from 80 mm to approximately 142 mm (Golder Associates, 2009; Domingue, 2017). As part of the same study, several pumping tests

done down to a depth of 360 m suggest the presence of five horizontal hydrostratigraphic units. Table 2.1 shows the properties of each unit.

Table 2.1: Hydrostratigraphic units at the Éléonore site (Golder Associates, 2009; Domingue, 2017)

Unit	Anisotropy	Hydraulic conductivity (m/s)	Specific storage (m ⁻¹)	Depth (m)
Shallow	K_x	3.0×10^{-5}		
	K_y	1.0×10^{-5}	2.0×10^{-7}	7 – 149
	K_z	1.5×10^{-6}		
Intermediate 1	$K_x = K_y = K_z$	1.0×10^{-6}	1.0×10^{-7}	150 – 299
Intermediate 2	$K_x = K_y = K_z$	6.4×10^{-8}	1.0×10^{-7}	300 – 359
Intermediate 1	$K_x = K_y = K_z$	1.0×10^{-6}	1.0×10^{-7}	360 – 499
Deep	$K_x = K_y = K_z$	1.0×10^{-8}	1.0×10^{-7}	500 – 2000

Properties of units below 360 m were extrapolated by performing numerical simulations.

The location of the mineral deposit beneath an area of the Opinaca reservoir compounded by the structural regime of the site contributes to the copious infiltration of water into the underground galleries. As of February 2018, water infiltration was in the order of 7200 m³/day, and the total process water consumption can reach 2650 m³/day. The current pumping system handles approximately 9850 m³/day. Two pumps were installed to manage the intensive pumping, one at 410 m and the other at 650 m below the surface. The pump at 410 m gathers the water above the 410 level, while the pump at level 650 collects water below 410 m and then sends it to level 410. Subsequently, water from level 410 circulates to the surface through the Gaumond production shaft. A new pump will be set up at level 1140 during work between levels 650 and 1190. The pump will send water flowing under level 650 to level 410 and then to the surface (Charland, 2018).

2.4 Energy Context

The Éléonore mine currently requires 37 MW of electricity per year. Presently, 62 % of the energy is consumed by the ore processing plant, 27 % by mining operations and 11 % by surface activities. Power consumption will reach 48 MW once the maximum extraction capacity of the mine is attained (Charland, 2018).

To meet their energy needs, Hydro-Québec's Eastmain power station, located 70 km south of the Éléonore site, supplies electricity through a 120 kV power line. The electricity distribution networks at the mine are designed to withstand the constraints imposed by the northern climate. Also, a 120/25 kV substation has been installed near the mine concentrator to avoid losses when the power demand is high (Charland, 2018). Notwithstanding, electrical heating systems have a high power demand. Therefore, a propane burner system provides the 37 MW of thermal power necessary annually to heat the underground workings.

2.5 Mine Plan and Future Works

Surface infrastructure on the Éléonore site includes a processing plant, waste storage facilities, fuel storage, distribution facilities, an industrial water treatment plant (WTP), a permanent camp with accommodation for 400 people, warehouse and garage facilities, an airstrip, and a concrete production plant (Figure 2.6). The underground mining-related infrastructure comprises a ventilation shaft, the production shaft, a shaft loading station, ore and waste passes and storage bins, a mine dewatering system, as well as a ramp that reaches 1130 m below the surface (Charland, 2018).

The underground mine is divided into two zones according to the location of the orebody. The upper mine located between 65 m and 650 m below the surface and the lower mine located between 650 m and 1370 m. Work started with the construction of two shafts, the production shaft, which currently reaches a depth of 1190 m, and the Gaumond ventilation shaft, which reaches a depth of 715 m. The construction of the main shafts continued by the mining at the 450 m and the 650 m levels. Work progressed from horizons 110 to 980. The totality of the orebody is currently divided into seven mining horizons, which are shown in Figure 2.6. The configuration and orientation of the underground workings are presented in Figure 2.7. Horizons 1 through 5 are presently being mined, and Horizons 6 and 7 will start production in late 2019 or early 2020. The production rate currently averages 5,000 t/d and is expected to reach 6,600 t/d in late 2019. According to actual production and estimated reserves, the mine is scheduled to be operational until 2026 (Charland, 2018).

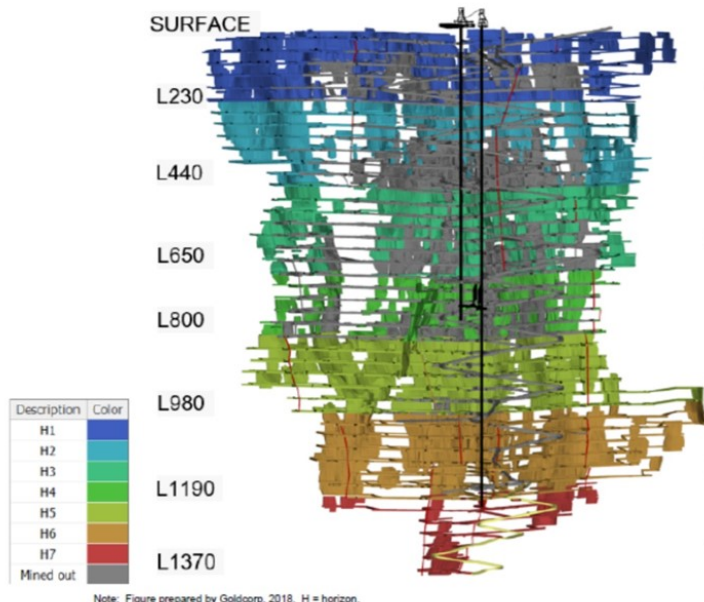


Figure 2.6: Surface and underground infrastructure at the Éléonore site . Areas that have been mined are shown in grey. Stope widths vary between 2.5 and 20 m, with an average length of 25 m, and can reach 30 m in height. Stopes are backfilled with paste fill. Paste mixture consists of 70% mill tailings, 25% sulphide concentrate, and 4–7% binder (Charland, 2018).

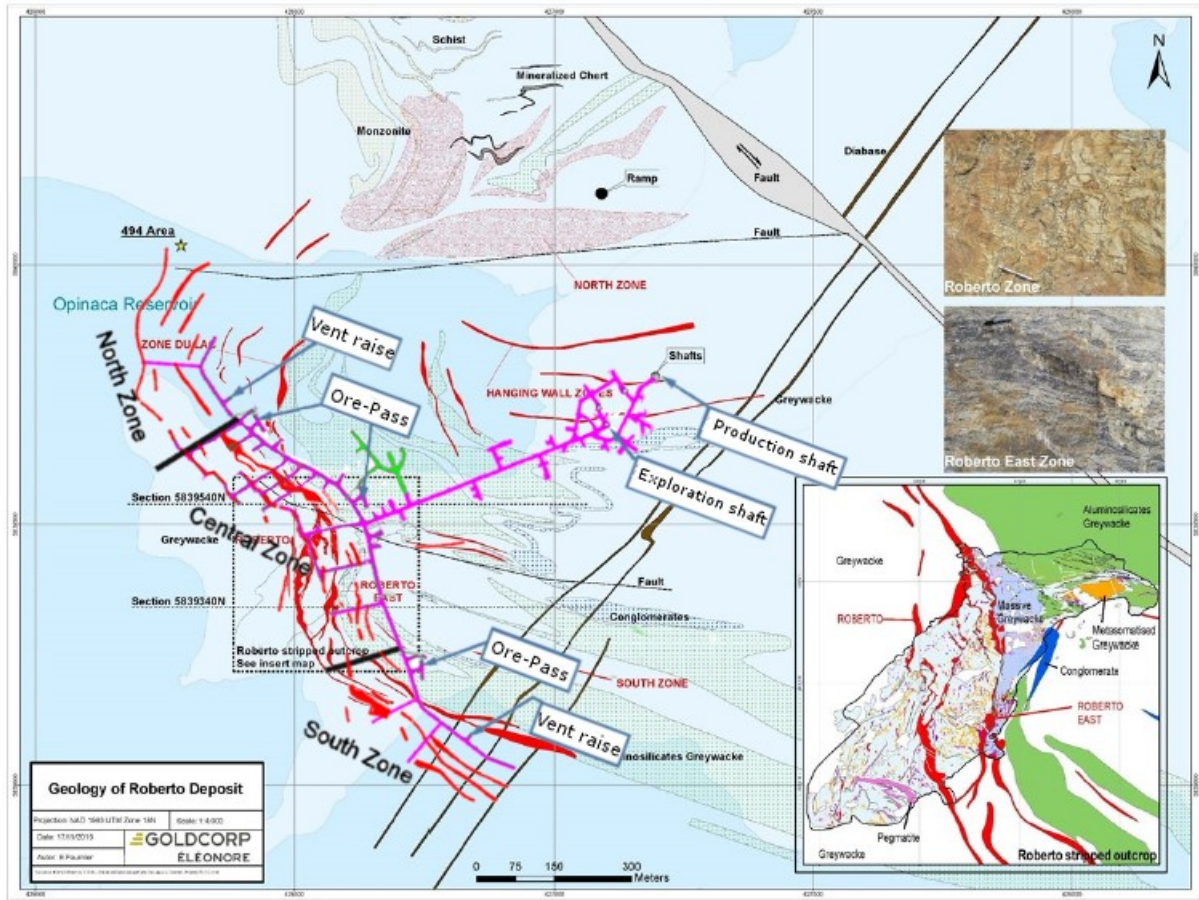


Figure 2.7: Map of the Éléonore site and the Roberto gold deposit. The mineralized zones are shown in red. The main underground workings at a depth of 650 m are shown in purple. A similar arrangement consisting of the main tunnel connecting the shafts to the Northern, Central and Southern mineralized zone is found at all other levels. Modified from Charland (2018). Geographical coordinates: NAD 1983 UTM Zone 18N.

2.6 Geothermal Setting

The thermal properties of rocks at the Éléonore site were evaluated by Levy et al. (2010). The thermal conductivity of the predominant lithology composed of massive greywacke is estimated to be $2.5 \text{ W m}^{-1} \text{ K}^{-1}$, with the Superior Province average being $3.4 \text{ W m}^{-1} \text{ K}^{-1}$ (Comeau, 2017). Subsequently, measurements from two boreholes estimate the subsurface heat flux at 31.3 mW m^{-2} , well below the 40 mW m^{-2} average of the Canadian Shield's Superior Province. The mean geothermal gradient is $0.0118 \text{ }^{\circ}\text{C m}^{-1}$ and heat generation is approximately 1.0 mW m^{-3} , exceeding the mean value of the region at 0.76 mW m^{-3} (Lévy et al., 2010; Majorowicz et Minea, 2015). Lastly, Comeau et al. (2017) used data available from the Éléonore site to calculate temperatures at depth by using a linearly decreasing relationship that characterizes heat production in the subsurface (Jessop, 1990). According to their results, a temperature of $8 \text{ }^{\circ}\text{C}$ is

expected at a depth of 500 metres. Meanwhile, a temperature of 15 °C and 27 °C are assumed at depths of 1000 and 2000 m, respectively. These properties will be used in the following chapters to assess the dewatering geothermal potential of the Éléonore site. The following chapter presents in detail the methodology used to design and evaluate the performance of a geothermal heat pump system adapted for the dewatering system of the mine, as well as the development of a hydrogeological numerical model used to assess the sustainability of the geothermal system.

3 METHODOLOGY

The evaluation of the geothermal potential of the Éléonore mine has two major components. The first is the design and adaptation of a geothermal heat pump system (GHPS) system for the dewatering system of the mine. This step entails determining the amount of energy needed to heat the underground workings, as well as the cost and the environmental impact incurred by the current propane burner system. Temperature and water flow data from potential sites have been collected and analyzed to assess the risk of corrosion and scaling. Furthermore, the thermal properties of rock samples from the main geological units at the Éléonore mine were also analyzed. The second component of the project involves the development of a hydrogeological numerical model to simulate the dewatering flow rate, drawdown and exiting water temperature to determine the sustainability of the geothermal resource. The following sections describe the methodology.

3.1 Design of the Geothermal Heat Pump System

3.1.1 Initial energy balance

To evaluate the geothermal potential of a site, first, it is crucial to determine the amount of energy needed to heat the underground workings of the mine, the costs incurred, as well as the environmental impact. The initial step was to calculate the monthly heating requirement using the propane consumption data provided by Newmont-Goldcorp as follows (Bergman et Incropera, 2011):

$$E = Q \times t \quad (3.1)$$

$$Q = [Q' \rho_{\text{air}} c_{\text{p,air}} (T_{\text{setpoint}} - T_{\text{initial}})]$$

Where:

E = energy consumed [kWh];

Q = power [kW];

Q' = airflow [$\text{m}^3 \cdot \text{s}^{-1}$];

$c_{\text{p,air}}$ = specific heat capacity of air [$\text{J} \text{ kg}^{-1} \text{K}^{-1}$] = 1.01

ρ_{air} = air density [$\text{kg} \cdot \text{m}^{-3}$];

T_{setpoint} = setpoint temperature [K] = 4°C;

T_{initial} = initial air temperature [K];

t = time [hours] = hours per day \times days in a month ;

Subsequently, the costs were determined with the following relationships:

$$Cost_{\text{total}} = consumption_{\text{propane}} \times price_{\text{propane}} \quad (3.2)$$

$$consumption_{\text{propane}} = \left[\left(\frac{Q \times t}{[\Delta_c H^0 \times \rho]} \right) \times f_{\text{gas-liquid}} \right]$$

Where:

$Cost_{\text{total}}$ = expenses [\$ CAD];

$consumption_{\text{propane}}$ = consumption in liquid [litres];

$price_{\text{propane}}$ = purchase price [\$/litre] + transportation price [0.0217\$/litre];

Q = power [kW or $MJ \cdot s^{-1}$];

t = time [s];

$\Delta_c H^0$ = enthalphy of combustion of propane [$MJ \cdot kg^{-1}$] = 46.3;

ρ = propane gas density [$kg \cdot m^{-3}$] = 1.83;

f = gas to liquid propane conversion factor = 0.003215

The monthly purchase and transportation cost of propane used to perform the above calculation was provided by the Éléonore mine. Finally, the environmental impact of the propane heating system was assessed by calculating CO₂ emissions as follows:

$$E_{\text{CO}_2} = E \times e_{\text{propane}} \quad (3.3)$$

Where:

E_{CO_2} = CO₂ emissions [kg or tonnes];

E = energy generated by the propane heating system [kWh];

e_{propane} = propane carbon footprint [$kg CO_2 \cdot kWh^{-1}$] = 0.21 (Koufos, 2012)

3.1.2 Site survey and selection

Two visits were conducted at the Éléonore mine to assess possible sites for the installation of a heat pump system. Four different locations were chosen along the industrial water treatment pathway, from the dewatering outlet area of the mine to the emissary (Figure 3.1). The purpose is to pinpoint the location with the highest flow rate and temperature, as well as the lowest risk of scaling and corrosion. The Éléonore mine operator provided water temperature and flow rate data. Additionally, rock samples from the main lithological units at the Éléonore site were analyzed to determine their thermal properties, which later aided in the development of the hydrogeological numerical model of the mine.

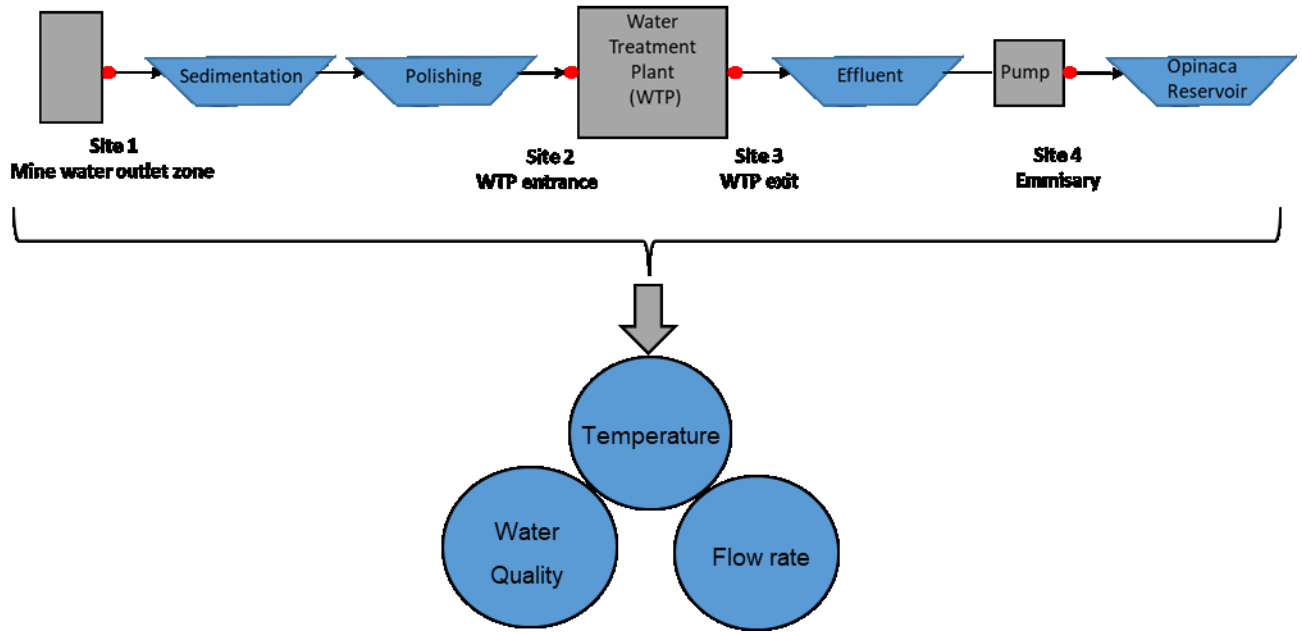


Figure 3.1: Potential GHPS sites at the Éléonore mine. The circles display the three parameters collected and studied at each site.

3.1.3 Flow and temperature

Groundwater flow and temperature have a marked influence on the performance of a GHPS and thus are critical parameters in the design process. An increase in groundwater flow enhances the performance of a heat pump, which corresponds to a higher coefficient of performance (COP). The increasing COP causes a decrease in power consumption resulting in financial savings. Nevertheless, an increase in groundwater flow represents an increase in pumping power. If the optimal flow rate is exceeded, the increase in pumping power will outweigh improvements in heat pump performance (Kavanaugh et Rafferty, 2014). It is, therefore, essential to determine the optimal entering groundwater flow. In the case of the Éléonore mine and other active mines, the dewatering system is already in place, and the flow rate is pre-established to prevent flooding of the underground workings. Since the entering groundwater flow cannot be modified, the ground-source heat pump (GHPS) was configured to handle the current dewatering system flow rate and its seasonal variations instead of determining the optimal flow and designing the system accordingly.

Groundwater temperature also has a significant effect on the efficiency of GHPS. Comparably to flow rate, higher entering water temperatures (EWT) improve system performance by increasing the COP, which results in savings and higher amounts of energy available for extraction

(Kavanaugh & Rafferty, 2014). Hence, a site with higher groundwater temperatures and flow rates is preferred.

3.1.4 Water Quality

A large number of impurities contained in water can hinder the performance of heat pump systems. For this reason, GHPs must be designed according to the quality of the water exiting the dewatering system of the mine. The purpose is to protect the system and the intermediate heat exchanger from corrosion and scaling, the most prevalent problems caused by water (Rafferty, 1999; Rafferty, 2004a; Kavanaugh et Rafferty, 2014; American Society of Heating et Air-Conditioning Engineers, 2015).

Four one-litre samples were collected from each of the four potential sites during the first visit to the mine. The samples were taken back to Québec City and analyzed at the *Institut national de la recherche scientifique* (INRS) laboratory for major and minor ions, as well as for total alkalinity and pH. From this data, total hardness and total dissolved solids were computed (Figure 3.2). Additionally, the mine provided hydrochemical data from 2014 to 2017 for the dewatering outlet zone and the emissary. Microbiological analyses were performed but were deemed invalid since samples must be analyzed no later than 24 hours after sampling. Due to the remoteness of the mine and the infrequent flight schedule, the samples could only be tested past the 24-hour limit.

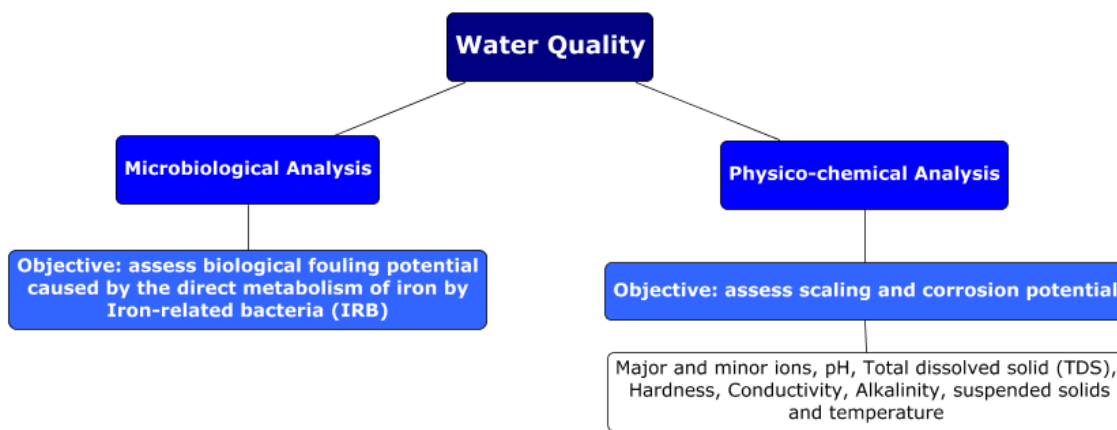


Figure 3.2: Physico-chemical and microbiological analyses carried out with samples from the Éléonore mine.

The results were used to calculate a series of stability indices that provide a quantitative prediction of water's corrosion and scaling potential. The Langelier, Ryznar, Puckorius and the Larson-Skold indices were chosen to assess water quality. The Langelier and Ryznar indices were initially

developed to determine the drinking water scaling potential by the precipitation of calcium carbonate (Langelier, 1936; Ryznar, 1944). They also serve to estimate the risk of corrosion. However, the Langelier and Ryznar indices do not take into account the buffer capacity of water and the maximum amount of deposits that can precipitate when water is at equilibrium (Puckorius et Brooke, 1991). Thus, the Puckorius saturation index was used since this method takes into account the capacity of water to regulate pH. Finally, the Larson-Skold index was utilized to evaluate the corrosion potential of water by employing the ratio between the concentration of chloride and sulphate to bicarbonate (Larson et Skold, 1958). Appendix I provides a detailed description of each index.

3.1.5 Geothermal Heat Pump System Design and Performance Assessment

The initial step is to design a heat pump system adapted to the conditions of the potential sites. Preliminary data provided by Newmont-Goldcorp suggested that the dewatering outlet zone (site 1) displays the highest average flow rate and temperature. Thus, a preliminary GHPS system was designed for this location with the assistance of Trane Inc. The GHPS system consists of three Multistack TRANE heat pumps to handle the mean flow rate of the dewatering system. Furthermore, the system contains an intermediate heat exchanger to prevent water from entering directly into the heat pump system. A plate heat exchanger (PHX) was chosen because of its high efficiency. The components of the plate heat exchanger can be made of type 304 and 316 stainless steel to protect the system against corrosion (Kavanaugh et Rafferty, 2014). The chosen heat transfer fluid is a standard aqueous solution of 30% propylene glycol. Although the volume of propylene glycol may vary, a concentration between 25 and 30% is recommended to prevent freezing, corrosion and bacterial growth (Dow Chemicals, 2009). Figure 3.3 shows the proposed system.

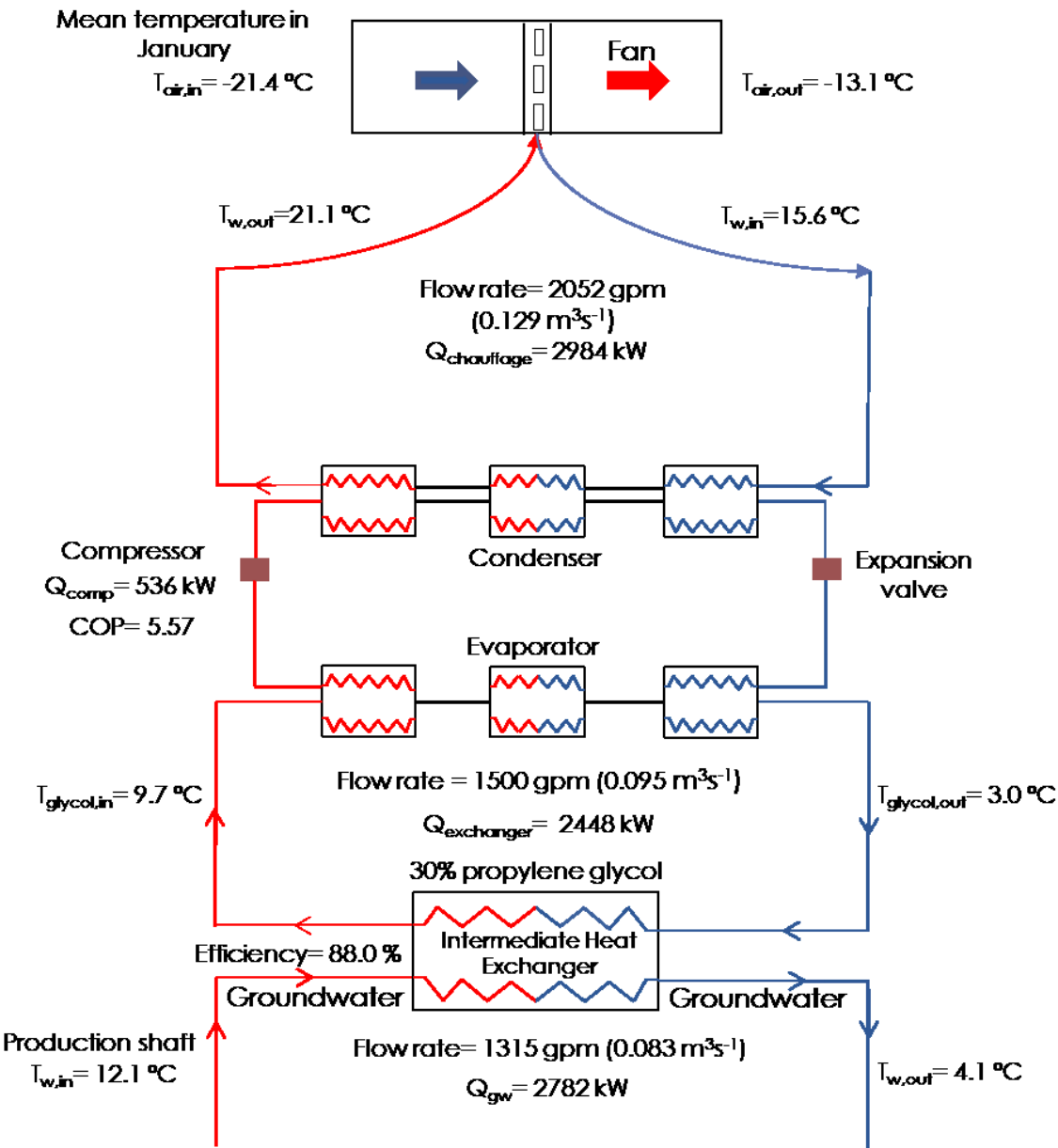


Figure 3.3: Geothermal heat pump system designed for the dewatering outlet area of the Éléonore mine. Values shown were calculated using average groundwater flow and temperatures.

The designed GHPS was used to determine the amount of energy generated throughout the year under varying conditions. The initial step was to calculate the energy content of the groundwater entering the system. Calculations were done for water at the outlet area of the dewatering system (site 1). Under average conditions, the water exiting the dewatering system enters the plate heat exchanger (PHX) at $12.1 \text{ }^{\circ}\text{C}$ and a flow rate of $0.083 \text{ m}^3 \text{s}^{-1}$ (1315 GUSPM). The water transfers the heat to the propylene glycol, entering the opposite side of the PHX at $3 \text{ }^{\circ}\text{C}$. The temperature of the heat-transfer fluid varies but was initially set to $3 \text{ }^{\circ}\text{C}$, knowing that the minimum desired

temperature of the water exiting the intermediate heat exchanger and into the polishing pond is 4 °C. The system, therefore, maintains a difference of 1.1 °C between the water exiting the PHX and the propylene glycol exiting the evaporator. The thermal power produced from the groundwater loop can be calculated with the following equation (Kavanaugh et Rafferty, 2014):

$$Q_{gw} = Q'_w \rho_w c_{p,w} (T_{w,in} - T_{w,out}) \quad (3.4)$$

Where:

Q_{gw} = heat extraction rate (groundwater loop) [W];

$c_{p,w}$ = specific heat capacity of water [$J \cdot kg^{-1} K^{-1}$] = 4190

Q'_w = groundwater flow rate [$m^3 \cdot s^{-1}$] = 0.083

ρ_w = water density [$kg \cdot m^{-3}$] = 999.8

$T_{w,in}$ = groundwater entering temperature [K] = 285.25

$T_{w,out}$ = groundwater leaving temperature [K] = 277.25

The thermal power transferred from the groundwater loop to the propylene glycol depends on the efficiency of the plate heat exchanger. Consequently, the efficiency of the PHX was determined by using equation 3.5 (Bergman et Incropera, 2011). Appendix II gives a complete description of each term in this expression.

$$\varepsilon = \frac{1 - \exp[-NTU(1 - C_r)]}{1 - C_r \exp[-NTU(1 - C_r)]} \quad (3.5)$$

Where:

ε = heat exchanger efficiency [%];

$NTU = \frac{U \times A}{C_{min}}$;

$C_r = C_{min}/C_{max}$

C_{min} = C_{glycol} or C_w , the lowest value;

C_{max} = C_{glycol} or C_w , the highest value;

C_{glycol} = heat capacity rate = $\dot{m}_{glycol} c_{p,glycol}$ [$W \cdot K^{-1}$];

C_w = heat capacity rate = $\dot{m}_w c_{p,w}$ [$W \cdot K^{-1}$];

The efficiency calculation indicates that the plate heat exchanger has an average efficiency of 88 %. It is, therefore, possible to determine the power transferred from the groundwater loop to the propylene glycol as follows (Bergman et Incropera, 2011):

$$Q_{exchanger} = \varepsilon \cdot Q_{gw} \quad (3.6)$$

$$Q_{gw} = Q'_w \rho_w c_{p,w} (T_{w,in} - T_{w,out})$$

Where:

$$Q_{\text{exchanger}} = \text{heat extraction rate (heat - carrier fluid loop)} [W]$$

$$Q_{\text{gw}} = \text{heat extraction rate (groundwater loop)} [W] = 2782$$

$$\varepsilon = \text{heat exchanger efficiency [\%]} = 88.0$$

$$c_{p,w} = \text{specific heat capacity of water} [J \cdot kg^{-1}K^{-1}] = 4190$$

$$Q'_{w} = \text{groundwater flow rate} [m^3 \cdot s^{-1}] = 0.083$$

$$\rho_w = \text{water density} [kg \cdot m^{-3}] = 999.8$$

$$T_{w,\text{in}} = \text{groundwater entering temperature} [K] = 285.25$$

$$T_{w,\text{out}} = \text{groundwater leaving temperature} [K] = 277.25$$

The thermal power produced from the propylene glycol loop is 2448 kW. Once the heat transfer between the mine water and the propylene glycol has occurred, the propylene glycol solution enters the evaporator at a pre-establish flow rate of $0.095 \text{ m}^3 \text{ s}^{-1}$ (1500 GUSPM). It returns to the plate heat exchanger at $3.0 \text{ }^\circ\text{C}$. However, it is necessary to determine the temperature of the propylene glycol entering the evaporator as follows (Bergman et Incropera, 2011):

$$T_{\text{glycol,in}} = \frac{Q_{\text{exchanger}}}{Q'_{\text{glycol}} \rho_{\text{glycol}} c_{p,\text{glycol}}} + T_{\text{glycol,out}} \quad (3.7)$$

Where:

$$Q_{\text{exchanger}} = \text{heat extraction rate (heat - transfer fluid loop)} [W] = 2448$$

$$c_{p,\text{glycol}} = \text{specific heat capacity} [J \cdot kg^{-1}K^{-1}] = 3713.7$$

$$Q'_{\text{glycol}} = \text{flow rate} [m^3 \cdot s^{-1}] = 0.095$$

$$\rho_{\text{glycol}} = \text{density} [kg \cdot m^{-3}] = 1037.5$$

$$T_{\text{glycol,in}} = \text{temperature of glycol entering the evaporator} [K] = 282.8$$

$$T_{\text{glycol,out}} = \text{temperature of glycol exiting the evaporator} [K] = 276.1$$

When the propylene glycol enters the evaporator, the heat is transferred to the refrigerant. The refrigerant circulates to a compressor to increase the pressure and, consequently, the temperature of the refrigerant gas. The electric power required by the compressor depends on the entering propylene glycol temperature and thus, the COP. Data provided by the manufacturer was used to determine the following relationship to estimate the COP for various entering temperatures (Figure 3.4):

$$T_{\text{glycol,in}} = 7.4958 \times COP - 31.86 \quad (3.8)$$

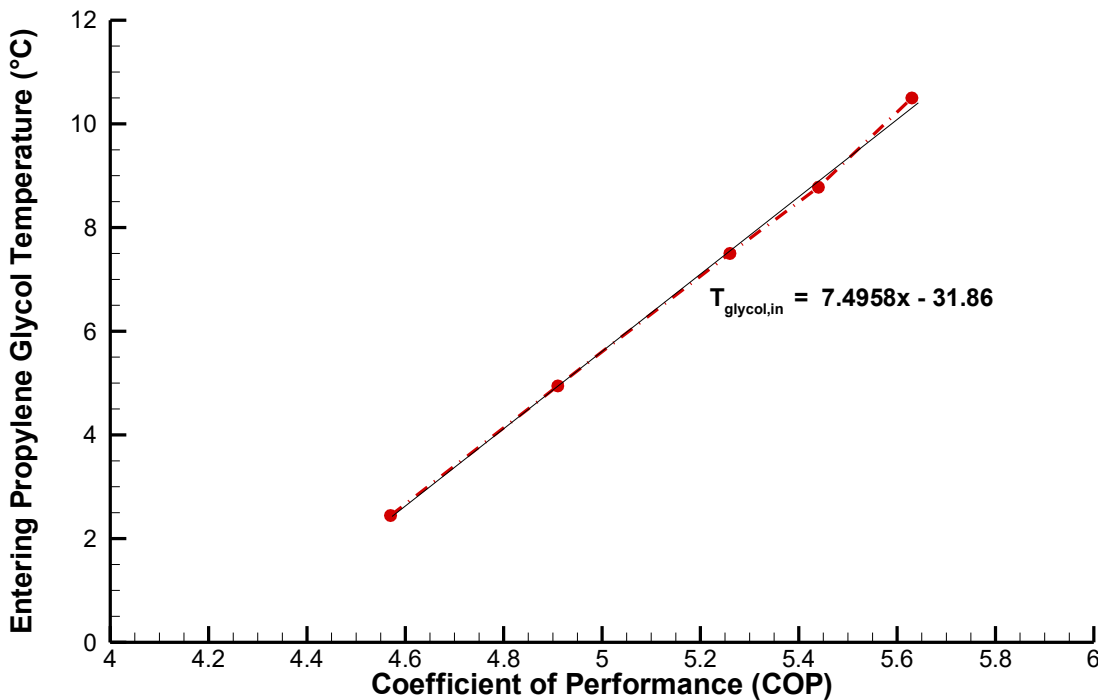


Figure 3.4: Coefficient of performance of the selected heat pump. The manufacturer TRANE supplied the performance data.

Thus, a propylene glycol entering the evaporator at 9.7 °C yields a COP of 5.57. With the COP and the thermal power produced from the propylene glycol loop, the electrical power needed by the compressor can be calculated as follows:

$$Q_{\text{comp}} = \frac{Q_{\text{exchanger}}}{COP - 1} \quad (3.9)$$

Where:

COP = coefficient of performance = 5.57

Q_{comp} = compressor power [W]

Finally, the refrigerant goes to the condenser at a pre-set flow rate of $0.129 \text{ m}^3 \text{s}^{-1}$ (2052 GUSPM) to heat the water circulating through the condenser loop to a temperature of 21.1 °C. The water is then directed to a water-to-air heat exchanger in the ventilation system to heat the mine.

Equation 3.10 gives the total power available to heat the mine:

$$Q_{\text{heating}} = Q_{\text{exchanger}} + Q_{\text{comp}} = 2984 \text{ kW} \quad (3.10)$$

With the thermal power produced by the heat pump, it is possible to determine either the water flow rate or the temperature difference inside the condenser loop with the following equation:

$$Q_{\text{heating}} = Q'_w \rho_w c_{p,w} (T_{w,\text{in}} - T_{w,\text{out}}) \quad (3.11)$$

$$Q'_w = \frac{Q_{\text{heating}}}{\rho_w c_{p,w} (T_{w,\text{in}} - T_{w,\text{out}})}$$

Where:

Q_{heating} = heating power [W];

Q'_w = water flow rate [$m^3 \cdot s^{-1}$];

$c_{p,w}$ = specific heat capacity of water [$J \ kg^{-1} K^{-1}$] = 4190

ρ_w = water density [$kg \cdot m^{-3}$] = 999.8

$T_{w,\text{in}}$ = temperature of water entering the condenser [K] = 288.75

$T_{w,\text{out}}$ = temperature of water exiting the condenser [K] = 294.25

The previous example calculations are all shown using average values from the dewatering outlet zone. The same method was employed to perform the calculations with the monthly groundwater flow and temperature data from each of the four sites. This approach enables the calculation of the amount of energy available throughout a year and the penetration levels of the geothermal system. A hydrogeological numerical model was subsequently developed to ascertain the amount of energy available and to assess the sustainability of the geothermal resource.

3.2 Numerical Model Development

The numerical model herein presented aims to assess present and future site conditions to quantify the amount of energy that can be produced with the geothermal heat pump system designed for the dewatering system of the Éléonore mine during the life of the mine, while evaluating the long-term sustainability of the system. HydroGeoSphere (HGS), which uses the control volume finite element method, was chosen to develop the three-dimensional hydrogeological model (Therrien et al., 2010). Transient simulations were performed over 18 years to simulate groundwater flow and heat transfer in the subsurface. The model was calibrated by replicating the water level drawdown caused by the dewatering of the mine and the temperature of the water exiting the dewatering system from 2013 to 2019. Predictive simulations were done from 2020 to 2031. Finally, the sensitivity of the model was assessed. The following sections provide an overview of the main steps involved in the development of the model.

3.2.1 Theoretical Approach and Governing Equations

To assess the sustainability of the geothermal resource, the groundwater flow and heat transport equations describing these physical phenomena are solved using numerical techniques through a numerical code or software. In the case of the Éléonore mine, a three-dimensional saturated transient groundwater flow model coupled with a heat transport model was developed. The governing equation describing transient subsurface flow in a three-dimensional saturated porous media with a hydraulic conductivity (K) and specific storage (S_s) is (Blessent, 2009):

$$\nabla(K_{ij}\nabla h) \pm \Gamma = S_s \frac{\partial h}{\partial t} \quad (3.12)$$

Where:

Γ = volumetric flux representing a source or a sink to the porous medium [$L^3 L^{-2} t^{-1}$]

K_{ij} = hydraulic conductivity tensor [$L \cdot t^{-1}$]

S_s = specific storage of the porous media [L^{-1}]

h = hydraulic head [L]

t = time [t]

Heat transfer by conduction, advection and mechanical dispersion in the porous medium is defined by:

$$-\nabla[q p_w c_w T - (k_b + c_b p_b D) \nabla T] \pm Q_{th} = [(\partial p_b c_b T) / \partial t] \quad (3.13)$$

Where:

ρ = density [$M \cdot L^{-3}$]
 c = heat capacity [$L^2 T^{-1} t^{-2}$]
 k = thermal conductivity [$LM t^{-3} T^{-1}$]
 T = temperature [T]
 t = time [t]
 q = Darcy flux in the subsurface [$L \cdot t^{-1}$]
 D = thermal dispersion term [$L^2 \cdot t^{-1}$]
 Q_{th} = thermal source or sink [$ML^2 t^{-3}$]
 b = bulk term
 w = aqueous phase

HydroGeoSphere, a numerical simulator capable of simulating fully or variably saturated surface and subsurface flow, as well as heat transport, was chosen to build the model and solve the governing equations (Therrien et al., 2010). To determine the numerical solutions, HGS employs the Control Volume Finite Element method (Therrien et Sudicky, 1996; Therrien et al., 2010). This method serves as a complement to the Finite Element technique by assigning a control volume to each of the nodes of the finite element grid used to discretize the model domain. The simulator then calculates the change in fluid mass inside each control volume (Blessent, 2009).

3.2.2 Modelling Strategy

The model was created in two steps. First, fully saturated transient groundwater flow and heat transport simulations were performed from 2013 to 2019, which is the six-year period spanning from the start of underground activities to present day. Groundwater level and temperature from these six years were used to calibrate the model. Posteriorly, conditions were simulated from 2020 to 2031. This period coincides with the estimated remaining life of the mine, namely from 2020 to 2026, plus five years for further developments. Lastly, a sensitivity analysis was performed to gain an improved insight into the system.

This model approximates the groundwater flow rate and heat transfer dynamics with a simplified system that captures the most important behaviours at the mine site (Voss, 2011). Various assumptions have been made to simplify the model. First, HydroGeoSphere assumes that the fluid is incompressible and that the porous medium is non-deformable. Furthermore, the simulations are performed under transient conditions in a fully saturated porous media. The model does not take into account variation in recharge. Thus, a mean value has been allocated to the surface. Water properties are constant, and convection caused by water density gradients are considered negligible (Raymond et Therrien, 2014). Moreover, the information provided by the mine suggests that approximately 95 % of the host rock is composed of massive greywacke, and

approximately 3 % is massive aluminosilicate-bearing greywacke. Based on this information, thermal properties assigned to the numerical model correspond to those of the massive greywacke. Finally, all hydrostratigraphic units are deemed horizontal, and fractures in the model site are represented as equivalent porous media due to the scale of the model.

3.2.3 Conceptual Model

The primary underground geological structures of the mine extend 2 km in the x -direction, 2.5 km in the y -direction and 2.0 km in depth (Domingue, 2017). The production shaft of the mine, located at the centre of the domain at 5839797N and 427179E, reaches a depth of 1190 m. From the production shaft, the main underground horizons extend approximately 690 m in the SW-NE direction. To enclose the main underground structures and to avoid undesirable boundary effects, the three-dimensional model of the Éléonore spreads 10 km in the x - and y - directions and reaches a depth of 2 km. The subsurface of the model is divided into five hydrostratigraphic units described in section 2.3. Thermal properties assigned correspond to the predominant geological unit, the massive greywacke.

The model domain was discretized using the interactive block grid instruction in HydroGeoSphere. This function generates a mesh made up of variably sized hexahedrons, which can be graded in each of the three main directions (Therrien et al., 2010). In the present study, the mesh has a discretization of 100 m to 200 m in the x , y and z -direction. However, the grid was refined near the underground workings, the production well, and the surface. From 4,300 m to 5,200 m in the x -direction and from 4,300 m to 5,700 m in the y -direction, elements vary in size from 20 m to 40 m. From the surface to 100 m below the surface (2,000 m to 1,900 m), element size is 10 m. In total, the domain is composed of 181,270 nodes and 171,216 elements (Figure 3.5).

Finally, the model uses an adaptive time step with an initial time step of 100 s, a maximal time step of 1.0×10^7 s and a time step increasing factor of 5.0. The maximum hydraulic head change per time step is 5 m, whereas the maximum temperature change is 3 °C. Three-dimensional finite elements were used to discretize the porous media, and one-dimensional linear elements were used for wells and tunnels.

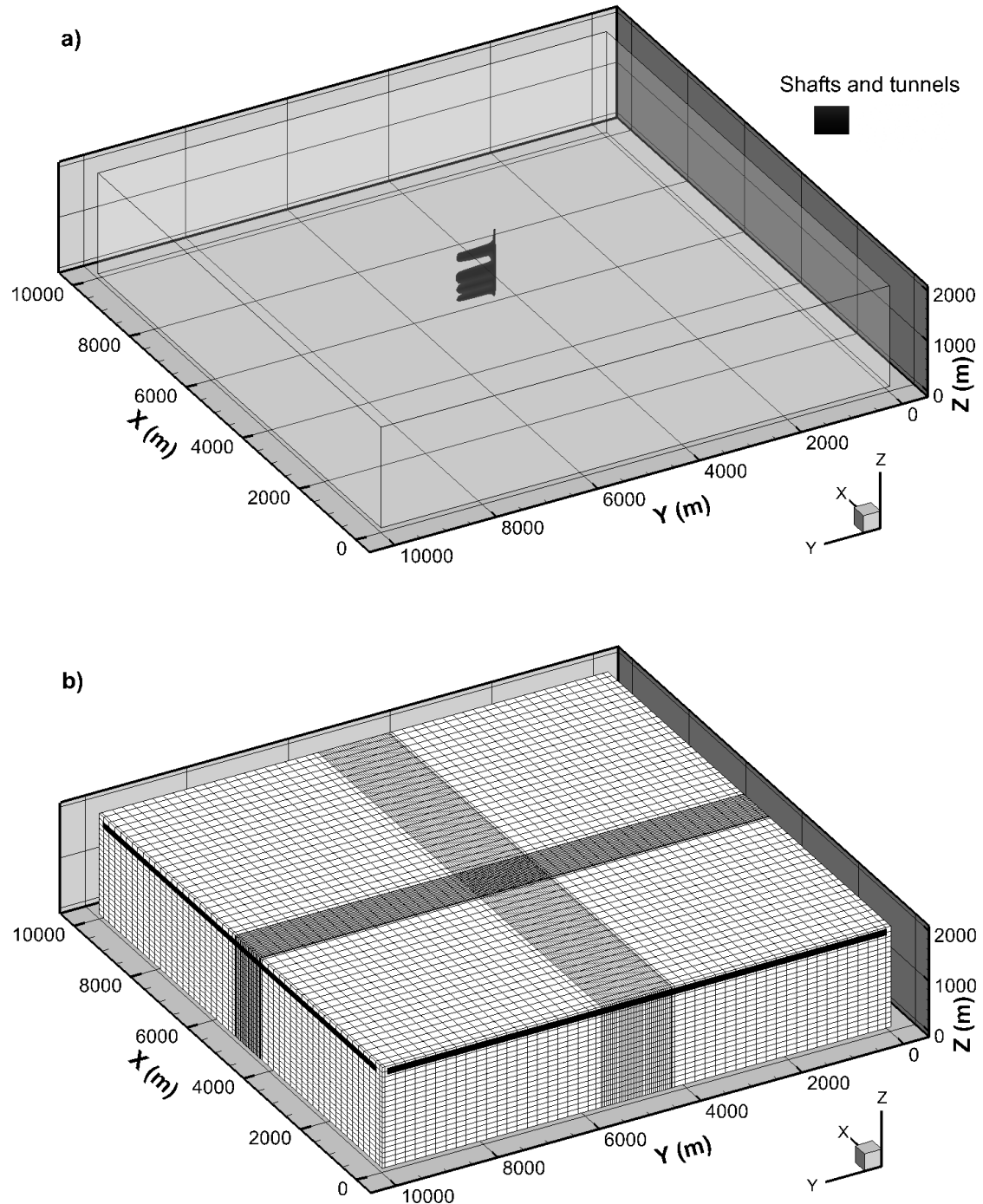


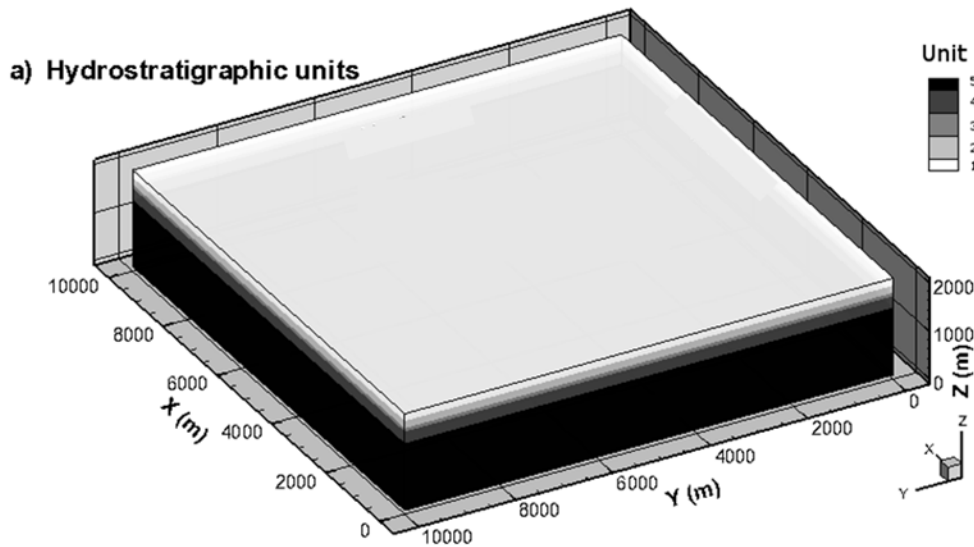
Figure 3.5: Three-dimensional representation of the Éléonore mine model showing a) the model geometry and the main underground workings. The production shaft is located at 5839797N and 427179E (NAD83, UTM zone 18N; b) The finite element mesh used to discretize the model domain.

3.2.3.1 Physical and Thermal Properties

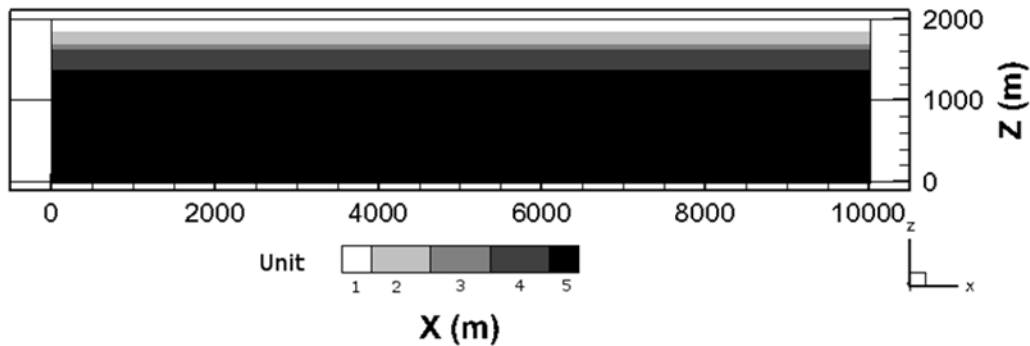
Thermal properties essential for heat transport modelling, including thermal conductivity and thermal diffusivity, were collected from rock samples analyzed at the *Laboratoire Ouvert de Géothermie* (LOG: <http://log.ete.inrs.ca/>). A total of 43 rock samples were examined twice each, parallel and perpendicular to foliation. Samples were left at room temperature 24 hours prior to analysis with a Thermal Conductivity Scanner (TCS) from Lippmann Geophysikalische Messgeräte. The analysis was performed in the Thermal Conductivity + Thermal Diffusivity mode, which possesses an accuracy of 5 %. Heat capacity was later determined by dividing the thermal conductivity by the thermal diffusivity. The remaining model properties were obtained from the literature. Table 3.1 summarizes the fundamental properties of the five units included in the model. Figure 3.6 shows the hydrostratigraphic units included in the model. Values were later modified to calibrate the model as well as to assess parameter sensitivity.

Table 3.1: Physical and thermal properties of the Éléonore mine model.

Parameter	Value	Unit	Reference
Hydraulic properties			
Hydraulic conductivity (x,y,z when specified)	Unit 1: 3.0×10^{-5} , 1.0×10^{-5} , 1.5×10^{-6} Unit 2: 1.0×10^{-6} Unit 3: 6.4×10^{-8} Unit 4: 1.0×10^{-6} Unit 5: 1.0×10^{-8}	m s^{-1} m s^{-1} m s^{-1} m s^{-1} m s^{-1}	(Golder Associates, 2009; Domingue, 2017)
Porosity	0.01		Mielke et al. (2016)
Longitudinal dispersivity	5.0	m	
Transversal dispersivity	0.5	m	Therrien et al. (2010)
Vertical dispersivity	0.05	m	
Tortuosity	0.1		
Specific storage	Unit 1: 2.0×10^{-7} Unit 2: 1.0×10^{-7} Unit 3: 1.0×10^{-7} Unit 4: 1.0×10^{-7} Unit 5: 1.0×10^{-7}	m^{-1} m^{-1} m^{-1} m^{-1} m^{-1}	(Golder Associates, 2009; Domingue, 2017)
Water density	1000	kg m^{-3}	Therrien et al. (2010)
Rock density	2640	kg m^{-3}	Mielke et al. (2016)
Thermal properties			
Thermal conductivity of rocks	2.54	$\text{W m}^{-1} \text{K}^{-1}$	Laboratory analysis
Thermal conductivity of water	0.59	$\text{W m}^{-1} \text{K}^{-1}$	Dinçer and Zamfirescu (2016)
Heat capacity of rocks	909	$\text{J kg}^{-1}\text{K}^{-1}$	Laboratory analysis
Heat capacity of water	4186	$\text{J kg}^{-1}\text{K}^{-1}$	Dinçer and Zamfirescu (2016)



b) Hydrostratigraphic units in two dimensions



c) Hydraulic conductivity

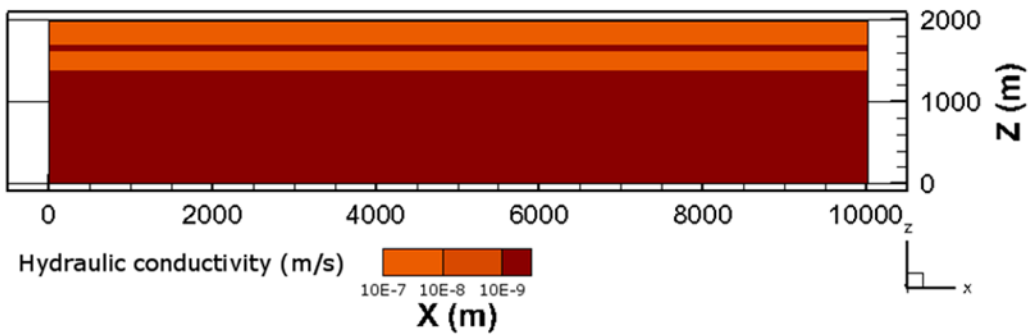


Figure 3.6: Hydrostratigraphic units included in the hydrogeological model shown in a) three dimensions and b) two dimensions. Figure c) displays the initial hydraulic conductivity of the model domain.

3.2.3.2 Dewatering system and flow rate

Four pumping stations were set up along the production shaft. The first pump is located at the 400 m level, followed by a pump at the 650 m level, one at 830 m and another at the 1140 m horizon (Figure 3.7 a). According to information provided by Goldcorp, the topmost pump is responsible for approximately 60 % of the annual dewatering flow rate, the following pump constitutes about 17%, and the two deepest stations pump the remaining 23 %. The Éléonore mine provided the dewatering flow rate for 2015 and 2016. The available data was used to perform a linear regression to forecast the mean annual dewatering flow rate for the calibration period, from 2013 to 2019 (Figure 3.7 b). The mean dewatering flow rate values for each year are given in Table 3.2.

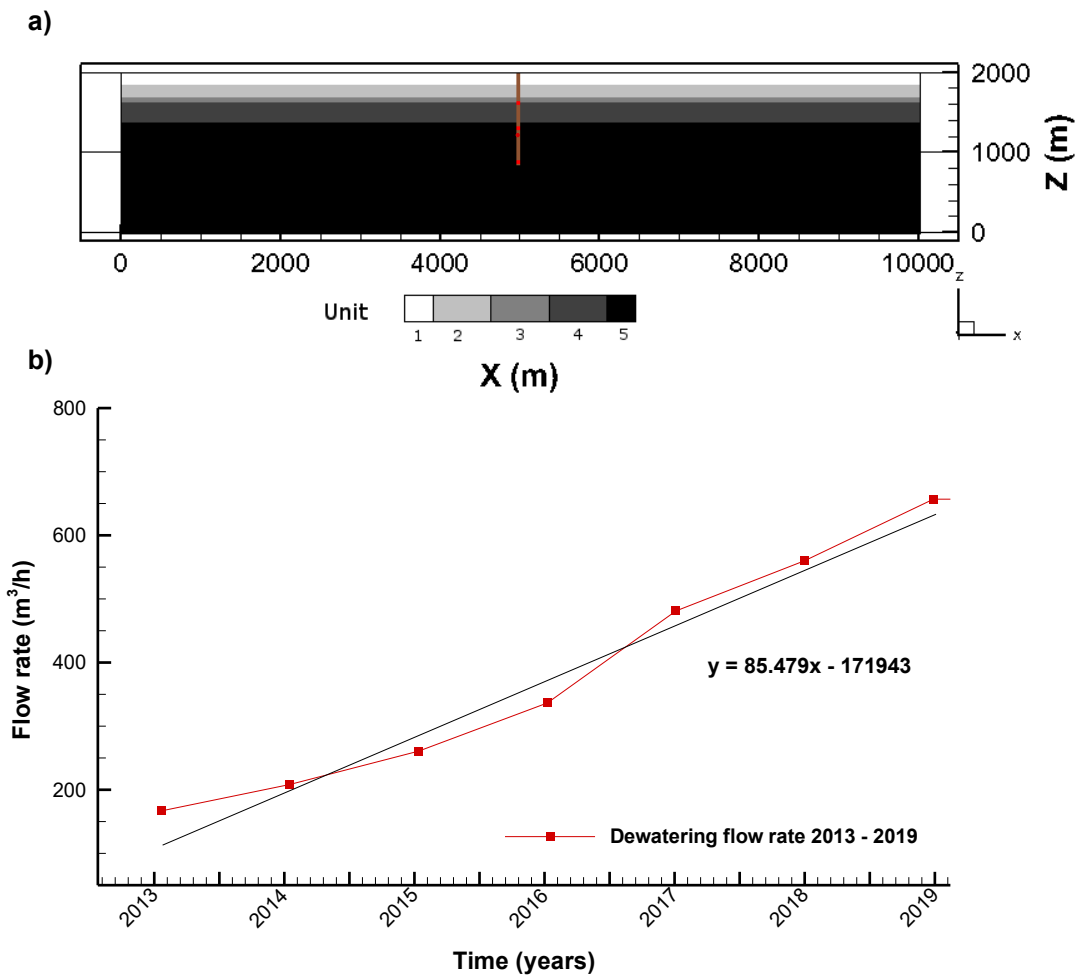


Figure 3.7: a) Two-dimensional representation of the Éléonore mine model showing the production shaft in brown and the pumping stations in red. b) Dewatering flow rate from 2013 to 2019. The 2015 and 2016 values are the observed values. The remaining values were estimated according to the mine's projections.

Table 3.2: Mean annual dewatering flow rate

Year	Flow rate (m^3h^{-1})
2013	166.8
2014	208.5
2015	260.9
2016	336.5
2017	481.1
2018	560.1
2019	656.8

3.2.3.3 Initial and Boundary Conditions

A Type-2 boundary condition, which corresponds to a mean local recharge of 80 mm y^{-1} was assigned to the surface of the domain. Flow at the base of the model is inferred negligible due to the minimally fractured nature of the host rock at this depth. Thus, the base of the model is considered impermeable. Since the water table is assumed to be free to move and follows the topography of the region closely, the system is considered saturated. For this reason, an initial hydraulic head of 2000 m was assigned to all the nodes in the model domain, and all the vertical boundaries of the system were imposed a hydraulic head equal to the surface elevation. Heat transfer in the subsurface was simulated after groundwater flow calibration. For the heat transfer simulation, all nodes were assigned an initial temperature specified by an imposed geothermal gradient of $0.0118 \text{ }^\circ\text{C m}^{-1}$. Vertical boundaries are considered adiabatic. The surface of the model has been attributed a constant temperature of $2.0 \text{ }^\circ\text{C}$, and a heat flux of 0.031 W m^{-2} is imposed at the base of the model. All boundary and initial conditions of the model are shown in Figure 3.8.

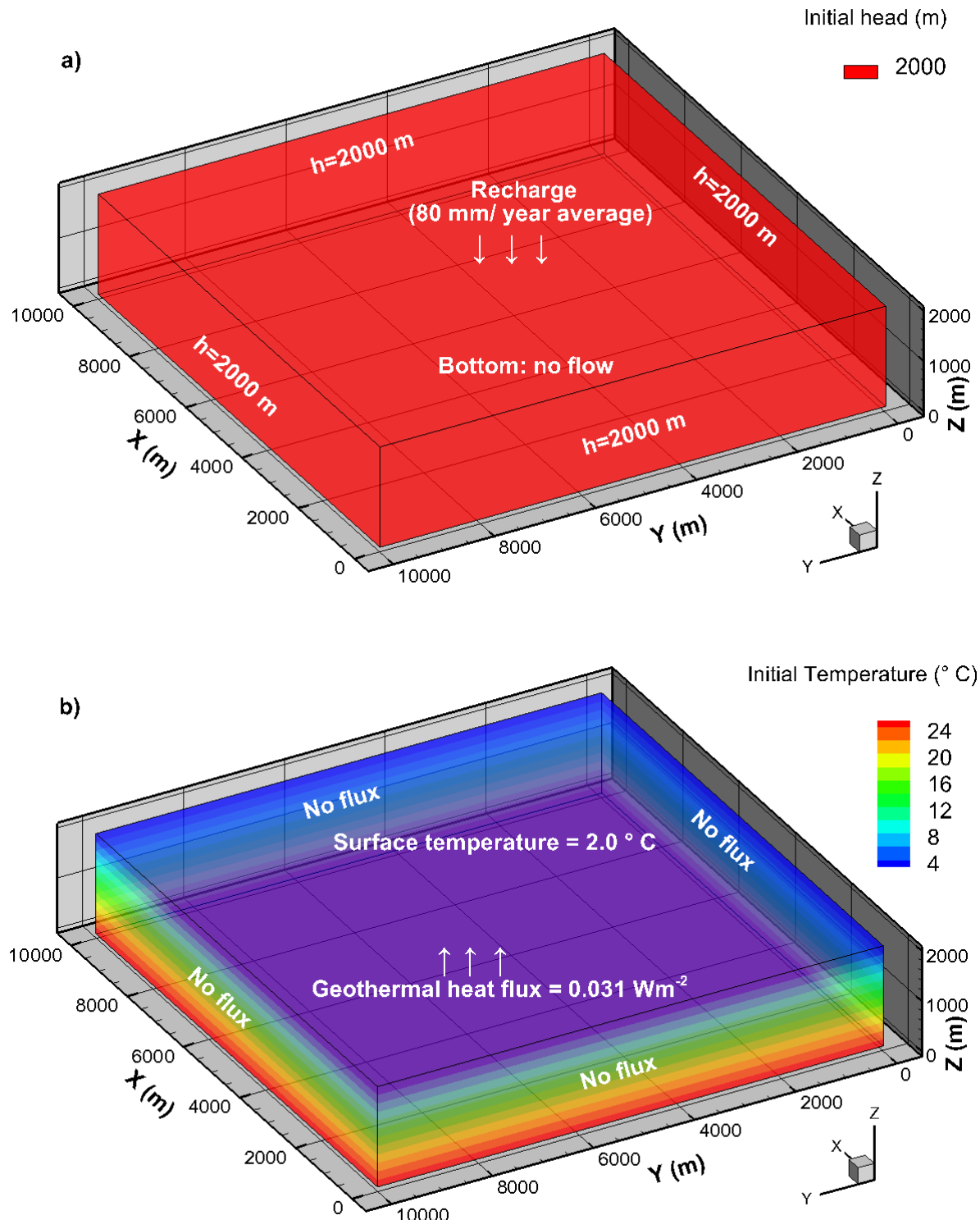


Figure 3.8: Three-dimensional representation of the mine model showing a) groundwater flow boundary and initial conditions and b) heat transport boundary and initial conditions used for the transient simulations.

3.2.4 Model Calibration

Calibration of the model aims to reproduce the observed water level drawdown generated by the dewatering of the Éléonore mine as well as the temperature of the water exiting the dewatering system. The calibration period is from 2013 to 2019. Newmont-Goldcorp provided dewatering temperatures. The drawdown was estimated by assuming that the water level corresponds to the date of construction of the primary underground levels. The initial physical and thermal parameters of the fully saturated coupled groundwater flow and heat transfer model were modified manually to fit the observed groundwater and temperature data. Table 3.3 provides the parameters that lead to the best representation of the modelled system. Only hydraulic conductivity and specific storage values are shown since the rest of the calibration parameters were not modified as their influence was found to be minimal. Values of hydraulic conductivity and specific storage utilized are lower than those reported by Golder Associates (2009) and tend towards values used to calibrate a flow model of the Éléonore mine previously developed by Domingue (2019).

Water exiting the dewatering outlet zone is exposed to atmospheric conditions and is a mix of waters coming from various depths, which create temperature fluctuations that cannot be replicated precisely (Figure 3.9). However, data from 2016 and 2017 indicate that at the dewatering outlet zone, water has a mean temperature of 12.1 °C. Therefore, the model created for this study aims to approximate the mean temperature at the dewatering outlet. Since the model solely provides underground temperatures, where surface conditions have minimal influence, the average temperature and flow rates at each pumping level were used to calculate the final temperature at the dewatering outlet zone after mixing. Calibration results indicate that during the initial year of dewatering, the mean temperature is lower since water is pumped exclusively from the 400 level. The overall temperature of pumped water increased, once deeper pumping stations were established. Aside from the initial year, simulated water temperatures at the dewatering outlet zone maintain an average temperature of 12.1 °C, which coincides with the mean of the observed data (Figure 3.9).

Moreover, total drawdown since the start of the dewatering is estimated at 1190 m, which corresponds to the deepest underground horizon. Nevertheless, data before the construction of the first horizon at 400 m in 2013 is not available. Thus, drawdown data and total time elapsed from the initial water level, at or near the surface, to the 400 m level is unknown. Therefore, although the total drawdown is 1,190 m, the drawdown spanning from the construction of the 400 m horizon in 2013 to present-day is 790 m. The calibration target of the conceived model is

the overall drawdown from 2013 to 2019. The simulated drawdown is displayed in Figure 3.10. Simulated heads reproduce the initial and final observed heads, but overestimate the hydraulic heads throughout most of the six years.

The simulated heads were compared to the observed heads obtained from a linear regression to evaluate the quality of the calibration (Figure 3.11). Computed heads show a root mean square error of 102 m, a mean absolute error of 89 m, a maximum absolute error of 158 m, and a mean absolute percentage error of 7 %. The Nash-Sutcliffe model efficiency coefficient (NSE), which is used to evaluate the efficiency of a model to make predictions and ranges from 0 to 1, is 0.9. A high NSE and a mean absolute error below 10% suggest that the model provides an adequate representation of the system at the Éléonore mine. The model was posteriorly used to perform a sensitivity analysis and to predict conditions to determine the amount of energy available in the future life of the mine.

Table 3.3: Physical and thermal properties of the Éléonore mine after model calibration.

Parameter	Initial value	Calibrated Value
Hydraulic conductivity (x,y,z when specified) (m s^{-1})	Unit 1: 3.0×10^{-5} , 1.0×10^{-5} , 1.5×10^{-6} Unit 2: 1.0×10^{-6} Unit 3: 6.4×10^{-8} Unit 4: 1.0×10^{-6} Unit 5: 1.0×10^{-8}	Unit 1: 1.0×10^{-7} , 1.0×10^{-7} , 1.0×10^{-5} Unit 2: 1.0×10^{-9} , 1.0×10^{-8} , 1.0×10^{-5} Unit 3: 1.0×10^{-9} , 1.0×10^{-8} , 1.0×10^{-7} Unit 4: 1.0×10^{-9} , 1.0×10^{-8} , 1.0×10^{-5} Unit 5: 7.5×10^{-8} , 7.5×10^{-8} , 9.1×10^{-8}
Specific Storage (m^{-1})	Unit 1: 2.0×10^{-7} Unit 2: 1.0×10^{-7} Unit 3: 1.0×10^{-7} Unit 4: 1.0×10^{-7} Unit 5: 1.0×10^{-7}	Unit 1: 1.0×10^{-8} Unit 2: 1.0×10^{-8} Unit 3: 1.0×10^{-8} Unit 4: 1.0×10^{-8} Unit 5: 9.0×10^{-8}

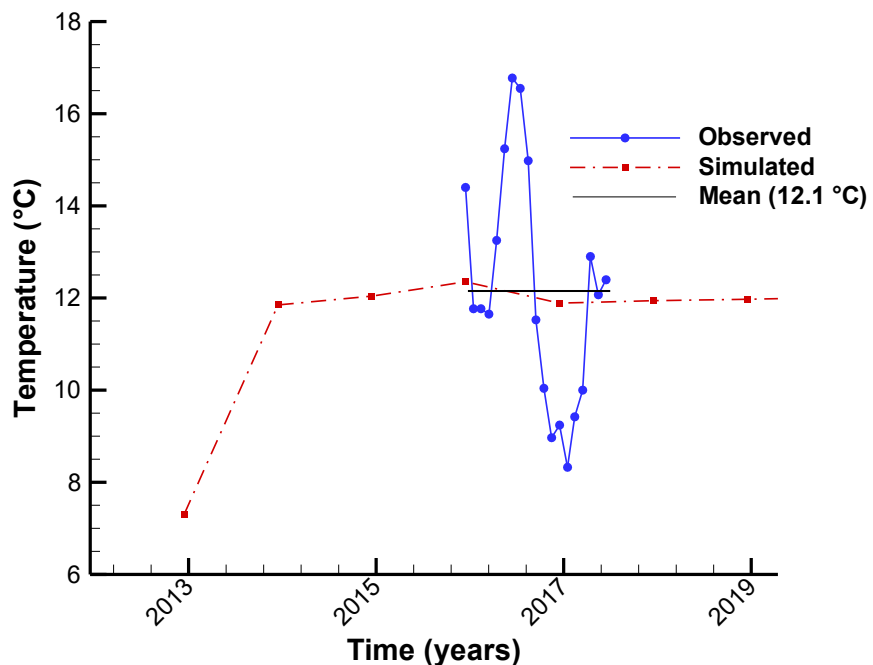


Figure 3.9: Observed and simulated temperature of water at the dewatering outlet zone. Observed data is for the year 2016 and the first half of 2017. The mean temperature value shown corresponds to the observed mean temperature of water at the dewatering outlet zone.

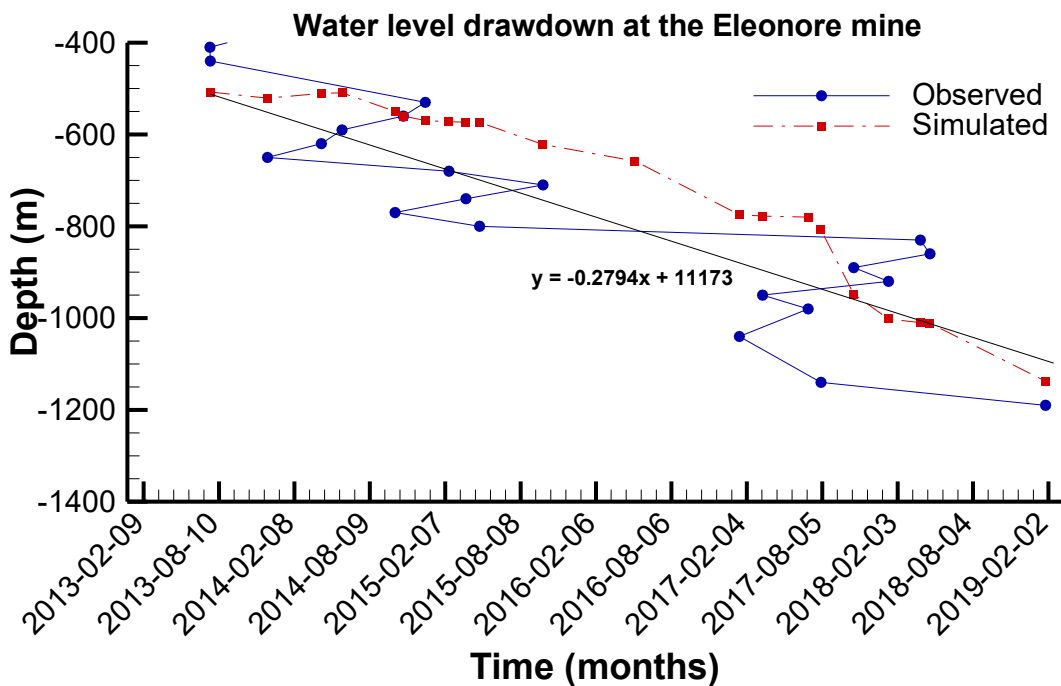


Figure 3.10: Observed and simulated water level drawdown at the Éléonore mine. Observed data was estimated from the construction date of the underground horizons.

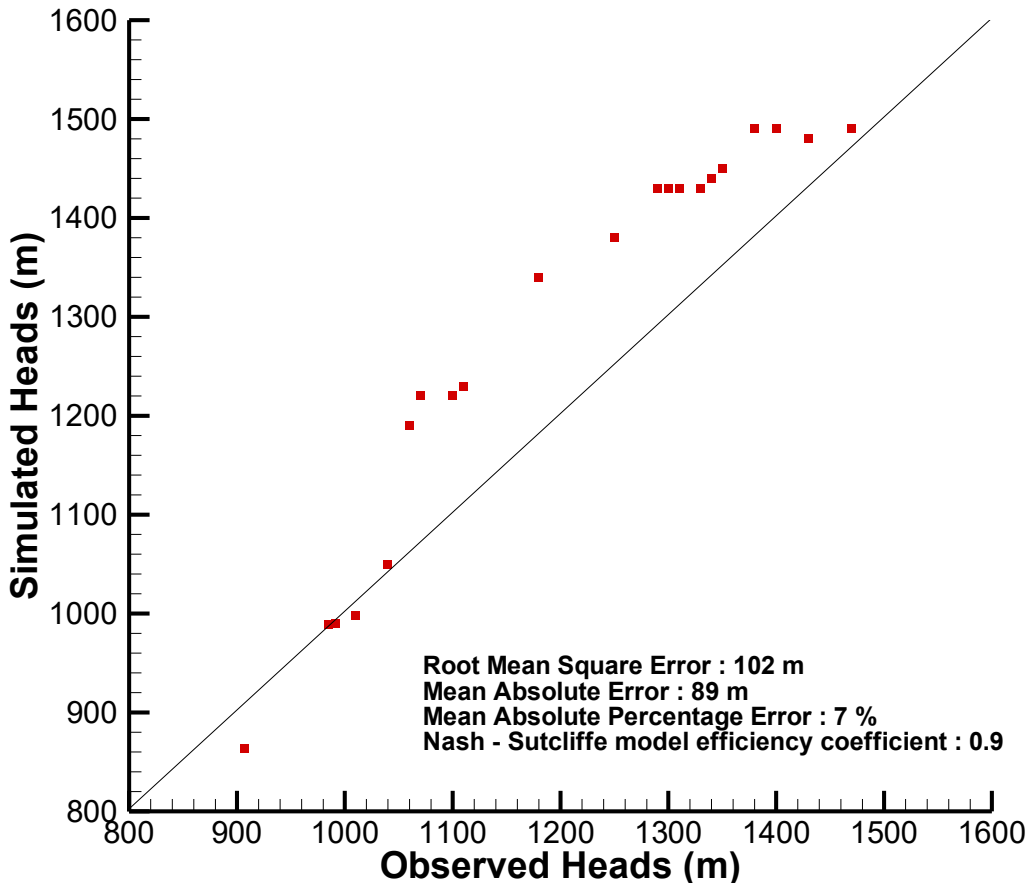


Figure 3.11: Observed vs simulated heads.

3.2.5 Model Predictions

To simulate future conditions, the model needs to consider the forthcoming underground development of the mine in addition to an increase in the dewatering flow rate. The production shaft is currently completed to 1190 m, and the deepest drilling holes report mineralization at 1500 m (Charland, 2018). Future development is thus planned at the 1370 m level. The 1370 horizon was added to the baseline calibrated model to account for the future development of the mine. The flow rate was gradually increased to reach the maximum expected dewatering flow rate of $718 \text{ m}^3 \text{ h}^{-1}$. All flow and heat transport boundary conditions, in addition to other physical and thermal properties, remain the same.

3.2.6 Sensitivity Analysis

During calibration, preliminary simulations suggest that hydraulic conductivity and flow rate have the most significant influence on system dynamics. A sensitivity analysis was performed to ascertain the influence of individual parameters on the drawdown and temperature of the water. Sixteen scenarios were evaluated by manually modifying key parameters such as hydraulic conductivity, specific storage, porosity, dispersivity, flow rate, and thermal conductivity (Table 3.4). The sensitivity assessment and the rest of the results are presented in the following chapter.

Table 3.4: Sensitivity analysis scenarios performed with the Éléonore mine model.

Scenario	Description
1	Hydraulic conductivity of host rock + 10%
2	Hydraulic conductivity of host rock - 10%
5	Porosity + 10%
6	Porosity - 10%
7	Dispersivities + 10%
8	Dispersivities - 10%
9	Specific storage + 10%
10	Specific storage - 10%
11	Flow rate + 11%
12	Flow rate - 11%
13	Thermal conductivity + 10%
14	Thermal conductivity - 10%
15	Specific heat capacity + 10%
16	Specific heat capacity - 10%

4 RESULTS

4.1 Design of the Geothermal Heat Pump System

The design of the geothermal heat pump system (GHPs) was adapted to the dewatering system of the Éléonore mine by considering the heating load of the underground workings, in addition to the temperature and flow rate data from potential sites. Subsequently, the water quality was evaluated to anticipate issues related to scaling and corrosion caused by mine water circulating through the system. The steps involved in the design of the GHPs and the resulting performance assessment are presented in the following sections.

4.1.1 Initial energy balance

The first step in the design of the GHPs was to determine the current heating load of the underground workings, the costs incurred, as well as the environmental impact. According to calculations performed with data from the year 2016, heating the underground workings demands 26 664 MWh or 37 thermal MW, which represents 22.5% of the total energy requirements of the mine. Heating is only required from October to April, with February having the highest thermal demand with 6 193 MWh. The propane-based heating system consumes 3.4 million litres annually, generating expenses of 1.5 million Canadian dollars per year while releasing 5 600 tonnes of carbon dioxide (Figure 4.1).

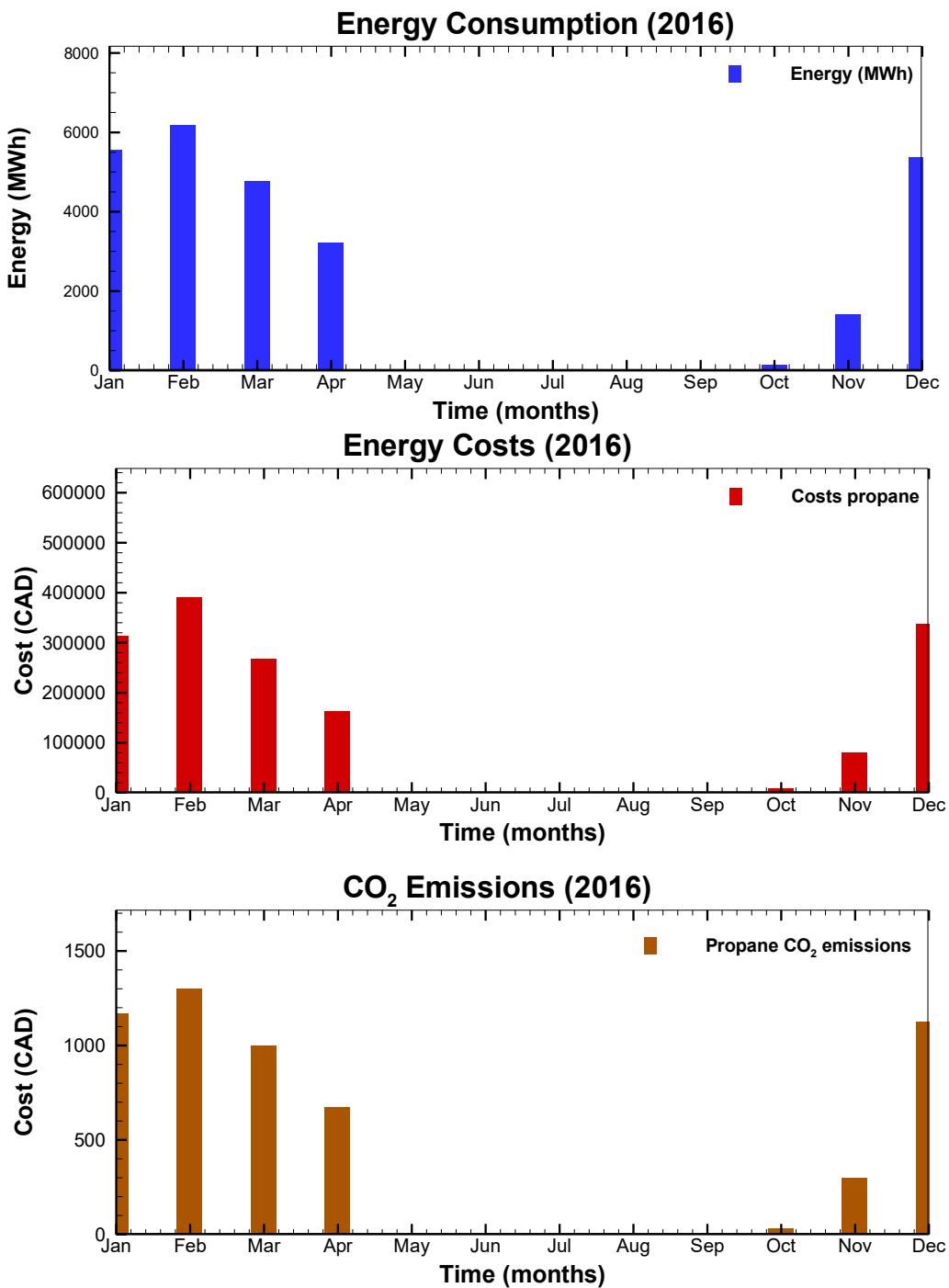


Figure 4.1: Initial economic, environmental and energy balance of the propane burner system used to heat the underground working of the Éléonore mine. No values are shown from May to September since the underground workings require no heating during this period.

4.1.2 Site assessment

The flow rate and temperature were first evaluated for the four potential sites along the industrial water treatment pathway. Based on information for the 2015-2017 period, the highest mean flow rate is located at the dewatering outlet zone, with an average flow of $299 \text{ m}^3 \text{ h}^{-1}$. The flow rate at the emissary is slightly lower, with $278 \text{ m}^3 \text{ h}^{-1}$. Meanwhile, the average flow at the entrance of the water treatment plant is $230 \text{ m}^3 \text{ h}^{-1}$, and at the plant exit, the mean flow is $167 \text{ m}^3 \text{ h}^{-1}$ (Figure 4.2 a and b). The dewatering flow at the exit of the water treatment plant is lower compared to the one at the exit of the mine because a portion of the water is used at the tailings management facility. The flow rate at the emissary is likewise lower relative to the dewatering outlet zone because part of the water is used for surface activities as well as freshwater.

Temperature analysis was performed for the 2016-2017 period (Figure 4.2 c). The highest temperature is found at the mine water outlet zone with a mean annual temperature of 12.1°C . The water at this location comes from a water reservoir located at level 400 m, where water that infiltrates the underground workings is collected. Water from the ramp and lower levels are also directed to the 400 m level and then pumped to the surface. Due to the geothermal gradient and the insulating effect of the ground, mine water coming from the underground workings maintains a higher temperature. However, the temperature measured at the dewatering outlet zone does exhibit minor seasonal fluctuations since the sampling site is located at the surface. At the entrance of the water treatment plant, the temperature is slightly lower, with an average temperature of 10.9°C . However, during the winter, the water entering the water treatment plant (WTP) has an average temperature of 8°C . It is indicating a loss of between 1.2 and 4.1°C between the dewatering outlet zone and the entrance of the WTP. Heat loss is the result of exposure to atmospheric conditions when the water remains in the polishing and sedimentation ponds. Water exits the WTP at approximately 10°C after it is treated with a *Moving Bed Biofilm Reactor* (MBBR). Finally, after leaving the effluent, the water at the emissary exits at an average of 9.0°C . Overall, the highest average temperature is located at the mine water outlet zone. The temperature is considerably higher compared to other sites during winter and spring and is slightly lower during the summer. These conditions are ideal for heating during the cold season and air conditioning during the summer.

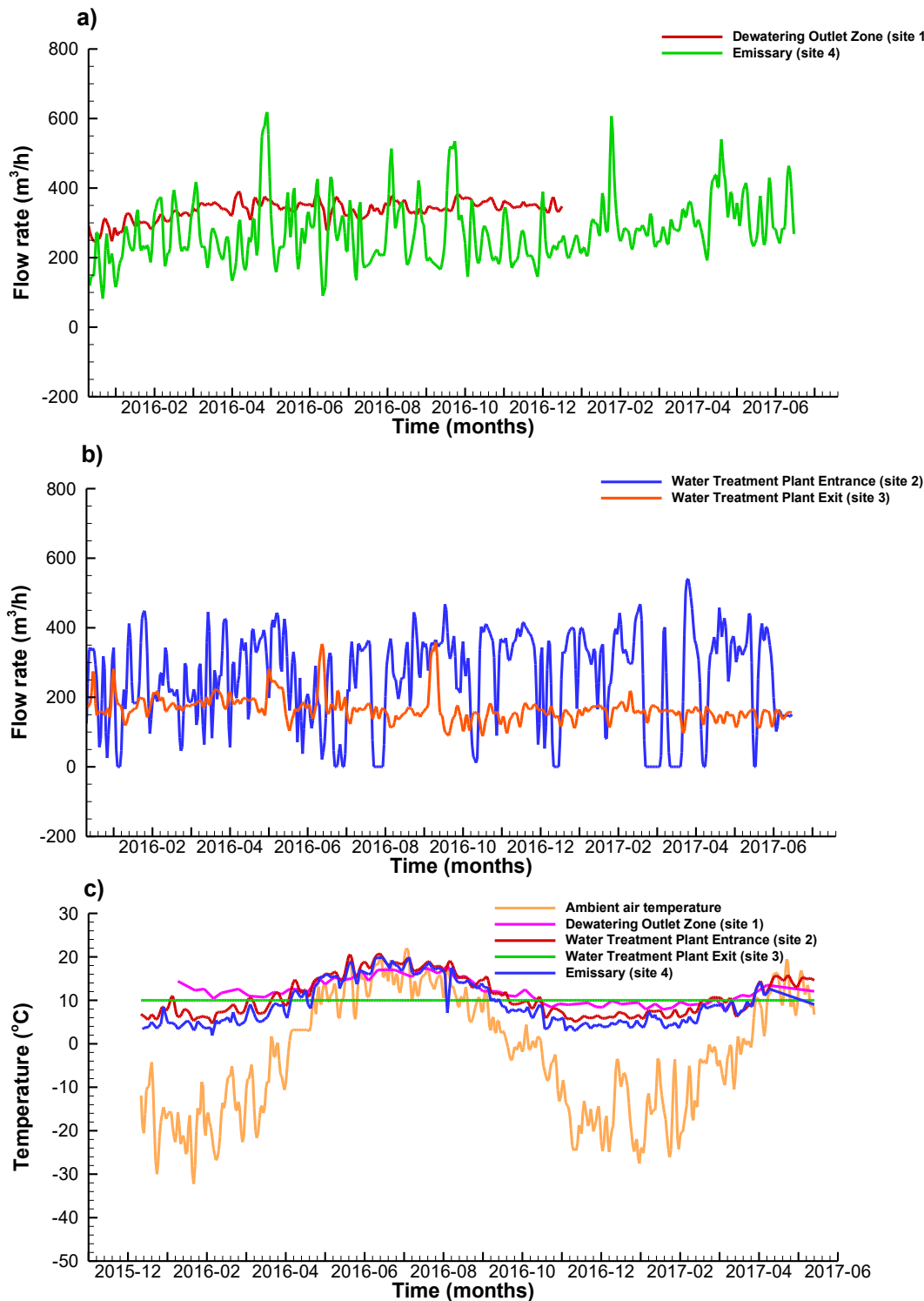


Figure 4.2: Assessment of initial conditions at the Éléonore mine. a) flow rate at the dewatering outlet zone and the emissary, b) flow rate at the entrance and exit of the water treatment plant, and c) temperature.

4.1.3 Water Quality

Following the dewatering flow rate and temperature analysis, water quality was studied to assess the risk of scaling and corrosion at each of the four sites. Hydrochemical data collected by Goldcorp at the mine water outlet zone (site 1 – process water) and the emissary (site 4 – treated water) are presented in Table 4.1. Results of the chemical analysis performed at the INRS laboratory for the four sites are included in Appendix III.

Table 4.1: Evolution of mine water chemistry from the dewatering outlet zone to the emissary.

Parameter (values in mg/L except when indicated)	Site # 1 : Mine water outlet zone	Site # 4 : Emissary	Recommended maximum values for GHPs (Kavanaugh et Rafferty, 1997; Ochsner, 2012)
	Values provided by Goldcorp from 2014 to 2017	Values provided by Goldcorp from 2014 to 2017	
Major Ions			
HCO ₃	88.5	36.4	
Ca	299.4	259.0	
K	58.7	68.3	
Mg	23.4	9.0	
Na	273.8	371.0	
Cl	654.4	720.9	400 - 600
SO ₄	270.3	563.4	50 - 200
Minor Ions			
Al	-	-	
As	-	-	
Ba	0.2	0.06	
Co	-	-	
Cr	-	-	
Cu	0.1	0.13	
Fe	46.2	0.5	0 - 5
Mn	0.8	0.04	
Mo	-	-	
Ni	-	-	
Pb	0.2	0.002	
Other parameters			
Total alkalinity (mg/L as CaCO ₃)	72.7	37.9	
Total hardness (mg/L as CaCO ₃)	855.2	696.4	15-200
Total dissolved solids	1 966.1	2 289.7	200 – 1 000
Total suspended solids	5 194.2	2.9	
Conductivity (µS/cm)	2 818.5	3 444.0	< 600
Temperature (°C)	12.2	9.6	
pH	8.6	7.1	6 - 8.5

Chemical data collected by Goldcorp indicate that water at the dewatering outlet zone (site 1) contains a high concentration of calcium and sodium, has a slightly basic pH of 8.6, and as a result, is classified as very hard ($> 200 \text{ mg/L}$; (Rafferty, 2004b). The latter constitute conditions favourable to scaling. The water sampled at this location also exhibits an elevated concentration of chloride, sulphate, and suspended solids, which makes it highly conductive and increases the risk of corrosion and clogging. Once the water reaches the emissary (site 4), calcium and magnesium concentration decreases but remains high. Water sampled at the emissary displays a gain in sodium and potassium ions, which become the major cations in solution. Chloride and sulphate show a further increase in concentration and remain the major anions. The amount of total suspended solids at the dewatering outlet zone is significant and can affect the performance of plate heat exchangers. The suspended solids concentration decreases towards the emissary, whereas the concentration of total dissolved solids and conductivity increases, leading to a considerable risk of corrosion. This could be a result of the release of ions in solution due to acidification. All values provided by the mine represent laboratory measured values. The tables containing the entirety of the analyzed parameters and the calculations of the saturation indices are presented in Appendix III.

Compared to the physicochemical data provided by Goldcorp, the samples analyzed at the INRS laboratory (Appendix III, Table III.1 – III.4) exhibit slightly lower concentrations overall. Also, except for an increasing Ca^+ concentration towards the emissary, all other major ions from samples analyzed at the INRS exhibit the same trend from the water outlet zone to the emissary, (Figure 4.3). The pH was measured in the field and varied from 8.5 at the dewatering outlet zone to 7.4 at the emissary. All samples were subsequently analyzed at the INRS laboratory and the pH had diminished significantly and varied from a mean pH of 5.7 at the dewatering outlet zone to a pH of 3 at the emissary (Appendix III, Table III.5). The acidification between the dewatering outlet zone and the emissary suggests that water is not in equilibrium. Since alkalinity depends on the pH, a reliable measure of alkalinity was not established. For this reason, and considering that hydrochemical data collected by the mine at sites 1 and 4 spans several years, this data was used to calculate the stability indices to quantify the risk of scaling and corrosion. Furthermore, the indices for sites 2 and 3 were not calculated, since no alkalinity data is available for these sites.

At the dewatering outlet zone, the Langelier Saturation Index (LSI) denotes slight scale-forming water, and the Ryznar Stability Index (RSI) suggests that water is neither scale forming nor corrosive. According to the Puckorius Scaling Index (PSI), which minimizes the effect of buffering

agents contained in water, there is potential for heavy corrosion. The Larson-Skold Corrosion Index (LSCI) also anticipates high rates of corrosion. At the emissary, no risk of scaling is present, but corrosion potential is higher relative to the mine water outlet zone. The decrease in pH, calcium and bicarbonate concentration and the increase in chloride, sulphate and total dissolved solids content towards the emissary contribute to the increased risk of corrosion. Overall, the dewatering outlet zone has the highest temperature and flow rate, as well as a lower risk of corrosion. Table 4.2 provides the complete results for the saturation indices of the mine water outlet zone and the emissary and Table 4.3 presents the interpretation for each of the indices. The entirety of the results and the files used to calculate the indices are included in Appendix IV.

Concentration of major ions in water samples from the Eleonore mine

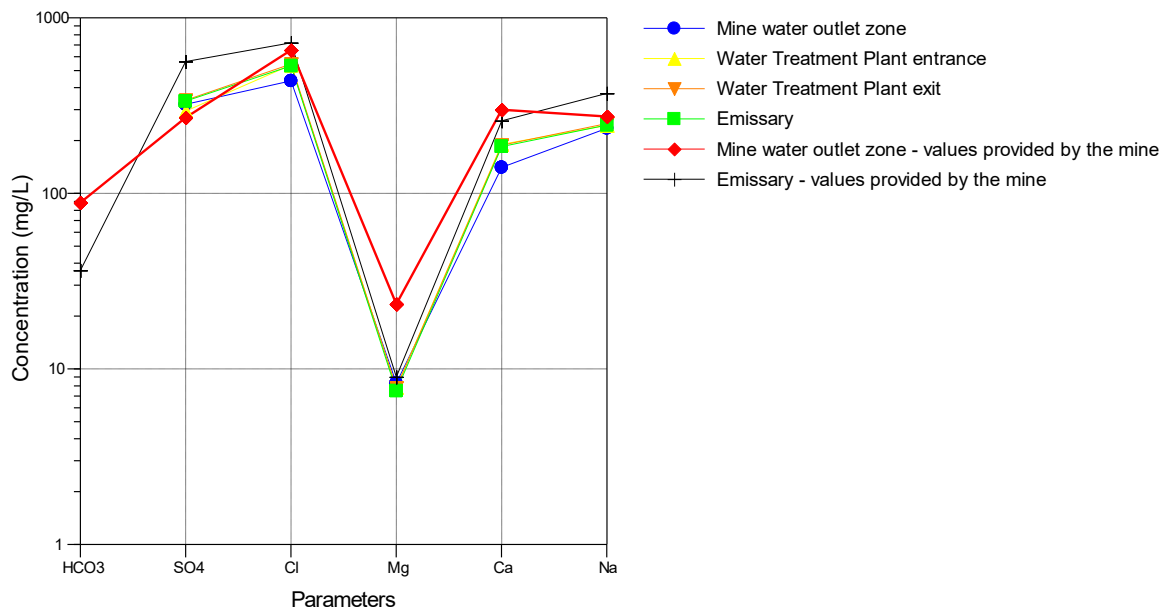


Figure 4.3: Major ion concentration.

Table 4.2: Scale and Corrosion indices results.

Site	Index			
	Langelier	Ryznar	Puckorius	Larson-Skold
Site # 1: Dewatering outlet zone	1.1	6.4	7.8	16.1
Site # 4 Emissary	-0.8	8.8	9.0	53.4

Table 4.3: Scale and Corrosion indices interpretation.

Langelier	Index	Ryznar	Puckorius	Larson-Skold
LSI > 2.0 Scale forming	4.0 – 5.0 Heavy scale	4.0 – 5.0 Heavy scale	4.0 – 5.0 Heavy scale	LSCI < 0.8 Chloride and sulfate will not interfere with natural film formation
0.5 < LSI < 2.0 Slightly scale forming	5.0 - 6.0 Light scale	5.0 - 6.0 Light scale	5.0 - 6.0 Light scale	
0.0 < LSI < 0.5 Balanced	6.0 – 7.0 Balanced: little scale or corrosion	6.0 – 7.0 Balanced: little scale or corrosion	6.0 – 7.0 Balanced: little scale or corrosion	0.8 < LSCI < 1.2 Chloride and sulphate may interfere with natural film formation;
-0.5 < LSI < 0.0 Slightly corrosive but non-scale forming	7.0 – 7.5 Corrosion	7.0 – 7.5 Corrosion	7.0 – 7.5 Corrosion	corrosion may occur
-2.0 < LSI < -0.5 Moderate to serious corrosion	7.5 – 9.0 Heavy corrosion	7.5 – 9.0 Heavy corrosion	7.5 – 9.0 Heavy corrosion	LSCI > 1.2 High corrosion rates are anticipated
LSI < -2.0 Serious corrosion	RSI > 9.0 Corrosion intolerable	PSI > 9.0 Corrosion intolerable	PSI > 9.0 Corrosion intolerable	

4.1.4 Geothermal Heat Pump System Design and Performance Assessment

The performance of the system was assessed from energy, economic and environmental standpoints using the procedure and the GHPs described in section 3.1.5. The geothermal heat pump system designed for the conditions of the site consists of three Multistack TRANE heat pumps capable of handling the mean flow rate of the dewatering system. Furthermore, due to the potential risk for corrosion, a plate heat exchanger was included to prevent water from entering directly into the heat pump system. The components of the plate heat exchanger are made of type 304 and 316 stainless steel to protect the system against corrosion (Kavanaugh et Rafferty, 2014). The system costs 325 000 \$CAD. This price includes the plate heat exchanger, the compressor and the evaporator as well as an air exchanger. It does not include the costs of operation and maintenance, installation, and inflation.

Calculations were performed for each site with the monthly dewatering flow rate and temperature values for the year 2015 and 2016. Results suggest that the proposed GHPs located at the dewatering outlet zone could generate between 9 471 and 10 283 MWh annually, which correspond to penetration levels between 35 and 39% (Table 4.4). During winter, the penetration level decreases due to an increase in the energy demand brought about by a decrease in ambient temperature. In February, the coldest month in both 2015 and 2016, the penetration level is 18% and 17%, respectively.

In terms of the energy production costs, the expenses incurred by the GHPs amounts solely to the electricity consumed by the compressor. According to the energy consumed by the GHPs designed for this study and the price of electricity at the mine, the costs of running such a system

would range between 56 000 and 60 000 CAD per year. Afterwards, the amount of energy generated by the heat pump system is subtracted from the total heating demand of the underground workings to obtain the remaining amount of energy that is fulfilled by the propane burner system. The net annual savings are then determined by comparing the costs incurred by the hybrid system to the actual propane-based heating system. In 2015, heating the underground workings with a hybrid heating system would have cost 1.4 \$ million — a 30% decrease in heating costs, which represents 600 000 \$ in net savings. Meanwhile, in 2016, such a system would have cost 1.04 \$ million, which constitutes a 33% decrease in heating costs or 514 000\$ in net savings (Table 4.5). Additionally, the incorporation of this system would decrease propane consumption by 1.24 and 1.36 million litres per year, while reducing CO₂ emissions by approximately 1,825 and 1,993 tonnes annually (Table 4.6). The results for the remaining sites are included in Appendix V.

Table 4.4: Monthly energy production rate and penetration level of the GHPs designed for the dewatering outlet zone.

Energy Analysis: Dewatering outlet zone						
Year	Month	¹ E _{exchanger}	E _{comp}	Total energy produced by the GHPs (² E _{heating})	Total heating energy demand of the underground workings	³ Penetration level
		(kWh)	(kWh)	(kWh)	(kWh)	(%)
2015	Jan	1 454 319	331 991	1 786 311	7 462 805	24
	Feb	1 142 697	257 740	1 400 437	7 857 609	18
	Mar	1 237 402	277 079	1 514 481	5 218 922	29
	April	1 133 010	254 009	1 387 019	1 820 607	76
	May	0	0	0	0	0
	June	0	0	0	0	0
	July	0	0	0	0	0
	Aug	0	0	0	0	0
	Sept	0	0	0	0	0
	Oct	514 810	112 571	627 380	298 220	210
	Nov	702 606	162 283	864 889	1 493 572	58
	Dec	1 548 956	341 753	1 890 709	3 022 661	63
Total		7 733 801	1 737 425	9 471 226	27 174 396	35
2016	Jan	2 145 316	453 537	2 598 852	5 564 374	47
	Feb	889 285	194 139	1 083 424	6 193 288	17
	Mar	1 277 591	276 829	1 554 420	4 763 296	33
	April	1 247 253	268 172	1 515 424	3 213 487	47
	May	0	0	0	0	0
	June	0	0	0	0	0
	July	0	0	0	0	0
	Aug	0	0	0	0	0
	Sept	0	0	0	0	0
	Oct	490 624	105 332	595 956	148 787	401
	Nov	765 102	172 461	937 564	1 418 548	66
	Dec	1 774 260	374 318	2 148 578	5 362 468	40
Total		8 589 431	1 844 787	10 434 218	26 664 248	39

¹Energy = power (kW) times the number of hours in a day, times the number of days in the respective month.

²E_{heating} = E_{exchanger} + E_{heating}.

³Penetration level = percentage of the total energy demand that can be supplied by the designed GHPs.

Table 4.5: Monthly energy production costs comparison between the propane-based system and a hybrid (geothermal-propane) heating system.

¹Economic Analysis : Dewatering outlet zone						
Year	Month	²Costs incurred by a propane-based heating system	³Costs for the GHPs	⁴Costs incurred by a hybrid heating system	⁵Net annual savings	Net annual savings (%)
		(CAD)	(CAD)	(CAD)	(CAD)	(%)
2015	Jan	571 991	10 823	445 901	126 090	22
	Feb	612 973	8 402	512 127	100 846	16
	Mar	428 493	9 033	313 181	115 312	27
	April	132 089	8 281	39 738	92 350	70
	May	0	0	0	0	0
	June	0	0	0	0	0
	July	0	0	0	0	0
	Aug	0	0	0	0	0
	Sept	0	0	0	0	0
	Oct	20 009	3 670	3 670	16 339	82
	Nov	102 248	5 290	48 329	53 918	53
	Dec	178 055	11 141	77 821	100 234	56
Total		2 045 856	56 640	1 440 767	605 090	30
2016	Jan	312 593	14 785	181 381	131 212	42
	Feb	390 179	6 329	328 252	61 927	16
	Mar	267 591	9 025	189 292	78 299	29
	April	162 987	8 742	94 867	68 119	42
	May	0	0	0	0	0
	June	0	0	0	0	0
	July	0	0	0	0	0
	Aug	0	0	0	0	0
	Sept	0	0	0	0	0
	Oct	8 155	3 434	3 434	4 722	58
	Nov	79 691	5 622	32 643	47 048	59
	Dec	337 837	12 203	214 679	123 158	36
Total		1 559 033	60 140	1 044 548	514 485	33

¹Energy production costs

²100 % of total heating energy demands

³Energy consumed by the compressor (E_{comp}) \times 3.26 ¢/kWh (Rate L, Hydro-Quebec) (personal communication, Newmont-Goldcorp, 2017)

⁴Cost of providing 100% of heating energy demand with a hybrid system = cost generated by a GHPs + cost incurred by the propane-based system once the penetration level of the GHPs has been deducted.

⁵Costs incurred by a propane burner system minus the costs incurred by a hybrid heating system.

Table 4.6: Monthly propane consumption and CO₂ emissions comparison between the present propane-based system and a hybrid (geothermal-propane) heating system.

Environmental Analysis : Dewatering outlet zone						
Year	Month	Propane-based system		Hybrid heating system		
		¹ Propane consumption (litres)	² CO ₂ emissions (tonnes)	³ Propane consumption (litres)	⁴ CO ₂ emissions (tonnes)	Propane savings (litres)
2015	Jan	1 018 321	1 567	774 574	1 210	243 747
	Feb	1 072 193	1 650	881 100	1 370	191 094
	Mar	712 136	1 096	505 482	793	206 655
	April	248 427	382	59 164	105	189 263
	May	0	0	0	0	0
	June	0	0	0	0	0
	July	0	0	0	0	0
	Aug	0	0	0	0	0
	Sept	0	0	0	0	0
	Oct	40 693	63	0	6	40 693
	Nov	203 802	314	85 786	141	118 017
	Dec	412 450	635	154 458	257	257 993
Total		3 708 024	5 707	2 460 563	3 882	1 247 461
2016	Jan	759 275	1 169	181 381	649	354 621
	Feb	845 092	1 301	328 252	1 084	147 836
	Mar	649 965	1 000	189 292	689	212 105
	April	438 489	675	94 867	372	206 784
	May	0	0	0	0	0
	June	0	0	0	0	0
	July	0	0	0	0	0
	Aug	0	0	0	0	0
	Sept	0	0	0	0	0
	Oct	20 302	31	3 434	6.0	20 302
	Nov	193 565	298	32 643	110	127 933
	Dec	731 724	1 126	214 679	696	293 180
Total		3 638 413	5 599	2 275 652	3 607	1 362 761

¹100% of heating needs provided by propane.

²kWh of energy produced by the propane heating system x [0.21 kgCO₂/kWh (Koufos, 2012)].

³Emissions generated by the propane heating system once the penetration level of the GHPs has been deducted.

⁴Emissions generated by the propane heating system once the penetration level of the GHPs has been deducted + emissions generated by the GHPs = kWh x [0.01 kgCO₂/kWh (Koufos, 2012)].

4.2 Numerical Model Development

The baseline calibrated model was used to perform predictive simulations of groundwater flow and heat transport conditions throughout the life of the mine. By predicting dewatering temperature and flow rates, it was possible to estimate the amount of energy that can be produced with the designed geothermal heat pump system, while simultaneously assessing the sustainability of the geothermal resource. The following sections present the results, including the thermal properties of rock samples used in the development of the numerical model, the model predictions, and the sensitivity analysis. The HGS input files are found in Appendix VI.

4.2.1 Physical and Thermal Properties

Rocks from the two main geological units at the Éléonore mine were analyzed with a Thermal Conductivity Scanner. Twenty-eight samples of massive greywacke, which constitutes approximately 95% of the subsurface, and 16 samples of aluminosilicate-bearing greywacke were examined. The samples come from six different locations and depths (Appendix VII, Table VII.1). A total of 2373 measurement points were recorded from the 28 massive greywacke samples, and 1498 measurement points were obtained from the 16 aluminosilicate-bearing greywacke samples. Both thermal conductivity and thermal diffusivity were analyzed. Volumetric heat capacity was determined by dividing the thermal conductivity by the diffusivity. Specific heat capacity used as input in HydroGeoSphere was calculated by dividing the volumetric heat capacity by the density of the rock (Mielke et al., 2016).

Statistical analyses were done with results from both geological units (Table 4.7). The data indicates that there is a difference between values from each unit, proving that samples come from distinct geological units. Despite being distinct lithologies, aside from the aluminosilicates, their composition is similar, and the differences in values are minor. The massive greywacke displays a mean thermal conductivity value of $2.4 \text{ W m}^{-1} \text{ K}^{-1}$, a mean thermal diffusivity of $1.0 \mu\text{m}^2 \text{ s}^{-1}$, and a mean volumetric heat capacity of $2.4 \text{ MJ m}^{-3} \text{ K}^{-1}$ or a specific heat capacity of $909 \text{ J kg}^{-1} \text{ K}^{-1}$. Meanwhile, the aluminosilicate-bearing greywacke displays slightly higher thermal conductivity and diffusivity, with a mean of $2.6 \text{ W m}^{-1} \text{ K}^{-1}$ and $1.2 \mu\text{m}^2 \text{ s}^{-1}$, respectively. The volumetric heat capacity is lower, with a mean of $2.3 \text{ MJ m}^{-3} \text{ K}^{-1}$ or $871 \text{ J kg}^{-1} \text{ K}^{-1}$. A graphical description of the statistical distribution of thermal properties according to geological units and location is included in Appendix VII.

Table 4.7: Thermal properties of rocks from the Éléonore mine.

Thermal Conductivity ($\text{W m}^{-1} \text{K}^{-1}$)									
Unit	Number of samples	Measure points	Mean	Median	Mode	Maximum	Minimum	Standard Deviation	Variance
Massive Greywacke	28	2373	2.4	2.3	2.2	4.1	1.6	0.4	0.15
Aluminosilicate Greywacke	16	1498	2.6	2.6	2.4	3.7	2.1	0.3	0.1
Thermal Diffusivity ($\mu\text{m}^2 \text{s}^{-1}$)									
Unit	Number of samples	Measure points	Mean	Median	Mode	Maximum	Minimum	Standard Deviation	Variance
Massive Greywacke	28	2373	1.0	1.0	1.0	2.0	0.4	0.2	0.03
Aluminosilicate Greywacke	16	1498	1.2	1.1	1.1	2.3	0.8	0.2	0.03
^{2,3} Volumetric Heat Capacity ($\text{MJ m}^{-3} \text{K}^{-1}$)									
Unit	Number of samples	Measure points	Mean	Median	Mode	Maximum	Minimum	Standard Deviation	Variance
Massive Greywacke	28	2373	2.4	2.4	2.1	4.5	1.7	0.3	0.1
Aluminosilicate Greywacke	16	1498	2.3	2.3	2.3	3.3	1.2	0.3	0.1

¹Thermal conductivity scanner data acquisition sampling interval of 2 mm.

²Values were obtained by dividing the thermal conductivity by the thermal diffusivity.

³Values were divided by the rock density obtained from the literature ($\rho = 2640 \text{ kg m}^{-3}$) to determine the specific heat capacity ($\text{J kg}^{-1} \text{K}^{-1}$) used in HydroGeoSphere

4.2.2 Model Results

4.2.2.1 Hydraulic head, drawdown and predicted temperature

According to mine plans, peak production would be achieved in 2019, and it is assumed that it will remain near this rate for several years. A linear regression done with observed flow rate values during the calibration period was utilized to predict flow rates (Figure 4.4). The predicted dewatering flow rate reaches $656.8 \text{ m}^3 \text{ h}^{-1}$ in 2019 and gradually increases until it attains the maximum expected dewatering flow rate of $718 \text{ m}^3 \text{ h}^{-1}$ in 2024 (Table 4.8; Beausoleil et al. (2014)). Once the maximum dewatering flow rate is reached, the rate of dewatering remains constant until mine closure in 2026 plus five additional years for further development. The increase in dewatering flow rate until mine reaches maximum production, followed by a plateau in dewatering until closure, is a behaviour previously observed in the life cycle of mines (Ugorets et Pereira, 2018).

From 2013 to early 2019, the dewatering of the mine has generated a total drawdown of 790 m, which is approximately 131 m per year. The current water level estimated from the depth of underground workings is 1190 m. With further underground development and the ensuing projected increase in dewatering flow rate, results suggest that level 1370 will be reached in early 2024. By 2027, the model reaches a quasi-steady-state, with a final drawdown of 1383 m and a radius of influence extending 2.26 km (Figure 4.5 a and b).

The increase in flow rate and drawdown has a considerable influence on the dewatering temperature. During the initial year of dewatering, the mean temperature of the water exiting the system is lower since water is pumped exclusively from the 400 level. In the first year, the average water temperature is 7.3 °C. As the development of the mine progresses, water is pumped from deeper locations, where the temperature is higher due to the geothermal gradient and the insulating effect of the ground. Once the 650 level pumping station starts dewatering, the mean temperature in 2014 increases to 11.8 °C. However, the dewatering flow rates at depth are significantly lower than flow rates from the main pumping stations situated close to the surface. Thus, temperature increases initially but reach a near-constant value departing minimally from the mean observed 12.1°C, with only a 0.3 °C increase from 2019 to 2031 (Figure 4.6 and Table 4.9).

Both predicted flow rate and temperature were used to calculate the maximal energy output of the proposed GHPs and the potential amount of energy and power available throughout the life of the mine. The results are presented in the following section.

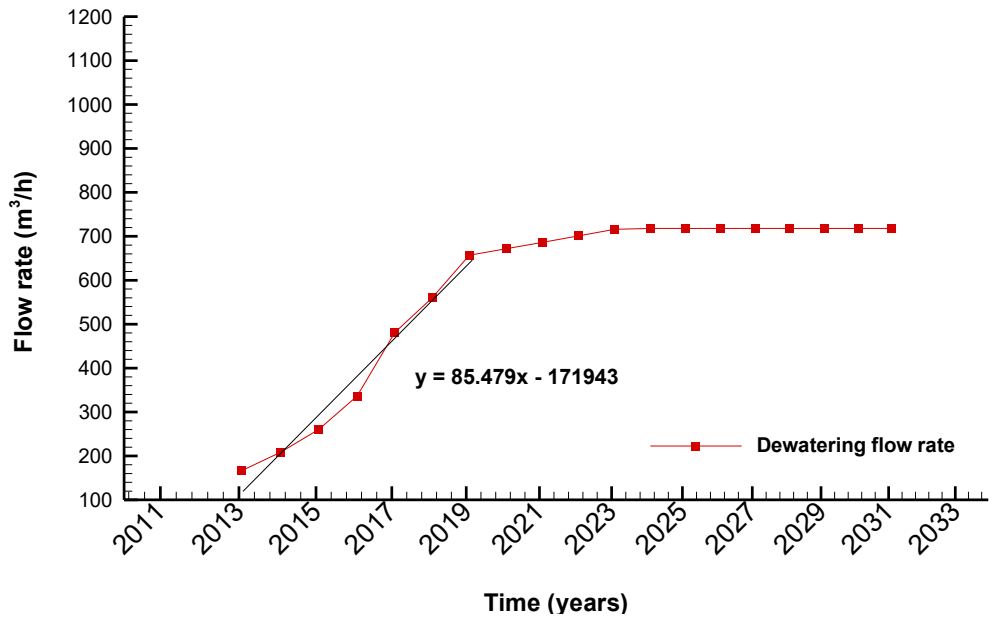
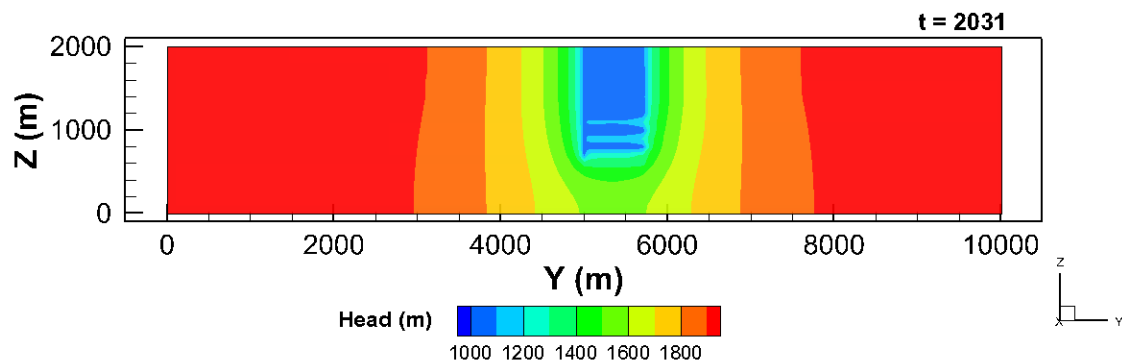


Figure 4.4: Calibrated and predicted dewatering flow rates

Table 4.8: Mean annual dewatering flow rate at the Éléonore mine

	Year	Flow rate ($\text{m}^3 \text{h}^{-1}$)
Calibration	2013	166.8
	2014	208.5
	2015	260.9
	2016	336.5
	2017	481.1
	2018	560.1
	2019	656.8
Prediction	2020	671.6
	2021	686.3
	2022	701.1
	2023	715.9
	2024	718.0
	2025 - 2031	718.0

a)



b)

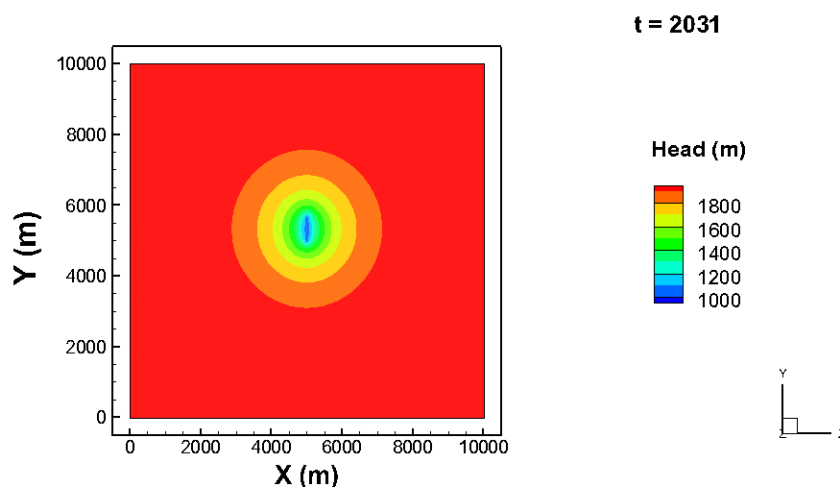


Figure 4.5: Predicted hydraulic heads at the Éléonore mine in 2031. Figure a) displays the hydraulic head at the Éléonore site, which reached a maximum depth of 1383 m. Figure b) shows the zone of influence caused by the dewatering of the mine, with a diameter of 4.5 km.

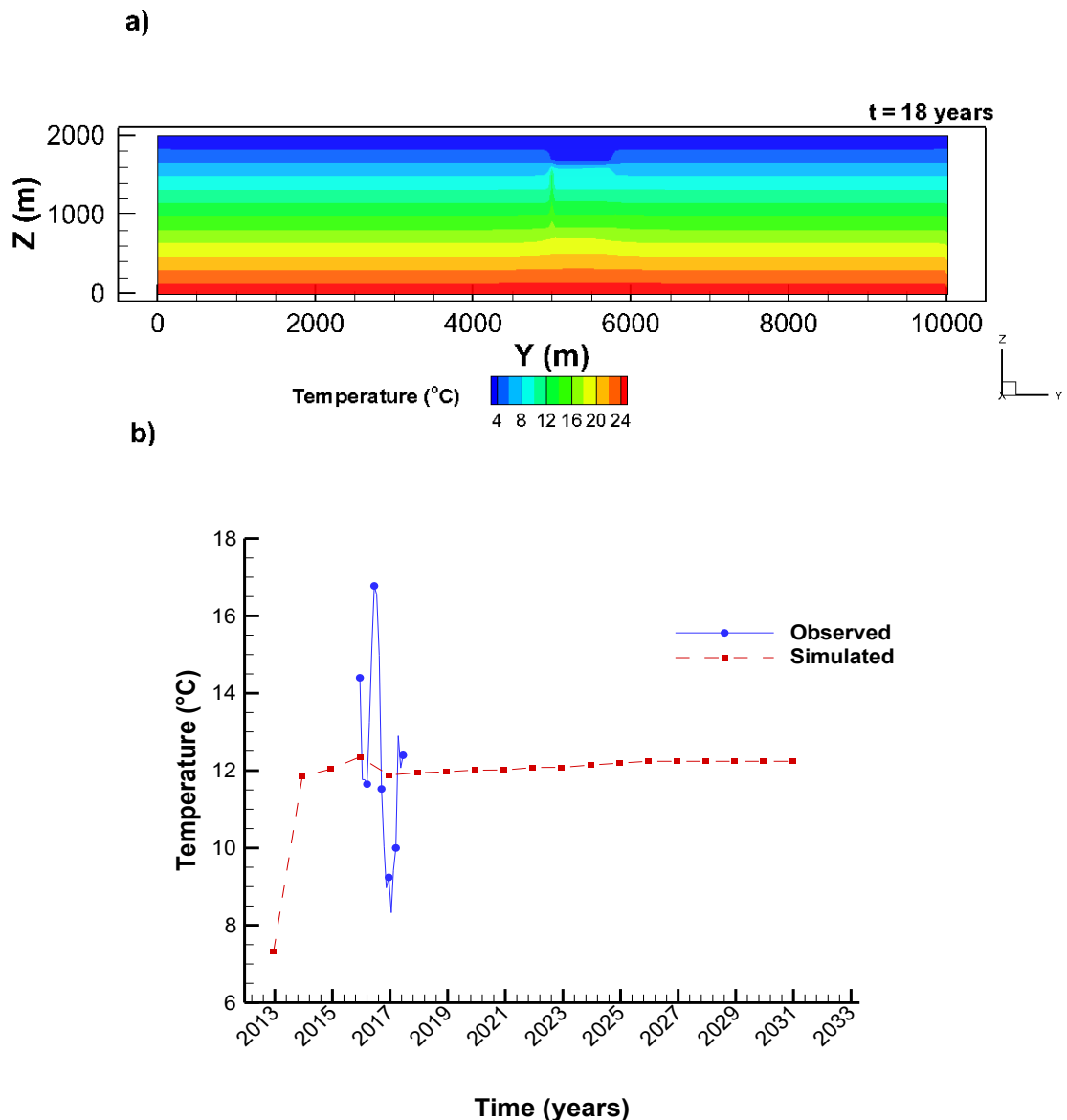


Figure 4.6: Predicted water temperature at the dewatering outlet zone.

Table 4.9: Simulated mean annual dewatering temperatures at the dewatering outlet zone of the Éléonore mine. As a reference, the observed annual mean in 2016 was 12.1 °C.

Dewatering outlet zone temperature ($^{\circ}\text{C}$)															
2013	2014	2015	2016	2017	2018	2019	2020	2021	2022	2023	2024	2025	2026	2027	2028-2031
7.3	11.8	12.0	12.4	11.9	11.9	12.0	12.0	12.0	12.1	12.2	12.2	12.2	12.2	12.2	12.3

4.2.2.2 Maximum and potential energy output

The GHPs was designed to handle a maximum entering flow rate of $481 \text{ m}^3 \text{ h}^{-1}$ (2118 GUSPM). The flow rate prediction indicates that this flow rate was achieved in 2017. Meanwhile, the simulated mean temperature of the water exiting the dewatering system in 2017 is 11.9°C . The maximum heating energy output of the GHPs was calculated using the previously mentioned conditions with the performance assessment procedure presented in section 3.1.5. A total of 26 664 MWh could be generated annually, an amount of energy that represents 45% of the total heating demands of the underground workings, assuming the heating load remains at the 2016 level. Heating costs would decrease by 36% while reducing greenhouse gas emissions by 2067 tonnes/year and displacing 1.6 million litres of propane (Table 4.10). Independent of the year, the maximum operating flow rate is reached; these values constitute the maximum energy output for the proposed system.

Notwithstanding, the selected GHPs is a modular system that can be easily upgraded to handle higher flow rates and extract greater quantities of energy. From 2018 onward, the amount of energy available rises significantly, as flow rate and temperature gradually increase. Results indicate that the amount of energy produced annually ranges from 29 215 MWh in 2018 to 39 183 MWh in 2031 (Table 4.11). Power output increases from 40 MW in 2018 to 53.9 MW in 2031. Ultimately, a cumulative total of 33 933 MWh would be generated until the expected end of life of the mine in 2026 and a total of 53 479 MWh by 2031.

Table 4.10: Maximum energy output of the proposed geothermal heat pump system.

Energy Analysis : Dewatering outlet zone					
Year	¹E_{exchanger}	E_{comp}	Energy generated by the GHPs ²(E_{heating})	Heating energy demand of the underground workings	³Penetration level
	(kWh)	(kWh)	(kWh)	(kWh)	(%)
2017	10 116 821	2 027 209	12 144 030	26 664 248	45

¹Economic Analysis : Dewatering outlet zone					
Year	²Costs incurred by a propane-based heating system	³Costs for the GHPs	⁴Costs incurred by a hybrid heating system	⁵Net annual savings	Net annual savings
	(CAD)	(CAD)	(CAD)	(CAD)	(%)
2017	2 045 856	66 187	1 316 162	729 695	36

Environmental Analysis : Dewatering outlet zone					
Year	¹Propane consumption	²CO₂ emissions	³Propane consumption	⁴CO₂ emissions	Propane savings
	(litres)	(tonnes)	(litres)	(CAD)	CO₂ savings
2017	3 701 442	5 599	2 043 565	3 532	1 657 877

Table 4.11: Heating energy and power potential

¹Predicted Energy Potential : Dewatering outlet zone			
Year	Power output (kW)	Energy output (kWh)	Total Cumulative Energy (MWh)
2017	16 540	12 144 030	1 214
2018	40 006	29 215 464	4 136
2019	47 394	34 448 633	7 581
2020	48 734	35 589 732	11 140
2021	49 822	36 213 082	14 761
2022	51 320	37 301 709	18 491
2023	52 421	38 102 449	22 302
2024	52 956	38 672 484	26 169
2025	53 262	38 713 917	30 040
2026	53 561	38 931 111	33 933
2027	53 552	38 924 401	37 826
2028	53 561	39 114 856	41 737
2029	53 785	39 093 660	45 647
2030	53 853	39 142 920	49 561
2031	53 908	39 183 204	53 479

¹Energy available from October to April.

4.2.3 Uncertainty Analysis

4.2.3.1 Sensitivity Analysis

Due to the inherent uncertainty in the parameters used to develop the numerical model and generate predictions, a sensitivity analysis was used to identify the properties that have the most influence on the model and to assess their impact on the results. The tested scenarios are presented in Table 3.4. All parameters were varied by $\pm 10\%$, and the analysis includes both the calibration period from 2013 to 2019 and the predictive model from 2020 to 2031. For the flow rate, variations begin in 2020 to examine the effect of changing dewatering rates on drawdown and temperature throughout the remaining life of the mine. The impact of parameter variation on model results was evaluated through the difference of hydraulic head, drawdown and temperature relative to the baseline calibrated model. Figure 4.7 shows the results of the sensitivity analysis. Only parameters having a considerable influence on results are shown.

According to the analysis, model results are most sensitive to hydraulic conductivity and the dewatering flow rate. A $\pm 10\%$ variation in hydraulic conductivity can generate a $\pm 85\text{ m}$ variation in drawdown. Meanwhile, a $\pm 10\%$ shift in flow rate can cause a $\pm 120\text{ m}$ change in drawdown. The dewatering temperature remains stable throughout the simulation period, with only a $0.15\text{ }^{\circ}\text{C}$ decrease caused by the change in hydraulic conductivity.

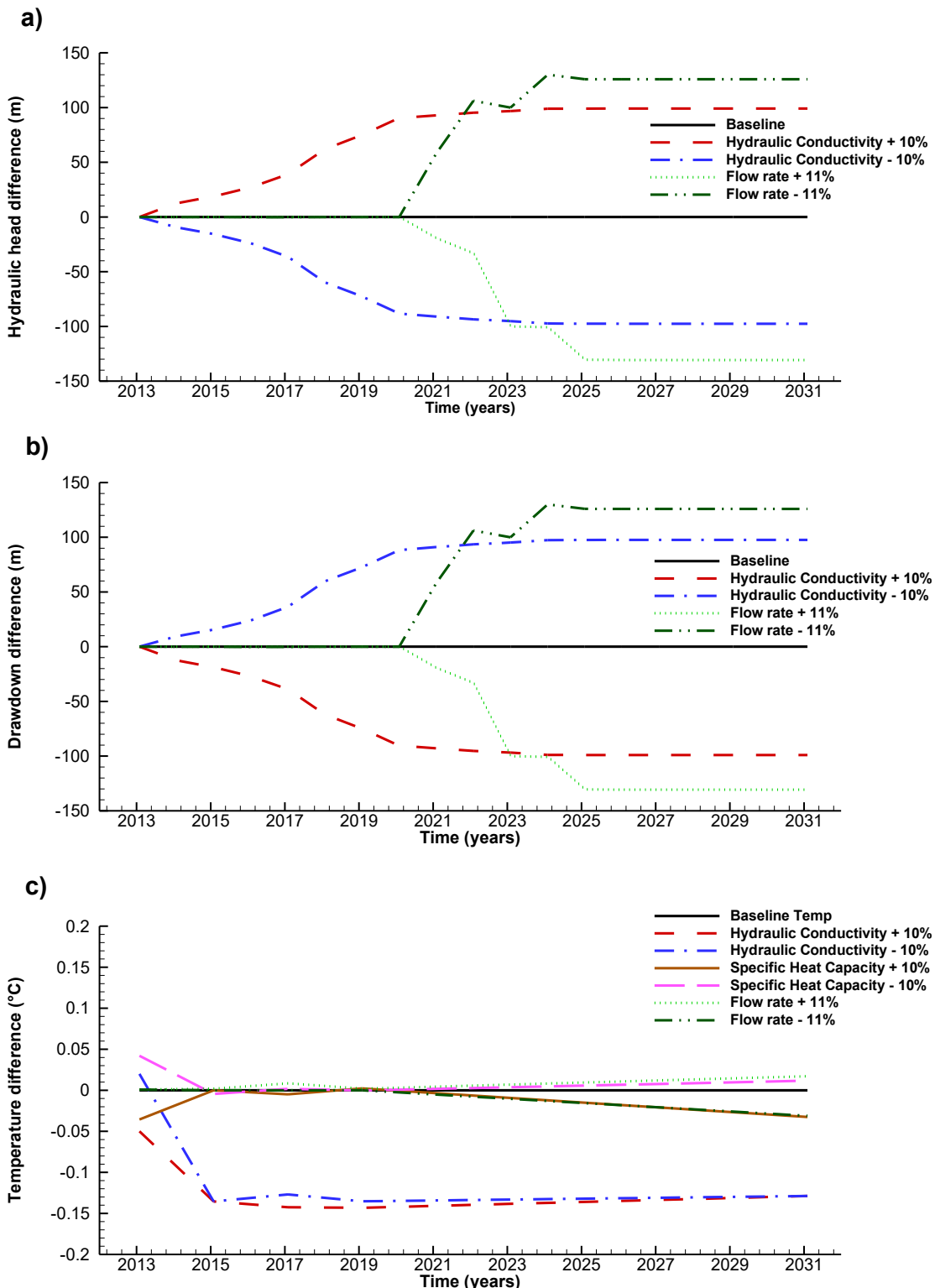


Figure 4.7: Sensitivity of the calibrated and predictive numerical model of the Éléonore mine a) Hydraulic head difference, b) Drawdown difference, and c) Dewatering temperature difference.

5 DISCUSSION

Background

Several active mines and future mining projects are situated in northern and remote locations, where the use of conventional energy sources, such as hydroelectricity, entails significant expenses due to their high power demand. Thus, presently, fossil fuels stand as the primary source of energy. Alternative energy sources should be implemented to increase profitability while decreasing the ecological footprint. The use of a geothermal heat pump system adapted to mining operations is one such option that appears attractive due to the large volume of water contained underground, the significant water flow rates used to dewater the mining operations, the higher temperature found underground, and the increased permeability of the subsurface making mines an ideal location for the installation of geothermal heat pump systems. Moreover, no drilling is necessary by coupling the geothermal system to the existing dewatering system. Therefore, the high costs of drilling and well installations are avoided, and the overall investment costs can potentially be reduced (Madiseh et al., 2012; Preene et Younger, 2014). Nevertheless, although the extraction of energy has been previously studied in the large volumes of water contained in flooded inactive mines (Hall et al., 2011; Raymond et Therrien, 2014; Bailey et al., 2016; Loredo et al., 2016; Banks et al., 2017; Al-Habaibeh et al., 2018; Menéndez et al., 2020), little research has been reported on the dewatering geothermal potential of active mines (Raymond et al., 2008).

Thereby, this study aimed to evaluate the dewatering geothermal potential of an active mine in a northern context to provide a technical portrait of geothermal heat pump systems as an eco-conscious alternative to the heating needs of mining sites. The Éléonore mine of Newmont-Goldcorp, which currently employs a propane-based heating system, was used as a case study. The procedure detailed in the ASHRAE publication by Kavanaugh and Rafferty (2014) for the design of Ground-Source Heat Pump consisting of — *initial energy balance, site assessment, system design, and performance assessment* served as a guideline in the assessment of the Éléonore site and the design of the heat pump system. The sustainability and the potential of the geothermal resource were further evaluated by developing a hydrogeological numerical model used to simulate the dewatering flow rate and temperatures throughout the life of the mine (Hamm et Sabet, 2010; Madiseh et al., 2012; Raymond et Therrien, 2014; Loredo et al., 2016).

Site assessment and Water Quality

Four sites were evaluated, and the most favourable conditions are found at the dewatering outlet zone, with a mean flow rate of $299 \text{ m}^3 \text{ h}^{-1}$ and a mean temperature of 12.1°C . Likewise, it is the closest site to the underground workings, which reduces the distance the water must travel and in turn, minimizes heat loss.

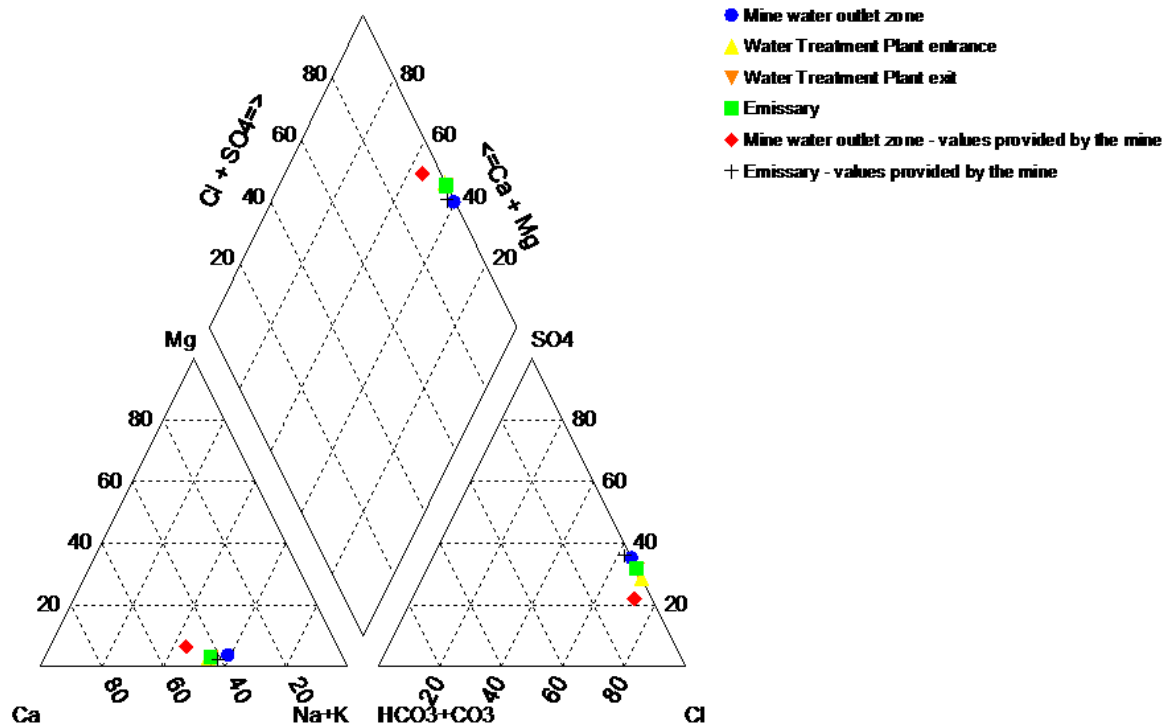
According to the hydrochemical data collected by the mine from 2014 to early 2017 and the calculated scaling and corrosion indices, the water transitions from slightly scale forming and corrosive at the dewatering outlet zone to more corrosive at the emissary. At the dewatering outlet zone, the water is very hard, has a higher concentration of $\text{Ca}^{2+} + \text{Mg}^{2+}$, and possesses a slightly basic pH of 8.1. These properties can be slight scale forming, as shown by the Langelier and Ryznar indices, which suggest that water is oversaturated with respect to calcite. Furthermore, the concentration of Cl^- , the high content of total dissolved solids, and the $\text{Ca}^{2+}/\text{Ca}^{2+} - \text{SO}_4^{2-}$ ratio, which is higher than 0.5, suggest that a carbonate source other than gypsum, such as the addition of alkalis to water to increase the pH is responsible for the high content of calcium ions (Hounslow, 1995). Also, according to the Puckorius index, which removes the buffering capacity of water, the potential for corrosion is high. Similarly, the Larson-Skold index reports a high corrosion potential due to the significant concentration of Cl^- and SO_4^{2-} . A critical issue found at the dewatering outlet zone compared to other sites is that the water has not been treated, and as a result, it contains a high amount of total suspended solids ($2.5 - 5.2 \text{ g L}^{-1}$), which constitutes a clogging risk for the plate heat exchanger.

Once the water reaches the emissary, there is a decrease in $\text{Ca}^{2+} + \text{Mg}^{2+}$, hardness, alkalinity and pH. The negative Langelier and Ryznar indices indicate that the water is now undersaturated with respect to calcite. Furthermore, there is an increase in $\text{Na}^+ + \text{K}^+$, Cl^- , and SO_4^{2-} . The gain in $\text{Na}^+ + \text{K}^+$ indicates that water is transitioning to a primarily brackish-saline type of water (Hounslow, 1995; Nordstrom et al., 2015). This change is induced as groundwater flows and interacts with the crystalline bedrock (water-rock interactions). Meanwhile, the increase in Cl^- and SO_4^{2-} can exacerbate the risk of corrosion. There is also a decrease in total suspended solids and pH, accompanied by an increase in total dissolved solids and conductivity, which suggest the release of ions in solution. Pyrite oxidation is a possibility since the water displays a decrease in iron, pH decreases from 7.1 to below 5.3, SO_4^{2-} concentration increases and the $\text{Ca}^{2+}/\text{Ca}^{2+} - \text{SO}_4^{2-}$ ratio is less than 0.5 (Hounslow, 1995; Rimstidt et Vaughan, 2003; Nordstrom et al., 2015). However, since the decrease of pH was registered several months after the initial measures, this particular phenomenon currently does not pose a risk to the system given that pH is presently neutral, and

the residence time of water inside the system is minimal. Nevertheless, as a result of all the changes in the composition of water at the emissary, the scaling and corrosion indices report a higher risk of corrosion compared to the dewatering outlet zone. Constant monitoring of water quality is critical since the water displays a tendency to decrease in pH, and the concentration of total key species conducive to corrosion is high (Hounslow, 1995; Nordstrom et al., 2015; Nogara et Zarrouk, 2018).

Chemical data from both sites were further analyzed with the Aquachem hydrochemical analysis software to examine the origin, hydrogeochemical facies, and the evolution of the water from the outlet zone to the emissary (Waterloo Hydrogeologic, 1999). Results indicate that the water at the dewatering outlet zone of the Éléonore mine is of the type Ca-Na-Cl. In a Piper diagram, the water plots between the Ca-Mg-SO₄ region, characteristic of mature mine water or leachates, and the Na-Cl region attributed to saline water (Figure 5.1). This water is located at the limit of both regions since it displays a lower content of Ca²⁺ and SO₄²⁻ and a higher concentration of Na⁺, K⁺ and Cl⁻ than typical mature mine water. A similar type of medium salinity mine water has been reported in other mines around the world and deep mines located in crystalline rocks, notably in the Canadian Shield (Fritz et Frape, 1982; Frape et al., 1984; Nuttall et Younger, 2004; Janson et al., 2009; Lghoul et al., 2014; Rivera, 2014). This type of water was also observed in the region of Saguenay-Lac-Saint-Jean, Québec by Walter et al. (2017). Both, the water in the Saguenay-Lac-Saint-Jean region and the mine water at the Éléonore mine show Na⁺/Cl⁻ depletion along with Ca⁺/Cl⁻ and Ca⁺/Na⁺ enrichment relative to seawater, which has been observed in deep brackish-saline groundwater aquifers in the Canadian Shield (Frape et al., 1984; Frape et Fritz, 1987). According to Gascoyne and Kamineni (1994), Gascoyne (2004), and Walter et al. (2017) the salinization is a possible product of prolonged low-temperature water/rock interaction, where the surface groundwater (Ca-HCO₃⁻) infiltrates the subsurface, then evolves into Na-HCO₃⁻ water and finally into Ca-Na-Cl type groundwater commonly found below 1000 m. The Na-Ca-Cl-SO₄²⁻ type water, water with slightly higher salinity and greater concentrations of SO₄²⁻ compared to the water at the outlet zone, may also be found at depth in the Canadian Shield as a consequence of sulphide rock weathering or oxidation. The latter type of water is found at the emissary of the Éléonore mine.

Eleonore mine water hydrochemistry



Eleonore mine water hydrochemistry

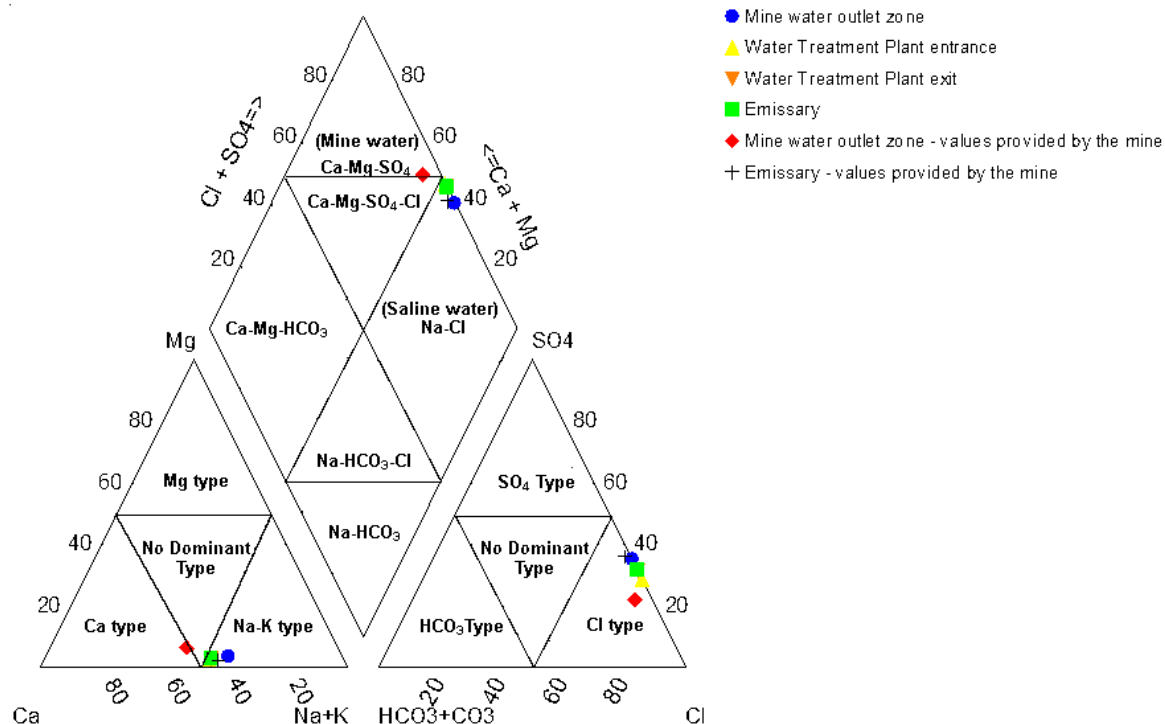


Figure 5.1: Piper diagram of the Éléonore mine water

Ultimately, water with characteristics similar to the waters present at the Éléonore mine can be found deep in the Canadian Shield and other mining sites around the world. According to the calculated scaling and corrosion indices, this type of mine water is slightly scale forming and predominantly corrosive. This information can serve as a guideline in preventing water quality issues by aiding in the design of geothermal heat pump systems for mining operations located in a similar context. Notwithstanding, it is important to keep in mind that the Langelier, Ryznar and Puckorius scaling indices were created to predict calcium carbonate scale in potable water, not scaling by other calcium salts. Also, although the use of these indices as indicators of the corrosion risk is common, their application for the prediction of corrosion in geothermal heat pump systems is not suggested (Rafferty, 2004a). Furthermore, these indices do not consider the flow rate, which is essential in scaling and corrosion. Higher temperatures and lower flow rates are ideal conditions for scale deposition (American Society of Heating et Air-Conditioning Engineers, 2015). The risk of corrosion, on the other hand, increases with a lower pH, as well as higher temperature and flow rate (Karlsdóttir, 2012). At the Éléonore mine, although water temperature is low, the dewatering flow rate is high, and the pH decreases with time. At other mines, temperature and flow rate can vary significantly depending on the local geothermal gradient and dewatering needs. On the other hand, the pH of saline mine waters typically varies from 6.5 to 9 (Nordstrom et al., 2015). It is recommended that these indices be used as possible and not absolute states. Thus, results should be verified with actual conditions of wells and conduits at the mine. Despite these limitations, the scaling and corrosion indices indicate a potential for slight scale formation and significant corrosion, and the heat pump system was designed accordingly.

Geothermal Heat Pump System Design

Since the dewatering outlet zone displays the highest mean flow rate and temperature conditions, a lower risk of corrosion, and is closest to the underground workings, the GHPs was explicitly designed for this location (Figure 5.2). A system located at the surface, nearest to the production shaft, seems to be the most effective location, according to Uhlík and Baier (2012). Nonetheless, the proposed system can be adapted and installed at any of the other locations. A report addressing a GHPs proposed for the water treatment plant is found in Appendix VIII.

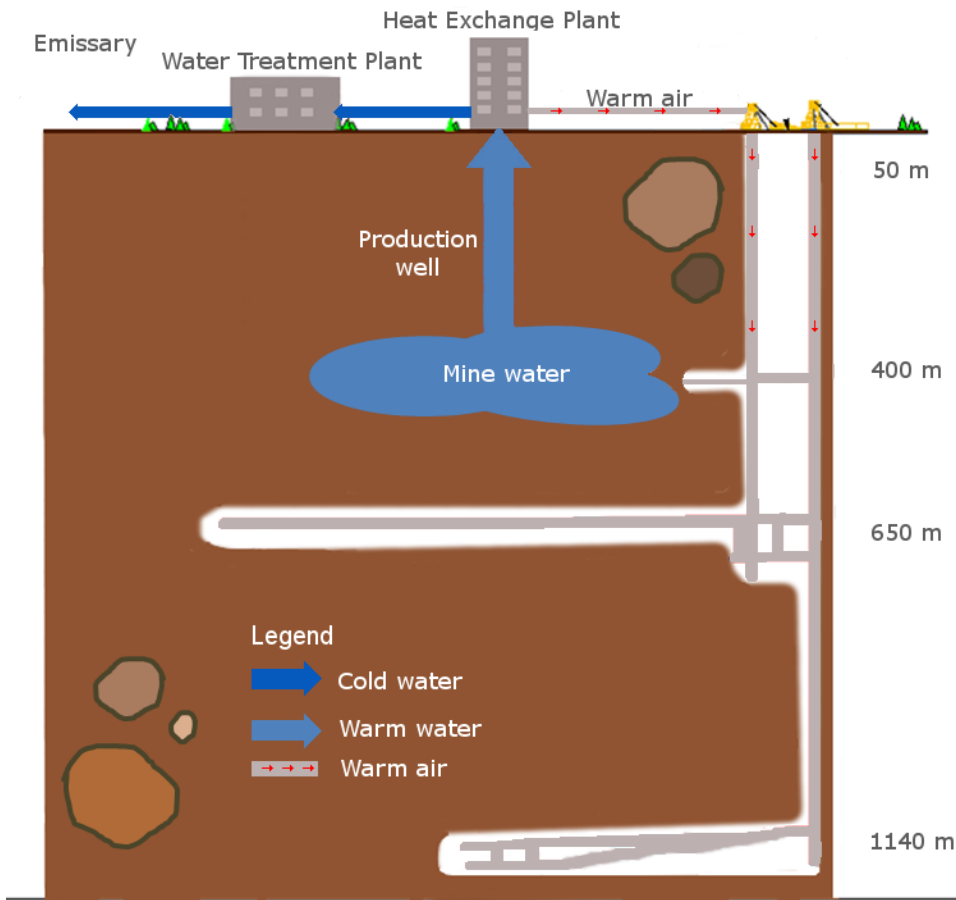


Figure 5.2: Schematic depiction of the geothermal system configuration proposed for the Éléonore mine.

An essential aspect of the design of an open geothermal heat pump system is the entering groundwater flow rate. In most heat pump system designs, the optimum entering groundwater flow rate must be determined first (Kavanaugh et Rafferty, 2014). Thus, the number of pumps, their location and the flow rate are configured to optimize heat extraction and costs. In geothermal systems, often a single submersible pump is assigned for injection and another for production, or in the case of a system with no reinjection, a single pump suffices. The number of pumps is usually kept to a minimum to reduce the overall electricity consumption of the system. In an active mine, the primary purpose of pumping is to dewater the underground workings to allow for efficient and safe work. The flow rate is pre-established according to the dewatering requirements. As the mine develops, the number of pumping stations and the dewatering flow rate are set as needed. Hence, at the Éléonore mine, the heat pump system was designed as a function of the minimal, maximal, and mean flow rate. Each of the three modules in the system is activated or deactivated according

to the entering water flow rate, making it capable of handling the minimum and maximum flow rates ranging from $80 \text{ m}^3\text{h}^{-1}$ to $481 \text{ m}^3\text{h}^{-1}$. As a result, the heat pump system has a constant output of energy. The approach temperature, which increases efficiency as the approach decreases, was fixed at 1.1°C (Kavanaugh et Rafferty, 2014). The heating coefficient of performance (COP) of heat pumps ranges typically from 3 to 6 and is most common in the range of 3 – 4.0 (Farr et al., 2016; Banks et al., 2017; Al-Habaibeh et al., 2018). To increase energy gain and decrease electricity consumption, the average heating COP of the proposed heat pump system is 5.6. Groundwater exiting the system is discharged into the sedimentation pond at a mean temperature of 6.7°C and subsequently flows to the water treatment plant, minimizing the environmental risk associated with the disposal of mine water and groundwater used for heating purposes.

All the major components of the GHPs are anticipated to be made of type 316 stainless steel to prevent issues associated with the risk of corrosion, as recommended by Kavanaugh and Rafferty (2014) and Rafferty (2004a). Furthermore, the system can also be equipped with a plate heat exchanger made of type 304 and 316 stainless steel to prevent mine water flowing directly into the evaporator. A geothermal heat pump system with similar specifications and materials was implemented at the Barredo abandoned mine in Spain (Lara et al., 2017). Furthermore, to reduce clogging issues due to the high total suspended solids content in untreated mine water, the plate heat exchanger would need to be disassembled occasionally for maintenance, and a filtering system capable of filtering 95% of the total suspended solids could be installed at the entrance of the exchanger (Rafferty, 2004a). A monitoring procedure could be employed to prevent fouling or clogging issues and to pinpoint the most appropriate time to execute the maintenance of the system, such as during the periods when the heating demand is low. Temperature and flow rate sensors could be incorporated into the GHPs to monitor the flow rate and temperature of the groundwater and the secondary heat-carrying fluid entering and exiting the system as proposed by Gjengedal et al. (2019). The initial performance of the system would be tested and utilized as a baseline to be compared to the actual performance of the system regularly. Unexpected variations in conditions and decline in overall performance would be used to specify the location along with the issue affecting the system. The surveillance procedure was proposed for open-loop GHPs used for district-heating systems with or without reinjection, containing a production well, an intermediate heat exchanger, and a heat pump unit. Nevertheless, the same monitoring program could be integrated into geothermal systems adapted for dewatering operations in active or inactive mines, since the components of the geothermal system are the same. Moreover, a compelling advantage for mines, which are often situated in remote or isolated locations, is that

the system can be tested in a few hours without having to stop the heat pump, and the conditions can be tracked off-site through the Internet.

As part of a holistic approach to reduce water quality issues and optimize system performance, in addition to a surveillance procedure, the geothermal heat pump system adapted to the dewatering system could incorporate a second plate heat exchanger set-up in parallel. An extra plate heat exchanger, which costs an additional \$CAD25 000, could ensure the continuous operation of the GHPs by redirecting the entering groundwater to the plate heat exchanger on standby while the other undergoes maintenance. This strategy is currently in use at a smaller scale in the National Coal Mining Museum in the United Kingdom (Athresh et al., 2016).

Finally, the possibility of replacing the plate heat exchanger with a shell and tube exchanger, which is capable of handling a greater amount of suspended solids, was discussed with the company TRANE. A similar approach was taken at the Barredo mine, where a shell and tube exchanger was installed instead of a plate heat exchanger, as the latter displayed significant accumulation of solids and required cleaning between 2 and 4 times per year. The shell and tube heat exchanger requires less cleaning relative to a plate heat exchanger, and under certain conditions, their efficiency can approach that of plate heat exchangers. Nevertheless, the efficiency of shell and tube heat exchangers has been reported to be 10 to 20% lower than plate heat exchangers (Bergman et Incropera, 2011; Walraven et al., 2014; Directorate-General for Research and Innovation - European Commission, 2019).

Performance Assessment

The feasibility of using mine water from abandoned mines has been widely studied (Banks et al., 2017; Álvarez et al., 2018; Menéndez et al., 2020). The energy available in abandoned (closed) flooded mines has been previously extracted successfully in Canada, Germany, Spain, the United Kingdom, and the United States for district heating (Jessop et al., 1995; Watzlaf et Ackman, 2006; Loredo et al., 2017). Recently, at the flooded Barredo mine in Spain, where groundwater temperature averages 20 °C, a GHPs with a COP of 6.7 was estimated to generate approximately 13,700 MWh year⁻¹(Ordóñez Alonso et al., 2010).

In the case of active mines, the energy extracted from the water exiting the dewatering system would be used for operations in the mine. According to Ghomshei and Meech (2005), 1 to 10 MW of energy could be available in operating mines.

In this study, a complete GHPs system was designed for the dewatering system of the active Éléonore mine. The system, located at the dewatering outlet zone, could generate between

9,471 MWh and 10,283 MWh year⁻¹ or provide a power of 12 MW to 13 MW, which represents 35 to 39% of the underground workings total heating demands. Heating costs would decrease by 33% or \$CAD514 000 in net annual savings. Additionally, the incorporation of this system would decrease propane consumption by 1.36 million litres per year, resulting in an offset of 1,993 tonnes of CO₂ annually. The capital cost for the purchase of the heat pump, including all the components related to the plate heat exchanger and the heat pump, is \$CAD 325 000. The price does not include the costs of installation, operation & maintenance, or inflation. Future research initiatives should include a complete life-cycle cost analysis to assess the economic feasibility of this type of system.

The calculations only consider energy produced during the months of the year, which require heating, from October to April. Higher quantities of energy are available throughout the rest of the year. The available energy could be employed for various underground or surface activities, such as air-conditioning during the summer, water heating, or minimizing fog build-up at the ramp entrance. Additionally, the performance was assessed using data from 2015 and 2016. The mean dewatering flow rate has increased since, resulting in greater amounts of energy available. Finally, energy losses incurred by downtime due to maintenance and the rise in energy demand due to the development of the mine must be taken into consideration in future analysis.

Geothermal Resource Sustainability and Potential

The three-dimensional transient saturated numerical model was developed with HydroGeoSphere as a means to assess the sustainability and the geothermal potential by simulating the evolution of the dewatering flow rate and temperature. Groundwater flow and heat transfer are simulated in a three-dimensional equivalent porous media where underground workings and wells are represented with highly conductive one-dimensional elements, as was done by Raymond and Therrien (2008). Thermal properties essential for heat transport modelling such as thermal conductivity and specific heat capacity were measured in the laboratory and subsequently calculated. The mean thermal conductivity of 2.54 W m⁻¹ K⁻¹ measured in this study for the two main units in the area, coincides with the mean thermal conductivity of 2.5 W m⁻¹ K⁻¹ measured by Lévy et al. (2010) at the Éléonore mine. Heat flux and geothermal gradient were both taken from the latter source. Remaining properties were obtained from the literature and later modified to calibrate the model against the estimated groundwater level and observed dewatering temperature.

The numerical model simulates an open-loop geothermal system without reinjection since, in the proposed system, the water circulates towards the heat pump and is disposed of in one of the

basins located before the water treatment plant. The absence of an injection well is advantageous as it decreases the thermal depletion observed in open geothermal systems with reinjection (Malolepszy et al., 2005; Renz et al., 2009). The risk of thermal short-circuiting is not an important concern like it can be for closed mines. Nevertheless, once pumping starts, an open-loop system without reinjection does display a slight decrease in temperature as shallow groundwater infiltrates the region of the underground workings. After the temperature drop, the overall temperature eventually stabilizes after the colder water from the surface mixes with deeper warmer water. Such a system was simulated and deemed optimal for geothermal heat extraction in underground flooded mines by Andrés et al. (2017), Uhlík and Baier (2012), and Baier et al. (2011).

Similar behaviour is seen in the results of the Éléonore mine numerical model, at the beginning of the dewatering operations. Once pumping starts, the region around the underground workings acts as a preferential pathway and displays the most significant change in head and drawdown. Furthermore, there is an inflow of shallow colder water, since water is pumped exclusively from the 400 m level. The resulting mean temperature during the first year of dewatering is 7.3 °C, which is five degrees Celsius lower than the present mean dewatering temperature. However, an important distinction emerges between numerical models developed for open-loop systems adapted for closed flooded mines and one for an active mine. In an active mine, as work progresses, pumps with varying flow rates are established in deeper locations, where the water temperature is higher due to the geothermal gradient and the insulating effect of the ground. Thus, the overall dewatering flow rate increases, and as deeper warmer water is pumped towards the 400 m level, the upward convection of warm water increases the temperature at the base of the model, as evidenced by the rising temperature isolines (Figure 5.3). At the 400 m level, the water is mixed with the shallow colder water and finally sent to the surface, resulting in a mean dewatering temperature of 12.1 °C. The dewatering temperature could rise further, as pumping depth increases. Even though the temperature at depth is higher and overall flow rate increases, the dewatering flow rates at depth are significantly lower than flow rates at the main pumping stations situated close to the surface given that water infiltration is greater in the uppermost levels. Thus, temperature increases initially, then reaches a plateau and remains near-constant throughout the life of the mine, with only a 0.3 °C increase from 2019 to 2031. Several parameters were modified during the sensitivity analysis, but the dewatering temperature remains stable throughout the simulation period.

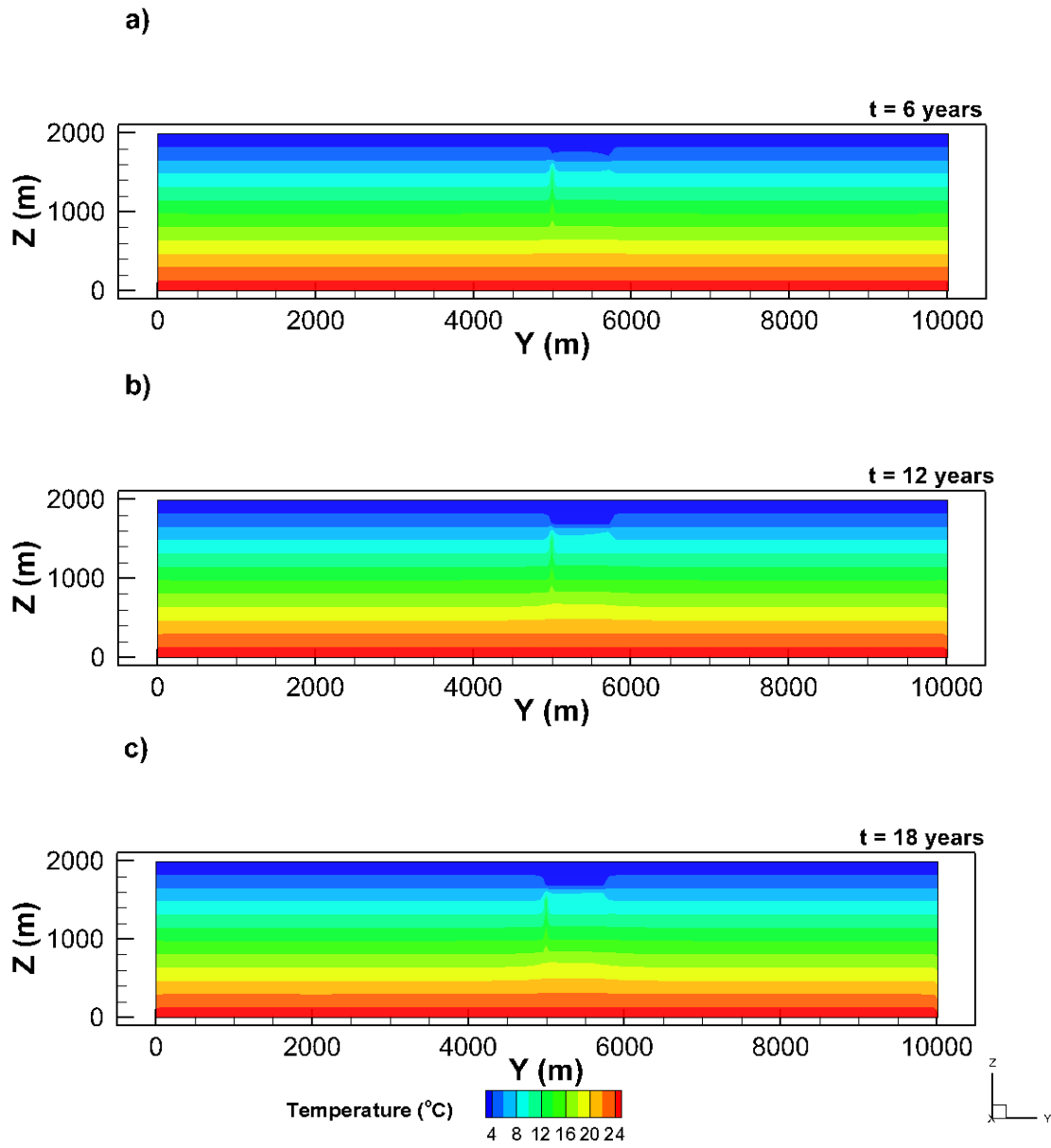


Figure 5.3: Simulated temperature in the underground workings after a) 6, b) 12, and c) 18 years.

The total dewatering flow rate, which has a significant influence on groundwater flow and the amount of energy produced by the heat pump, is predicted to increase from the observed value of $336.5 \text{ m}^3 \text{ h}^{-1}$ in 2016 to the expected maximum of $718 \text{ m}^3 \text{ h}^{-1}$ in 2024. Although there is inherent uncertainty regarding the evolution of the dewatering flow rate, according to information provided by the mine, a flow rate of $410 \text{ m}^3 \text{ h}^{-1}$ has been reached. The latter flow rate approaches the maximum operating flow rate of the proposed GHPs system, which denotes that it is possible to generate the predicted energy values needed to reach a penetration level, or the percentage of energy that can be supplied by the GHPs system relative to the total amount of heating energy

required by the underground workings, of 45%. This, in turn, would further reduce net annual expenses, carbon emissions and the payback period.

It appears that apart from heat flux and the geothermal gradient, the depth and the proportion of the total volume of water each pump handles have a significant influence on the dewatering temperature. For instance, results suggest that at the studied site, the mean dewatering temperature would be 10.2 °C if only the 400 level pump were in service. Flow rate, on the other hand, has a significant impact on groundwater flow and heat pump performance. All these factors play a vital role in the long-term sustainability and the dewatering geothermal potential of an active mine. At the Éléonore mine, the results suggest that the mean dewatering temperature will remain near 12 °C to 12.3 °C throughout the life of the mine, which is optimal for heat extraction. Moreover, since the mine is situated underneath the Opinaca reservoir, the abundant quantities of water infiltrating the mine and the required dewatering flow rate constitute suitable conditions for the installation of a geothermal system. In the case of other active mines, a thorough study is required in a case-by-case basis, given that heat flux, geothermal gradient, mine depth, pumping configuration, and dewatering flow rate depend on mine location, the type of mine, the depth of mineralization, the water inflow and the stage of life of the mine.

Strengths, Weaknesses, Opportunities and Threats (SWOT) Analysis

The overall strengths, weaknesses, opportunities, and threats (Table 5.1) of implementing a GHPs system at the Éléonore mine are shown in the following sections.

Strengths

A geothermal heat pump system is a technology that has been employed successfully in various settings. It is being utilized successfully for district heating in abandoned flooded mines. In this study, a GHPs was designed specifically for the dewatering system of an active mine. The system has no reinjection well, and water is discharged at a water basin located before the water treatment plant, reducing overall environmental risks and legislative constraints. Also, since the system is coupled to the existing dewatering system, no additional drilling is required, and investment costs could be reduced significantly. Further, the heat pump, equipped with an intermediate heat exchanger and installed at the exit of the dewatering system, where water exits at a mean of 12.1 °C and $299 \text{ m}^3 \text{ h}^{-1}$, could provide 39% of the 26.6 GWh/year needed to heat the underground workings. The supply of energy would be constant, given the high capacity factor of geothermal heat pumps. The high efficiency of the system could reduce costs by 33%, equivalent to \$CAD 514K. Moreover, due to its low emissions, propane consumption could be reduced by

1.36 million litres annually, and carbon dioxide emissions could decrease by 36% or 1,993 tons per year. Also, the hydrogeological numerical model developed for the Éléonore mine suggests that the dewatering temperature will remain stable, and the dewatering flow rate will increase. Thereby, the geothermal heat pump system adapted for the dewatering system of the mine is sustainable throughout the life of the mine and could attain a penetration level of 45% once the GHPs system reaches its maximum output, which would further decrease costs by \$CAD 700K annually. Since the heat pump system is highly modular, it could be modified to handle the increasing flow rate and can also be adapted for other locations in the mine. The purchase costs of the geothermal heat pump system, including intermediate heat exchanger, evaporator and condenser, is \$CAD 325K. Finally, from a circular economy standpoint, at the end of life of the mine, the geothermal equipment can be re-used at other sites with adequate characteristics.

Weaknesses

The primary technical challenge is the corrosion and clogging risk of the system due to the mine water. As a result, the system was designed with corrosion-resistant materials. Correspondingly, maintenance of the system is required, but the incorporation of a monitoring program can determine the best period to schedule maintenance, such as during periods of low heating demand. A second intermediate heat exchanger set in parallel could also be incorporated to reduce further issues related to water quality and ensure the constant output of heating. From an economic standpoint, renewable energy projects may have higher capital expenditure (CAPEX) and operating expenses (OPEX) than fossil fuels, especially given the northern and remote locations of many mining projects. Furthermore, the mine life span and the time of inception of the project plays a crucial role in the economic feasibility. The longer the life span of the mine and the earlier the alternative energy project is implemented, the greater the chances for positive economic returns. For this reason, the study for the possible installation of a GSHP at an active mine is recommended during the development and design phase, and its installation is preferred before the mine is operational. Nevertheless, the performance of the system depends on individual site conditions, and it can still be feasible once production has started. Thus, a complete techno-economic analysis must be performed on a case-by-case basis to establish the viability of the project.

Opportunities

At the Éléonore mine, the extra energy produced by the GHPs during the warmer months of the year, from May to September, could be employed to air-condition the underground workings during the summer and to minimize fog build-up at the ramp entrance. Also, with certain modifications, the geothermal system can be installed at other locations such as the exit of the water treatment plant to provide heating and air-conditioning for nearby surface infrastructure. Although the installation of this type of system would be more convenient prior to the start of production, it can also be implemented in existing mines that are set to expand and require additional energy. There are various opportunities to finance the implementation of such a project, for instance, the *ÉcoPerformance* program offered by Québec's provincial government through *Transition Énergétique Québec*. Finally, through the integration of alternative sources of energy, mining companies can strengthen their corporate identity, and active mines in northern and remote locations can increase energy security by decreasing the risk associated with the future cost of fossil fuels and logistics.

Threats

Some of the factors that can prevent the implantation of a geothermal heat pump system as a source of heating would be a lack of interest from decision-makers due to the relative newness of this approach in active mines, lower prices of fossil fuels, and the lack of government policies that stimulate investment in alternate energy sources. Policies could specify that a certain percentage of the energy in mines be produced with renewable energy.

Table 5.1: Strengths, Weaknesses, Opportunities, and Threats (SWOT) analysis of implementing a geothermal heat pump system at the Éléonore mine.

Strengths	Weaknesses
<ul style="list-style-type: none"> - The GHPs could provide 39% of the 26.6 GWh/year needed to heat the underground workings. - Annual heating costs could be reduced by 33%, equivalent to CAD\$ 514K. - Propane consumption could be reduced by 1.36 million litres annually. - CO₂ emissions could decrease by 36% or 1993 tons per year. - The geothermal system adapted to the mine's operations is sustainable throughout the life of the mine. - Since the dewatering system is already present, the installation of the GHPs does not require drilling. - At the end of the life of the mine, the geothermal equipment can be repurposed at other sites with adequate characteristics. - GHPs systems have been employed successfully for district heating in abandoned flooded mines. - Decreased risk associated with the future cost of fossil fuels and logistics issues. 	<ul style="list-style-type: none"> - The primary technical challenge is the corrosion and clogging risk due to the mine water. - Renewable energy projects can have higher capital expenditure (CAPEX) and operating expenses (OPEX) than fossil fuels, especially given the northern and remote locations of many mining projects. - This study was done once the mine had started production, but the evaluation and installation of a GHPs should preferably be done before the mine is operational.
Opportunities	Threats
<ul style="list-style-type: none"> - There are various opportunities to finance the implementation of this project, for example, the <i>ÉcoPerformance</i> program offered by Québec's provincial government through <i>Transition Énergétique Québec</i>. - The integration of alternative sources of energy can strengthen the corporate identity of mining companies. - Active mines in northern and remote locations can increase energy security by diversifying their sources of energy. - The GHPs could be employed to air-condition the underground workings during the summer. - The GHPs could also be utilized as a source of heating or air-conditioning for other surface activities. - A GHPs could be installed if the mining project expands and the heating demand increases. 	<ul style="list-style-type: none"> - Lack of interest from decision-makers due to the relative newness of this approach in active mines. - Low fossil fuel prices. - Lack of governmental policies that stimulate investment in alternate energy sources.

6 CONCLUSIONS

Unlike mining projects located at lower latitudes, a contributor to production costs for active mines in northern regions is the need to heat the underground workings seven to eight months a year due to the cold weather conditions to maintain operations and to ensure the safety of the workers. Nevertheless, in a northern context, infrastructure is lacking, electric power transmission lines are on occasions unavailable, and their construction is not economically viable owing to the significant distances separating the energy source and the mining project. In cases where the power grid is accessible, heating with an electrical system is not economical because of the high power demand. As a result, fossil fuels currently stand as the primary source of energy for mining projects, but the environmental consequences present a challenge. Efforts must be undertaken in an attempt to establish sustainable mining operations while increasing profitability. Some mines in northern Canada have already incorporated alternative energy sources (Vision Biomasse Québec, 2015; Bertoli, 2015; Natural Resources Canada, 2018a, 2019b), such as wind and biomass, which have reduced fossil fuel consumption and greenhouse gas emissions. For instance, at the Casa Berardi mine in the James Bay municipality in the Abitibi region, a biomass system has been reported to reduce propane consumption by 1.9 M litres per year. Meanwhile, at the Raglan mine in Nunavik, Québec, a wind turbine system with energy storage reduced diesel consumption by 2.2 M litres annually and has displaced 6,000 tons of greenhouse gases per year. Geothermal heat pump systems are low-emission, have a high capacity factor, and are highly efficient. Such systems have been successfully implemented for district heating in abandoned flooded mines around the world, but a complete technical assessment of the geothermal dewatering potential in active mines has not been reported. Therefore, to contribute to the energy transition of the mining industry, this study aimed to provide a technical portrait of geothermal heat pump systems as an eco-conscious, affordable, constant, and accessible source of heating for mines operating in a northern context. The Éléonore mine of Newmont-Goldcorp, an active mine located in the Eeyou-Istchee James Bay territory, was selected as a case study. The geothermal potential was assessed by designing a GHPs system adapted to the conditions at the dewatering system. A hydrogeological numerical model aided in evaluating the sustainability and the energy available during the life of the mine. Under present conditions, a system equipped with an intermediate heat exchanger installed at the exit of the dewatering system could provide 39% of the 26.6 GWh/year needed to heat the underground workings, reducing heating costs by 33% and greenhouse gas emissions by 1993 tons/year. The hydrogeological numerical model developed for the Éléonore mine suggests that a geothermal heat pump system adapted for the

dewatering system of the mine is sustainable throughout the life of the mine and could supply up to 45% of the underground workings heating demands in the upcoming years. Thus, this research indicates that with adequate assessment, geothermal heat pump systems can be adapted to active mining operations in a northern context and can contribute to their energy needs in an environmental, affordable, and constant manner.

Perspectives and recommendations

A geothermal heat pump system adapted to the dewatering system of an active mine appears technically feasible and sustainable throughout the life of the mine under the given conditions of water temperature and flow rate. The water quality constitutes the major technical challenge, but it can be managed with adequate prevention and mitigation measures. Furthermore, the brackish-saline characteristics of the mine water at the Éléonore site is typically found in the Canadian Shield and is likely to be found in other mines. Notwithstanding, other active mines should be studied on a case-by-case basis, since critical factors influencing the geothermal potential depend on the local heat flux, geothermal gradient, mine depth, mine water quality, pumping configuration, and dewatering flow rate can vary across locations. Overall, the proposed geothermal heat pump system can significantly contribute to the heating needs of the Éléonore mine in an ecological, affordable, consistent, and sustainable manner. This research can serve as a guideline and point of comparison in the evaluation of the dewatering geothermal potential of other active mines situated in northern regions, as well as to aid in the design of geothermal heat pump systems for operating mines with similar water properties. Finally, the implementation of this pilot project at the Éléonore mine, which could be supported by various stakeholders, would provide the operational data needed to validate the results, contributing thus to the integration of alternative sources of energy in the mining industry.

Future research is needed to establish the economic viability of the geothermal heat pump system as an alternative energy source for the Éléonore mine. Moreover, it is necessary to investigate the cooling potential of the GHPs during the warmer months of the year. Likewise, new studies could be done to evaluate the operational performance of the water quality monitoring system and the two intermediate heat exchangers working in parallel. The research could further study water quality at other active mining sites to create a database of mine water that could be analyzed and verified against actual conditions to create a tool better suited to ascertain the risk of scaling and corrosion of mine water. Ultimately, other active mines and future mining projects in the early phases of development should be identified to assess the feasibility of implementing the geothermal heat pump technology as a contributor to the energy needs of mining operations.

7 BIBLIOGRAPHY

- Aachener-Zeitung. (2018). Geothermie aus Grubenwasser: Alter Schacht wird aufgebohrt. <https://bit.ly/2FJPlpp> (Accessed: 28/03/2019).
- Adams, R., & Younger, P. (2001). A strategy for modeling ground water rebound in abandoned deep mine systems. *Groundwater*, 39(2), 249-261. <https://doi.org/10.1111/j.1745-6584.2001.tb02306.x>
- Al-Habaibeh, A., Athresh, A. P., & Parker, K. (2018). Performance analysis of using mine water from an abandoned coal mine for heating of buildings using an open loop based single shaft GSHP system. *Applied Energy*, 211, 393-402. <https://doi.org/10.1016/j.apenergy.2017.11.025>
- Álvarez, R., Ordóñez, A., García, R., & Loredo, J. (2018). An estimation of water resources in flooded, connected underground mines. *Engineering Geology*, 232, 114-122. <https://doi.org/10.1016/j.enggeo.2017.11.016>
- American Society of Heating, R., & Air-Conditioning Engineers, I. (2015). ASHRAE Handbook - Heating, Ventilating, and Air-Conditioning Applications (SI Edition). In *Chapter 49, Water Treatment: Deposition, Corrosion, and Biological Control* (pp. 1-22): American Society of Heating, Refrigerating and Air-Conditioning Engineers, Inc. <https://www.ashrae.org/technical-resources/ashrae-handbook>
- Amiri, L., Hassani, F., & Ghoreishi-Madiseh, S. A. (2016). *Harvesting geothermal energy from active mines of Canada; a field study*. Paper presented at the Canadian Institute of Mining, Metallurgy and Petroleum Convention, Ottawa, Ontario.
- Andrés, C., Ordóñez, A., & Álvarez, R. (2017). Hydraulic and Thermal Modelling of an Underground Mining Reservoir. *Mine Water and the Environment*, 36(1), 24-33. <https://doi.org/10.1007/s10230-015-0365-1>
- Athresh, A. P., Al-Habaibeh, A., & Parker, K. (2016). The design and evaluation of an open loop ground source heat pump operating in an ochre-rich coal mine water environment. *International Journal of Coal Geology*, 164, 69-76. <https://doi.org/10.1016/j.coal.2016.04.015>
- Baier, J., Polák, M., Šindelář, M., & Uhlík, J. (2011). *Numerical modeling as a basic tool for evaluation of using mine water as a heat source* (Vol. 143): WIT Press <https://doi.org/10.2495/ESUS110071>.
- Bailey, M. T., Gandy, C. J., Watson, I. A., Wyatt, L. M., & Jarvis, A. P. (2016). Heat recovery potential of mine water treatment systems in Great Britain. *International Journal of Coal Geology*, 164, 77-84. <https://doi.org/10.1016/j.coal.2016.03.007>
- Bandyayera, D., Rhéaume, P., Maurice, C., Bédard, É., Morfin, S., & Sawyer, E. (2010). *Synthèse géologique du secteur du réservoir Opinaca, Baie-James* (RG 2010-02). Québec, Canada. <http://collections.banq.qc.ca/ark:/52327/1998821>
- Banks, D., Athresh, A., Al-Habaibeh, A., & Burnside, N. (2017). Water from abandoned mines as a heat source: practical experiences of open- and closed-loop strategies, United Kingdom. *Sustainable Water Resources Management*, 5(1), 29-50. <https://doi.org/10.1007/s40899-017-0094-7>

- Beausoleil, C., Fleury, D., Fortin, A., Brisson, T., & Joncas, L. (2014). *Éléonore Gold Project Quebec, Canada* (Technical Report NI 43-101). Québec, Québec. <https://bit.ly/2MBDQnm>
- Belzile, P., Comeau, F.-A., Raymond, J., & Lamarche, L. (2017). *Revue technologique: efficacité énergétique et énergies renouvelables au nord du Québec*. Institut national de la recherche scientifique. Québec, Canada. <http://espace.inrs.ca/id/eprint/5308>
- Bergman, T. L., & Incropera, F. P. (2011). *Fundamentals of heat and mass transfer* (6th ed.). Hoboken, NJ: John Wiley & Sons <https://bit.ly/2Yvk4IX>.
- Bertoli, C. (2015). *Parc éolien de Diavik*. Rio Tinto. Montréal, Québec, présentation. <https://bit.ly/2WDHxLm>
- Blessent, D. (2009). *Integration of 3D Geological and Numerical Models Based on Tetrahedral Meshes for Hydrogeological Simulations in Fractured Porous Media*. (Doctoral dissertation), Université Laval, Québec, Québec. <http://hdl.handle.net/20.500.11794/21218>
- Charland, A., Perron, M., Rispoli, A., Bussières, M., Bergeron, S. (2018). *Éléonore Gold Project Quebec, Canada* (Technical Report NI 43-101). <https://bit.ly/32K9ULy>
- Comeau, F.-A., Raymond, J., Malo, M. (2017). *Potentiel géothermique du nord du Québec: évaluation préliminaire*. (Rapport : 1660). Institut national de la recherche scientifique. Québec, Québec. <http://espace.inrs.ca/id/eprint/7118>
- Dincer, I., & Zamfirescu, C. (2016). *Drying phenomena: theory and applications* (1st ed.). West Sussex, United Kingdom: John Wiley & Sons <https://doi.org/10.1002/9781118534892>.
- Directorate-General for Research and Innovation - European Commission. (2019). *Sustainable use of flooded coal mine voids as a thermal energy source : a baseline activity for minimising post-closure environmental risks (LoCAL) : final report*. Brussels, Belgium. <https://doi.org/10.2777/715020>
- Domingue, C. (2017). *Modélisation 3D de l'écoulement de l'eau souterraine et évaluation de l'efficacité de différentes méthodes de cimentation pour la réduction d'infiltrations d'eau à la mine Éléonore*. (Master's Thesis), Université Laval, Québec, Québec. <http://hdl.handle.net/20.500.11794/27922>
- Dow Chemicals. (2009). *DOWFROST™ HD Heat Transfer Fluid: Why a Minimum 25% Glycol Concentration is Recommended in GSHP Applications*. Dow Chemical Company. United States. <https://bit.ly/2OXTBVy>
- Farr, G., Sadasivam, S., Manju, Watson, I. A., Thomas, H. R., & Tucker, D. (2016). Low enthalpy heat recovery potential from coal mine discharges in the South Wales Coalfield. *International Journal of Coal Geology*, 164, 92-103. <https://doi.org/10.1016/j.coal.2016.05.008>
- Fontaine, A., Dubé, B., Malo, M., McNicoll, V., Brisson, T., Doucet, D., & Goutier, J. (2015). Geology of the metamorphosed Roberto gold deposit (Éléonore Mine), James Bay region, Quebec: diversity of mineralization styles in a polyphase tectonometamorphic setting. In *Targeted Geoscience Initiative 4: Contributions to the understanding of Precambrian lode gold deposits and implications for exploration* (pp. 209-225). Ottawa: Natural Resources Canada. <https://doi.org/10.4095/296624>
- Frape, S., & Fritz, P. (1987). Geochemical trends for groundwaters from the Canadian Shield. In *Saline water and gases in crystalline rocks* (Vol. 33, pp. 19-38). Ottawa, Canada: Geological Association of Canada.

- Frape, S. K., Fritz, P., & McNutt, R. H. (1984). Water-rock interaction and chemistry of groundwaters from the Canadian Shield. *Geochimica et Cosmochimica Acta*, 48(8), 1617-1627. [https://doi.org/10.1016/0016-7037\(84\)90331-4](https://doi.org/10.1016/0016-7037(84)90331-4)
- Fritz, P., & Frape, S. K. (1982). Saline groundwaters in the Canadian Shield — A first overview. *Chemical Geology*, 36(1), 179-190. [https://doi.org/10.1016/0009-2541\(82\)90045-6](https://doi.org/10.1016/0009-2541(82)90045-6)
- Gascoyne, M. (2004). Hydrogeochemistry, groundwater ages and sources of salts in a granitic batholith on the Canadian Shield, southeastern Manitoba. *Applied Geochemistry*, 19(4), 519-560. [https://doi.org/10.1016/S0883-2927\(03\)00155-0](https://doi.org/10.1016/S0883-2927(03)00155-0)
- Gascoyne, M., & Kamineni, D. C. (1994). The Hydrogeochemistry Of Fractured Plutonic Rocks In The Canadian Shield. *Applied Hydrogeology*, 2(2), 43-49. <https://doi.org/10.1007/s100400050044>
- Ghomshei, M., & Meech, J. (2005). Usable heat from mine waters: Coproduction of energy and minerals from "mother earth". In J. Meech (Ed.), *Intelligence in a Small Materials World* (pp. 401). Lancaster, Pennsylvania: Destech.
- Ghoreishi-Madiseh, S. A., Hassani, F., & Abbasy, F. (2015). Numerical and experimental study of geothermal heat extraction from backfilled mine stopes. *Applied thermal engineering*, 90, 1119-1130. <https://doi.org/10.1016/j.applthermaleng.2014.11.023>
- Gjengedal, S., Ramstad, R. K., Hilmo, B. O., & Frengstad, B. S. (2019). Fouling and clogging surveillance in open loop GSHP systems. *Bulletin of Engineering Geology and the Environment*. <https://doi.org/10.1007/s10064-019-01556-5>
- Golder Associates. (2009). *Hydrogeological study of the proposed underground mine (original 2007 design - 3500 t/day), Eleonore Project*. (Internal report).
- Gouvernement du Québec. (2014). *Règlement sur le prélèvement des eaux et leur protection, RLRLQ c Q-2, r.* Retrieved from <http://www.mddelcc.gouv.qc.ca/eau/prelevements/reglement-prelevement-protection/index.htm>.
- Grasby, S., Allen, D., Bell, S., Chen, Z., Ferguson, G., Jessop, A., et al. (2011). Geothermal energy resource potential of Canada. *Geological Survey of Canada, Open file 6941 (revised)*, 302. <https://doi.org/10.4095/288745>
- Hall, A., Scott, J. A., & Shang, H. (2011). Geothermal energy recovery from underground mines. *Renewable & Sustainable Energy Reviews*, 15(2), 916-924. <https://doi.org/10.1016/j.rser.2010.11.007>
- Hamm, V., & Sabet, B. B. (2010). Modelling of fluid flow and heat transfer to assess the geothermal potential of a flooded coal mine in Lorraine, France. *Geothermics*, 39(2), 177-186. <https://doi.org/10.1016/j.geothermics.2010.03.004>
- Hounslow, A. (1995). *Water quality data: analysis and interpretation* (1st ed.). Boca Raton, Florida: CRC press <https://doi.org/10.1201/9780203734117>.
- Janson, E., Gzyl, G., & Banks, D. (2009). The occurrence and quality of mine water in the Upper Silesian Coal Basin, Poland. *Mine Water and the Environment*, 28, 232-244. <https://doi.org/10.1007/s10230-009-0079-3>
- Jessop, A. M. (1990). Developments in Solid Earth Geophysics: Thermal geophysics. In (Vol. 17). Amsterdam: Elsevier Science Limited. <https://doi.org/10.1016/B978-0-444-88309-4.50006-3>

- Jessop, A. M., Macdonald, J. K., & Spence, H. (1995). Clean energy from abandoned mines at Springhill, Nova Scotia. *Energy Sources*, 17(1), 93-106. <https://doi.org/10.1080/00908319508946072>
- Karlsdóttir, S. N. (2012). 7.08 - Corrosion, Scaling and Material Selection in Geothermal Power Production. In A. Sayigh (Ed.), *Comprehensive Renewable Energy* (pp. 241-259). Oxford: Elsevier. <https://doi.org/10.1016/B978-0-08-087872-0.00706-X>
- Kavanaugh, S. P., & Rafferty, K. D. (2014). *Geothermal heating and cooling: design of ground-source heat pump systems*. Atlanta, GA: American Society of Heating Refrigerating and Air-Conditioning Engineers <https://bit.ly/2GyMrUb>.
- Kavanaugh, S. P., & Rafferty, K. D. (1997). *Ground-source heat pumps : design of geothermal systems for commercial and institutional buildings*. Atlanta: American Society of Heating, Refrigerating and Air-Conditioning Engineers
- Koufos, K. (2012). *Assessing the potential to implement open loop geothermal systems in Canadian underground mines*. (Mémoire de maîtrise), McGill University, Montréal, Québec. <http://digitool.library.mcgill.ca/thesisfile107715.pdf>
- Langelier, W. F. (1936). The analytical control of anti-corrosion water treatment. *American Water Works Association*, 28(10), 1500-1521. <https://doi.org/10.1002/j.1551-8833.1936.tb13785.x>
- Lara, L., Colinas, I., Mallada, M., Hernández-Battez, A., & Viesca, J. (2017). Geothermal use of mine water. *European Geologist*, 43, 40-45. <https://bit.ly/33dVdAi>
- Larson, T. E., & Skold, R. V. (1958). Laboratory studies relating mineral quality of water to corrosion of steel and cast iron. *Corrosion*, 14(6), 43-46. <https://doi.org/10.5006/0010-9312-14.6.43>
- Lefebvre, R., Hockley, D., Smolensky, J., & Gélinas, P. (2001). Multiphase transfer processes in waste rock piles producing acid mine drainage: 1: Conceptual model and system characterization. *Journal of Contaminant Hydrology*, 52(1), 137-164. [https://doi.org/10.1016/S0169-7722\(01\)00156-5](https://doi.org/10.1016/S0169-7722(01)00156-5)
- Lévy, F., Jaupart, C., Mareschal, J. C., Bienfait, G., & Limare, A. (2010). Low heat flux and large variations of lithospheric thickness in the Canadian Shield. *Journal of Geophysical Research: Solid Earth*, 115(B6). <https://doi.org/10.1029/2009JB006470>
- Lghoul, M., Maqsoud, A., Hakkou, R., & Kchikach, A. (2014). Hydrogeochemical behavior around the abandoned Kettara mine site, Morocco. *Journal of Geochemical Exploration*, 144, 456-467. <https://doi.org/10.1016/j.gexplo.2013.12.003>
- Loredo, C., Ordóñez, A., García-Ordiales, E., Alvarez, R., Roqueni, N., Cienfuegos, P., et al. (2017). Hydrochemical characterization of a mine water geothermal energy resource in NW Spain. *Science of the Total Environment*, 576, 59-69. <https://doi.org/10.1016/j.scitotenv.2016.10.084>
- Loredo, C., Roqueñí, N., & Ordóñez, A. (2016). Modelling flow and heat transfer in flooded mines for geothermal energy use: A review. *International Journal of Coal Geology*, 164, 115-122. <https://doi.org/10.1016/j.coal.2016.04.013>
- Madiseh, S. A. G., Ghomshei, M. M., Hassani, F. P., & Abbasy, F. (2012). Sustainable heat extraction from abandoned mine tunnels: A numerical model. *Journal of Renewable and Sustainable Energy*, 4(3), 1-16. <http://dx.doi.org/10.1063/1.4712055>

- Majorowicz, J. A., & Minea, V. (2015). Shallow and deep geothermal energy potential in low heat flow/cold climate environment: northern Québec, Canada, case study. *Environmental Earth Sciences*, 74(6), 5233-5244. <https://doi.org/10.1007/s12665-015-4533-1>
- Malolepszy, Z., Demollin-Schneiders, E., & Bowers, D. (2005). *Potential use of geothermal mine waters in Europe*. Paper presented at the Proceedings of the World Geothermal Congress, Antalya, Turkey.
- Marshall, B. (2016). *Facts and figures of the Canadian mining industry*. Ottawa, Ontario : Mining Association of Canada (MAC). <http://mining.ca/fr/documents/faits-et-chiffres-2016>
- Menéndez, J., Ordóñez, A., Fernández-Oro, J. M., Loredo, J., & Díaz-Aguado, M. B. (2020). Feasibility analysis of using mine water from abandoned coal mines in Spain for heating and cooling of buildings. *Renewable Energy*, 146, 1166-1176. <https://doi.org/10.1016/j.renene.2019.07.054>
- Mielke, P., Weinert, S., Bignall, G., & Sass, I. (2016). *Thermo-physical rock properties of greywacke basement rock and intrusive lavas from the Taupo Volcanic Zone, New Zealand* (Vol. 324) <https://doi.org/10.1016/j.jvolgeores.2016.06.002>.
- Miller, L. M., & Keith, D. W. (2018). Observation-based solar and wind power capacity factors and power densities. *Environmental Research Letters*, 13(10), 8. <http://dx.doi.org/10.1088/1748-9326/aae102>
- Ministère de l'Énergie et des Ressources naturelles. (2015). Carte 6 - La production électrique sur le territoire du Plan Nord. (2015). Ministère de l'Énergie et des Ressources naturelles, Direction générale de l'information géographique. Québec, Québec. <https://bit.ly/2UJCHQI>
- Ministère de l'Énergie et des Ressources naturelles. (2012). Carte - Les grands ensembles géologiques du Québec. <https://mern.gouv.qc.ca/publications/mines/provinces-geologiques-8x11.pdf>
- Natural Resources Canada. (2016). Base de données complète sur la consommation d'énergie. <https://bit.ly/2I32ono> (Accessed: 15/03/2019).
- Natural Resources Canada. (2005). *Benchmarking the energy consumption of Canadian underground bulk mines*. Ottawa, Ontario. <http://publications.gc.ca/pub?id=9.688105&sl=0>
- Natural Resources Canada. (2019a). Canadian Climate Normals 1981-2010 Station Data, Aéroport La Grande Rivière. http://climate.weather.gc.ca/climate_normals/index_e.html (Accessed: 12/04/2019).
- Natural Resources Canada. (2018a). Canadian Industry Program for Energy Conservation (CIPEC), Ottawa, Canada. <https://bit.ly/33nXA2U> (Accessed: 28/11/2019).
- Natural Resources Canada. (2018b). Map of Top 100 Exploration Projects. <https://www.nrcan.gc.ca/mining-materials/exploration/17179> (Accessed: 09/03/2019).
- Natural Resources Canada. (2019b). Nunavik Mining: RAGLAN 2.0 Large Scale Renewable Energy Smart Grid, Ottawa, Ontario. <https://bit.ly/2XSJTrJ>.
- Nogara, J., & Zarrouk, S. J. (2018). Corrosion in geothermal environment: Part 1: Fluids and their impact. *Renewable and Sustainable Energy Reviews*, 82, 1333-1346. <https://doi.org/10.1016/j.rser.2017.06.098>

- Nordstrom, D. K., Blowes, D. W., & Ptacek, C. J. (2015). Hydrogeochemistry and microbiology of mine drainage: An update. *Applied Geochemistry*, 57, 3-16. <https://doi.org/10.1016/j.apgeochem.2015.02.008>
- Nuttall, C. A., & Younger, P. L. (2004). Hydrochemical stratification in flooded underground mines: an overlooked pitfall. *Journal of Contaminant Hydrology*, 69(1), 101-114. [https://doi.org/10.1016/S0169-7722\(03\)00152-9](https://doi.org/10.1016/S0169-7722(03)00152-9)
- Ochsner, K. (2012). *Geothermal Heat pumps: a Guide for planning and Installing*. London, United Kingdom: Routledge <https://doi.org/10.4324/9781849771443>.
- Ordóñez Alonso, M. A., Andrés Arias, C., Álvarez García, R., & Jardón Palacio, J. S. (2010). *Aprovechamiento de las aguas subterráneas como recurso hídrico y energético. Aplicación al embalse minero Barredo-Figaredo*. (Tesis de doctorado), Universidad de Oviedo, España. <http://hdl.handle.net/10651/12824>
- Ouzzane, M., Eslami-Nejad, P., Badache, M., & Aidoun, Z. (2015). New correlations for the prediction of the undisturbed ground temperature. *Geothermics*, 53, 379-384. <https://doi.org/10.1016/j.geothermics.2014.08.001>
- Patsa, L., Van Zyl, D., Zarrouk, S., & Arianpoo, N. (2015). *Geothermal Energy in Mining Developments: Synergies and Opportunities Throughout a Mine's Operational Life Cycle*. Paper presented at the World Geothermal Congress 2015, Melbourne, Australia.
- Perron, Y. (2016). *Utilisation du GNL pour la production d'électricité*. Stornoway Diamonds. Longueuil, Québec. <https://bit.ly/2OFDBa9>
- Preene, M., & Younger, P. (2014). Can you take the heat?—Geothermal energy in mining. *Mining Technology*, 123(2), 107-118. <https://doi.org/10.1179/1743286314y.0000000058>
- Puckorius, P., & Brooke, J. (1991). A new practical index for calcium carbonate scale prediction in cooling tower systems. *Corrosion*, 47(4), 280-284. <https://doi.org/10.5006/1.3585256>
- Rafferty, K. (1999). *Scaling in geothermal heat pump systems*. Klamath Falls, OR : United States Department of Energy. <http://citeseerx.ist.psu.edu/viewdoc/download?doi=10.1.1.558.3349&rep=rep1&type=pdf>
- Rafferty, K. D. (2004a). Water Chemistry Issues in Geothermal Heat Pump Systems. *ASHRAE Transactions*, 110(1), 550-555. <https://bit.ly/2K3jKkw>
- Rafferty, K. D. (2004b). *Water chemistry issues in geothermal heat pump systems*. Paper presented at the 2004 Winter Meeting - Technical and Symposium Papers, American Society of Heating, Refrigerating and Air-Conditioning Engineers.
- Ravenelle, J.-F. (2013). *Amphibolite facies gold mineralization: an exemple from the Roberto deposit, Éléonore property, James Bay, Quebec*. (Doctoral dissertation), Université du Québec, Institut national de la recherche scientifique, Québec, Québec. <http://espace.inrs.ca/1945/>
- Ravenelle, J.-F. (2010). *Insights on the geology of the world-class Roberto gold deposit, Éléonore property, James Bay area, Quebec*. Geological Survey of Canada, Current Research 2010-1, 26 p. <https://doi.org/10.4095/261482>
- Raymond, J. (2010). *Geothermal system optimization in mining environments*. (Thèse de doctorat), Université Laval, Québec, Québec. <http://hdl.handle.net/20.500.11794/21596>
- Raymond, J., & Therrien, R. (2008). Low-temperature geothermal potential of the flooded Gaspe Mines, Quebec, Canada. *Geothermics*, 37(2), 189-210. <https://doi.org/10.1016/j.geothermics.2007.10.001>

- Raymond, J., & Therrien, R. (2014). Optimizing the design of a geothermal district heating and cooling system located at a flooded mine in Canada. *Hydrogeology Journal*, 22(1), 217-231. <https://doi.org/10.1007/s10040-013-1063-3>
- Raymond, J., Therrien, R., & Gosselin, L. (2010). Low-temperature geothermal energy in mining environments. *CIM Journal*, 1(2), 140-149.
- Raymond, J., Therrien, R., & Hassani, F. P. (2008). Overview of geothermal energy resources in Québec (Canada) mining environments. *10th International Mine Water Association Congress*. <https://bit.ly/2Nvm0mn>
- Ren, G., Liu, J., Wan, J., Guo, Y., & Yu, D. (2017). Overview of wind power intermittency: Impacts, measurements, and mitigation solutions. *Applied Energy*, 204, 47-65. <https://doi.org/10.1016/j.apenergy.2017.06.098>
- Renz, A., Ruhaak, W., Schatzl, P., & Diersch, H. J. G. (2009). Numerical Modeling of Geothermal Use of Mine Water: Challenges and Examples. *Mine Water and the Environment*, 28(1), 2-14. <https://doi.org/10.1007/s10230-008-0063-3>
- Rimstidt, J. D., & Vaughan, D. J. (2003). Pyrite oxidation: a state-of-the-art assessment of the reaction mechanism. *Geochimica et Cosmochimica Acta*, 67(5), 873-880. [https://doi.org/10.1016/S0016-7037\(02\)01165-1](https://doi.org/10.1016/S0016-7037(02)01165-1)
- Rivera, A. (2014). *Canada's groundwater resources*. Markham, Ontario: Fitzhenry & Whiteside <https://doi.org/10.4095/293431>.
- Ryznar, J. W. (1944). A New Index for Determining Amount of Calcium Scale Formed by a Water. *J. Am. Water Work Assoc*, 36, 472-483. <https://doi.org/10.1002/j.1551-8833.1944.tb20016.x>
- Sarbu, I., & Sebarchievici, C. (2014). General review of ground-source heat pump systems for heating and cooling of buildings. *Energy and Buildings*, 70, 441-454. <https://doi.org/10.1016/j.enbuild.2013.11.068>
- Shortall, R., Davidsdottir, B., & Axelsson, G. (2015). Geothermal energy for sustainable development: A review of sustainability impacts and assessment frameworks. *Renewable and Sustainable Energy Reviews*, 44(Supplement C), 391-406. <https://doi.org/10.1016/j.rser.2014.12.020>
- SNC - Lavalin. (2016). *Propriété de la mine Raglan au-delà de 2020 (phases II et III) poursuite des opérations minières à l'est de Katinniq*. Rapport - étude d'impact. Montréal, Québec.
- Stratego. (2016). *Multi-level actions for enhanced Heating and Cooling plans*. Report. Brussels, Belgium. <https://bit.ly/35ZydX5>
- Therrien, McLaren, R., Sudicky, E., & Panday, S. (2010). HydroGeoSphere: A three-dimensional numerical model describing fully-integrated subsurface and surface flow and solute transport. *Groundwater Simulations Group, University of Waterloo, Waterloo, Ontario*. <https://bit.ly/2FsW72d>
- Therrien, & Sudicky, E. A. (1996). Three-dimensional analysis of variably-saturated flow and solute transport in discretely-fractured porous media. *Journal of Contaminant Hydrology*, 23(1-2), 1-44. [https://doi.org/10.1016/0169-7722\(95\)00088-7](https://doi.org/10.1016/0169-7722(95)00088-7)
- Tugliq. (2019). Raglan II - Réseau hybride éolien, diesel et stockage d'énergie dans l'Arctique Canadien. <https://bit.ly/2I75bvR> (Accessed: 23/03/2019).

- Ugorets, V., & Pereira, C. (2018). *Dependence Of Predicted Dewatering On Size Of Hydraulic Stress Used For Groundwater Model Calibration*. Paper presented at the Mine Water Solutions 2018, Vancouver, British Columbia.
- Uhlík, J., & Baier, J. (2012). Model Evaluation of Thermal Energy Potential of Hydrogeological Structures with Flooded Mines. *Mine Water and the Environment*, 31(3), 179-191. <https://doi.org/10.1007/s10230-012-0186-4>
- Vision Biomasse Québec. (2015). *Le chauffage à la biomasse forestière résiduelle*. Mémoire. Québec, Québec. <https://bit.ly/2WDFMhe>
- Voss, C. I. (2011). Editor's message: Groundwater modeling fantasies —part 1, adrift in the details. *Hydrogeology Journal*, 19(7), 1281-1284. <https://doi.org/10.1007/s10040-011-0789-z>
- Walraven, D., Laenen, B., & D'haeseleer, W. (2014). Comparison of shell-and-tube with plate heat exchangers for the use in low-temperature organic Rankine cycles. *Energy Conversion and Management*, 87, 227-237. <https://doi.org/10.1016/j.enconman.2014.07.019>
- Walter, J., Chesnaux, R., Cloutier, V., & Gaboury, D. (2017). The influence of water/rock – water/clay interactions and mixing in the salinization processes of groundwater. *Journal of Hydrology: Regional Studies*, 13, 168-188. <https://doi.org/10.1016/j.ejrh.2017.07.004>
- Waterloo Hydrogeologic. (1999). AquaChem Computer Code: Aqueous geochemical analyses, plotting and modelling. *Waterloo Hydrogeologic*, Waterloo, Ontario, Canada. <https://www.waterloohydrogeologic.com/aquachem/>
- Watzlaf, G. R., & Ackman, T. E. (2006). Underground Mine Water for Heating and Cooling using Geothermal Heat Pump Systems. *Mine Water and the Environment*, 25(1), 1-14. <http://dx.doi.org/10.1007/s10230-006-0103-9>
- Wieber, G., & Pohl, S. (2008). *Mine water: a source of geothermal energy—examples from the Rhenish Massif*. Paper presented at the Proceedings of the 10th international mine water association congress, Karlovy Vary, Czech Republic.

8 APPENDIX I SCALING AND CORROSION INDICES

Langelier and Ryznar Saturation Indices

The Langelier and Ryznar indices were developed to determine the scaling potential of drinking water by precipitation of calcium carbonate (CaCO_3). The assessment of the risk of scaling is obtained by using equations 1 and 2 with data obtained from the chemical analysis of water samples such as total alkalinity data, total hardness, total dissolved solids, temperature and pH (Raymond et Therrien, 2008; American Society of Heating et Air-Conditioning Engineers, 2015).

The Langelier index is given by the following relation (Langelier, 1936):

$$LSI = pH_{\text{mes}} - pH_{\text{sat}} \quad (1)$$

Where:

LSI = Langelier Saturation Index

pH_{mes} = measured pH;

pH_{sat} = saturation pH = $(9.3 + A + B) - (C + D)$;

Where:

$A = (\log_{10}(\text{Total Dissolved Solids } [\text{mg} \cdot l^{-1}]) - 1)/10$

$B = -13.12 \log_{10}(T_k) + 34.55$

$C = \log_{10}(\text{Ca}^+ \text{hardness } [\text{mg} \cdot l^{-1} \text{ of } \text{CaCO}_3]) - 0.4 \text{ [mg} \cdot l^{-1} \text{ of } \text{CaCO}_3]$

$D = \log_{10}(\text{Alkalinity } [\text{mg} \cdot l^{-1} \text{ of } \text{CaCO}_3])$

$T_k = pH_{\text{sat}}$ calculation temperature (temperature of water entering the system) [K]

If the value of the Langelier index is greater than zero, the water presents a risk of scaling. On the contrary, if the value is less than zero, the water carries a risk of corrosion. The Langelier index was posteriorly modified by using field measurements and values. An alternative method for assessing the risk of scaling, known as the Ryznar Stability Index (RSI), was developed. The RSI is calculated as follows (Ryznar, 1944):

$$RSI = 2pH_{\text{sat}} - pH_{\text{mes}} \quad (2)$$

In the case of the Ryznar index, the water exhibits a risk of scaling when the value is less than 6.0. In contrast, a value greater than 6.0 suggests a corrosive tendency.

Puckorius Scaling Index

The Langelier and Ryznar indices do not take into account two essential aspects, which are the buffering capacity of the water and the maximum amount of deposits that can be precipitated when the water is at equilibrium. The Puckorius Saturation Index (PSI) accounts for the link

between scaling and water supersaturation by considering the buffer capacity of water. The calculation of the PSI is done as follows (Puckorius et Brooke, 1991):

$$PSI = 2pH_{\text{sat}} - pH_{\text{eq}} \quad (3)$$

Where:

$PSI = \text{Puckorius Scaling Index}$

$pH_{\text{eq}} = 1.465 \log_{10}(\text{Alkalinity [mg} \cdot l^{-1} \text{ of } CaCO_3]) + 4.54;$

$pH_{\text{sat}} = \text{saturation pH} = (9.3 + A + B) - (C + D);$

Where:

$A = (\log_{10}(\text{Total Dissolved Solids [mg} \cdot l^{-1}]) - 1)/10$

$B = -13.12 \log_{10}(T_k) + 34.55$

$C = \log_{10}(\text{Ca}^+ \text{hardness [mg} \cdot l^{-1} \text{ of } CaCO_3]) - 0.4 \text{ [mg} \cdot l^{-1} \text{ of } CaCO_3]$

$D = \log_{10}(\text{Alkalinity [mg} \cdot l^{-1} \text{ of } CaCO_3])$

$T_k = pH_{\text{sat}} \text{ calculation temperature (temperature of water entering the system) [K]}$

Larson-Skold Corrosion Index

The purpose of the Larson-Skold Corrosion Index (LSCI) is to evaluate the risk of corrosion of water in contact with mild steel (carbon steel). The LSCI is given by (Larson et Skold, 1958):

$$LSCI = \frac{C_{Cl^-} + C_{SO_4^{2-}}}{C_{HCO_3^-}} \quad (4)$$

Where:

$LSCI = \text{Larson - Skold Corrosion Index}$

$C_{Cl^-} = \text{Chlorine concentration [meq} \cdot l^{-1}];$

$C_{SO_4^{2-}} = \text{Sulfate concentration [meq} \cdot l^{-1}];$

$C_{HCO_3^-} = \text{Bicarbonate concentration [meq} \cdot l^{-1}];$

If the value of the index is less than 0.8, chlorides and sulphates do not pose a risk of corrosion.

If the value is between 0.8 and 1.2, a higher corrosion rate than desired may occur. Finally, if the index is greater than 1.2, the risk of corrosion is high.

9 APPENDIX II PLATE HEAT EXCHANGER EFFICIENCY CALCULATION

Plate Heat Exchanger Efficiency Calculation

$$\varepsilon = \text{efficiency} = \frac{1 - \exp[-NTU(1 - C_r)]}{1 - C_r \exp[-NTU(1 - C_r)]} [\%] \quad (1)$$

The first step is to determine the number of transfer units (*NTU*) which is given by:

$$NTU = \frac{U \times A}{C_{min}};$$

Where *U* is the overall heat transfer coefficient, *A* represents the active surface inside the plate heat exchanger, which is 68.3 m^2 , and C_{min} is equal to the heat capacity rate of water or the heat-transfer fluid, whichever value is lower. The following relation gives the term necessary to obtain the overall heat transfer coefficient:

$$U = 1/h_{glycol} + 1/h_w \quad [W \text{ m}^{-2}K^{-1}];$$

Where:

$$h_w = \text{heat transfer coefficient of water} = \frac{0.023Re^{0.8}Pr^{0.4} \times k}{2a} \quad [W \text{ m}^{-2}K^{-1}];$$

$$h_{glycol} = \text{heat transfer coefficient of glycol} = \frac{0.023Re^{0.8}Pr^{0.4} \times k}{2a} \quad [W \text{ m}^{-2}K^{-1}];$$

Therefore, the individual heat transfer coefficient of water and propylene glycol must be calculated to obtain the overall heat transfer coefficient. In the two previous relations, *a* is the distance between plates inside the plate heat exchanger, which is equal to 0.004 m and *k* [$\text{W m}^{-1}\text{K}^{-1}$] is the thermal conductivity of the fluid. Reynold's number (*Re*) and Prandtl's number (*Pr*) are described by:

$$Re = (2\rho u_m a)/\mu; \\ Pr = c_p \mu/k;$$

Where:

$$\rho = \text{density} \quad [kg \cdot m^{-3}];$$

$$u_m = \text{average fluid velocity} \quad [m \cdot s^{-1}] = \dot{m}/(\rho(a \times L));$$

$$a = \text{distance between plates} \quad [m] = 0.004$$

$$\mu = \text{dynamic viscosity} \quad [N \text{ s}^{-1} \text{ m}^{-2}];$$

$$c_p = \text{specific heat capacity} \quad [J \text{ kg}^{-1}K^{-1}];$$

$L = \text{plate length [m]}$

The next step is to determine C_{\min} by calculating the heat capacity rate of water and propylene glycol as follows:

$$C_w = \dot{m}_w c_{p,w} [W \cdot K^{-1}] \text{ and } C_{\text{glycol}} = \dot{m}_{\text{glycol}} c_{p,\text{glycol}} [W \cdot K^{-1}];$$

Where:

$c_{p,w}$ = specific heat capacity of water [$J \ kg^{-1}K^{-1}$];

$c_{p,\text{glycol}}$ = specific heat capacity of propylene glycol [$J \ kg^{-1}K^{-1}$];

\dot{m}_w = mass flow rate of water [$kg \cdot s^{-1}$];

\dot{m}_{glycol} = mass flow rate of propylene glycol [$kg \cdot s^{-1}$];

The final step in calculating the efficiency of the heat exchanger involves computing the heat capacity ratio C_r , which is the ratio between C_{\min} and C_{\max} . The latter is given by the heat capacity rate of water or propylene glycol, whichever is higher.

10 APPENDIX III WATER QUALITY

Table III.1: Site 1 - Mine Water Outlet Zone

Site # 1 : Mine water outlet zone					
Parameter (values expressed in mg/L except when indicated)	Sample : EJA-SM-1	Sample : EJA-SM-2	Sample : EJA-SM-3	Sample : EJA-SM-4	Mean
Major ions					
HCO ₃	N/A	N/A	N/A	N/A	N/A
Ca	146	136	132	148	140.5
K	40.7	36.3	35.3	40.0	38.1
Mg	8.22	8.27	8.35	8.42	8.3
Na	236	230	229	245	235
Cl	443	416	427	464	437.5
SO ₄	321	321	294	339	318.8
Minor ions					
Al	0.025	0.024	0.027	0.029	0.026
As	0.290	0.300	0.300	0.304	0.298
Ba	0.033	0.031	0.029	0.032	0.031
Cd	< 5.0x10 ⁻⁴	0.001	< 6. 0x10 ⁻⁵	< 5. 0x10 ⁻⁵	0.001
Co	0.054	0.048	0.047	0.058	0.051
Cr	0.005	0.005	0.005	0.005	0.005
Cu	0.001	< 0.0005	< 0.0005	< 0.0005	0.001
Fe	0.051	0.045	0.046	0.059	0.050
Mn	0.0117	0.009	0.008	0.010	0.009
Mo	0.021	0.021	0.020	0.022	0.021
Ni	0.011	0.010	0.010	0.010	0.010
Pb	0.002	< 0.001	< 0.001	< 0.0016	0.002
Sb	0.230	0.230	0.220	0.250	0.233
Zn	0.001	0.008	5.00x10 ⁻⁴	9.6x10 ⁻⁴	0.0045
Other parameters					
Total alkalinity (mg/L as CaCO ₃)	N/A	N/A	N/A	N/A	N/A
Total hardness (mg/L as CaCO ₃)	398.4	373.6	364.0	364.3	375.1
Total dissolved solids	1 426.0	1 329.6	1 331.5	1 487.9	1393.8
Total suspended solids	2 469.0	2 583.0	N/A	N/A	2526
Conductivity (μ S/cm)	2260	2190	N/A	N/A	2225
Temperature (°C)	8.9	10.4	N/A	N/A	9.65
pH-field (15/11/2017)	N/A	N/A	N/A	N/A	N/A
pH-laboratory (13/06/2018)	6.4	6.8	2.8	6.8	5.7

Table III.2: Site 2 - Water Treatment Plant Entrance

Site # 2 : Water Treatment Plant Entrance					
Parameter (values expressed in mg/L except when indicated)	Sample : EJA-WTPE-1	Sample : EJA-WTPE-2	Sample : EJA-WTPE-3	Sample : EJA-WTPE-4	Mean
Major ions					
HCO ₃	N/A	N/A	N/A	N/A	N/A
Ca	195.0	190.0	189.0	187.0	190.3
K	35.3	35	34.9	34.9	35.0
Mg	7.91	7.85	7.77	7.88	7.85
Na	249	243	243	241	244
Cl	532	527	555	540	539
SO ₄	287	292	299	299	294
Minor ions					
Al	0.0197	0.021	0.027	0.027	0.024
As	0.22	0.22	0.22	0.22	0.22
Ba	0.037	0.037	0.037	0.036	0.037
Cd	0.00009	0.00006	0.00008	0.00006	0.00007
Co	0.042	0.042	0.041	0.042	0.042
Cr	0.0059	0.0059	0.006	0.0061	0.0059
Cu	0.0024	0.0035	0.0049	0.0043	0.0038
Fe	0.0139	0.0143	0.019	0.0189	0.017
Mn	0.0259	0.0205	0.0184	0.018	0.0207
Mo	0.02	0.021	0.021	0.021	0.0207
Ni	0.0134	0.0137	0.0138	0.0135	0.0136
Pb	< 0.0016	0.0022	0.0017	< 0.0016	0.0019
Sb	0.154	0.154	0.153	0.156	0.1542
Zn	0.00128	0.00112	0.0008	0.0009	0.0010
Other parameters					
Total alkalinity (mg/L as CaCO ₃)	N/A	N/A	N/A	N/A	N/A
Total hardness (mg/L as CaCO ₃)	519.5	506.8	503.9	499.4	507.4
Total dissolved solids	1 544.1	1 524.0	1 553.7	1 534.4	1539.1
Total suspended solids	54.0	115.0	N/A	N/A	84.5
Conductivity (µS/cm)	2410	2490	N/A	N/A	2450
Temperature (°C)	9.1	12.2	N/A	N/A	10.7
pH-field (15/11/2017)	N/A	N/A	N/A	N/A	N/A
pH-laboratory (13/06/2018)	5.9	3.0	3.0	2.8	3.7

Table III.3: Site 3 - Water Treatment Plant Exit

Site # 3 : Water Treatment Plant Exit			
Parameter (values expressed in mg/L except when indicated)	Sample : EJA-WTPE-1	Sample : EJA-WTPE-2	Mean
Major Ions			
HCO ₃	N/A	N/A	N/A
Ca	188.0	188.0	188
K	34.9	35.9	35.4
Mg	7.8	7.8	7.8
Na	250	250	250
Cl	536	555	546
SO ₄	330	349	3340
Minor Ions			
Al	0.0123	0.0128	0.013
As	0.003	0.003	0.003
Ba	0.033	0.033	0.033
Cd	0.00009	0.00037	0.00023
Co	0.041	0.042	0.042
Cr	0.0045	0.0044	0.0045
Cu	0.0037	0.0044	0.0041
Fe	0.122	0.127	0.125
Mn	0.0196	0.0195	0.0196
Mo	0.0159	0.0159	0.0159
Ni	0.0153	0.015	0.0152
Pb	0.0016	0.0016	0.0016
Sb	0.121	0.121	0.121
Zn	0.00133	0.0034	0.0024
Other parameters			
Total alkalinity (mg/L as CaCO ₃)	N/A	N/A	N/A
Total hardness (mg/L as CaCO ₃)	501.6	501.5	501.6
Total dissolved solids	1 575.1	1 621.4	1598.2
Total suspended solids	8.3	N/A	8.3
Conductivity (µS/cm)	2520	N/A	2520
Temperature (°C)	9.7	N/A	9.7
pH-field (15/11/2017)	N/A	N/A	N/A
pH-laboratory (13/06/2018)	2.7	3.1	2.9

Table III.4: Site 4 - Emissary

Site # 4 : Emissary					
Parameter (values expressed in mg/L except when indicated)	Sample : EJA-EM-1	Sample : EJA-EM-2	Sample : EJA-EM-3	Sample : EJA-EM-4	Mean
Major ions					
HCO ₃	N/A	N/A	N/A	N/A	N/A
Ca	186	185	184	184	185
K	35.6	36	34.9	35.1	35.4
Mg	7.53	7.54	7.54	7.51	7.53
Na	247	245	243	245	245
Cl	538	525	545	521	532.3
SO ₄	335	334	339	333	335.3
Minor ions					
Al	0.0128	0.0133	0.0125	0.0132	0.0129
As	0.004	< 0.003	0.003	< 0.003	0.0035
Ba	0.032	0.032	0.033	0.033	0.0325
Cd	0.00021	0.00015	0.00016	0.0001	0.00015
Co	0.043	0.042	0.043	0.043	0.0428
Cr	0.0049	0.0048	0.0048	0.0049	0.0049
Cu	0.0038	0.0029	0.0033	0.0034	0.0034
Fe	0.108	0.0988	0.111	0.108	0.1065
Mn	0.02	0.0202	0.02	0.0199	0.0200
Mo	0.016	0.0162	0.0164	0.0166	0.0163
Ni	0.0155	0.0151	0.0154	0.0155	0.0154
Pb	0.0016	0.0017	0.0016	0.0016	0.0016
Sb	0.119	0.122	0.123	0.122	0.1215
Zn	0.0035	0.0025	0.00138	0.00187	0.0023
Other parameters					
Total alkalinity (mg/L as CaCO ₃)	N/A	N/A	N/A	N/A	N/A
Total hardness (mg/L as CaCO ₃)	677.7	495.5	493.0	490.4	539.2
Total dissolved solids	1 581.1	1 569.4	1 586.5	1 556.2	1573.3
Total suspended solids	1.2	8.3	N/A	N/A	4.75
Conductivity (µS/cm)	2480	2520	N/A	N/A	2500
Temperature (°C)	8.9	10.6	N/A	N/A	9.75
pH-field (15/11/2017)	N/A	N/A	N/A	N/A	N/A
pH-laboratory (13/06/2018)	3.1	3.0	2.9	3.0	3.0

Table III.5: Evolution of water pH and conductivity

Location	pH		Conductivity ($\mu\text{S}/\text{cm}$)	
	Field (mean)	Laboratory (mean)	Field (mean)	Laboratory (mean)
Dewatering outlet zone (SM)	8.5	5.9	2225	3243
Water Treatment Plant entrance (EUTEI)	8.1	4.2	2450	3993
Water Treatment Plant exit (SUTEI)	7.2	4.1	3260	5746
Emissary (EMI)	7.4	3.7	3189	5082

11 APPENDIX IV SCALING AND CORROSION INDICES CALCULATOR FILE AND RESULTS

Scaling and Corrosion indices calculator file

FR : Fichier utilisé pour calculer les indices de saturation et corrosion. Voir les fichiers accompagnant le mémoire pour télécharger ce fichier.

EN: File used to calculate the saturation and corrosion indices. See the files accompanying the thesis to download the calculator file.

Scaling and Corrosion indices results

Scaling and Corrosion Indices		
Langelier Saturation Index	$LSI = pH - pH_s$	
Ryznar Saturation Index	$RSI = 2pH_s - pH$	
Puckorius Scaling Index	$PSI = 2pH_s - pH_{eq}$	
Larson-Skold Corrosion Index	$LSCI = \frac{Co_{Cl^-} + Co_{SO_4^{2-}}}{Co_{HCO_3^-}}$	
Saturation pH (pH_s) = $(9.3 + A + B) - (C + D)$		
A = $(\log_{10} [\text{Total dissolved solids}] - 1) / 10$		
B = $-13.12 * \log_{10} (T^\circ C + 273) + 34.55$		
C = $\log_{10} [\text{Calcium hardness}] - 0.4$		
D = $\log_{10} [\text{alkalinity}]$		
Equilibrium pH (pH_{eq}) = $1.465 \log_{10} [\text{alkalinity}] + 4.54$		
Co = concentration in [meq/l]		
Results		
Parameters	Sample: EJA-SM Location: Dewatering outlet zone	Sample: EJA-ARO Location: Emissary
Total alkalinity (mg/l en CaCO ₃)	72.7	37.9
Calcium hardness (mg/l en CaCO ₃)	749	648
Total dissolved solids (mg/l)	1966.1	2289.7
Cl ⁻ (meq/l)	18.5	20.3
SO ₄ (meq/l)	5.6	11.7
HCO ₃ (meq/l)	1.5	0.60
pH at equilibrium (pH _{eq})	7.3	6.9
pH (measured)	8.6	7.1
T ₁ °C (maximum)	17.9	21.6
T ₂ °C (mean)	12.2	9.6
T ₃ °C (minimum)	7.7	1.2
Parameters needed to calculate saturation pH (pH_s)		
A	0.23	0.24
B at T ₁	2.22	2.15
B at T ₂	2.34	2.39
B at T ₃	2.43	2.56
C	2.47	2.41
D	1.86	1.58
pH _s at T ₁	7.42	7.70
pH _s at T ₂	7.53	7.93
pH _s at T ₃	7.62	8.11
Index calculation		
LSI @ T ₁	1.2	-0.6
LSI @ T ₂	1.1	-0.8
LSI @ T ₃	1.0	-1.0
RSI @ T ₁	6.2	8.3
RSI @ T ₂	6.4	8.8
RSI @ T ₃	6.6	9.1
PSI @ T ₁	7.6	8.5
PSI @ T ₂	7.8	9.0
PSI @ T ₃	8.0	9.4
LSCI	16.1	53.4

12 APPENDIX V GEOTHERMAL HEAT PUMP PERFORMANCE ASSESSMENT SITE 2 - 4

Table V.1: Site 2 – Water Treatment Plant Entrance

Energy Balance : Water Treatment Plant Entrance						
Year	Month	¹ E _{exchanger}	E _{comp}	Total energy generated by the GHPS (² E _{heating})	Total heating energy demand of the underground workings	³ Penetration level
		(kWh)	(kWh)	(kWh)	(kWh)	(%)
2016	Jan	638 132	122 206	596 976	5 564 374	11
	Feb	1 155 256	211 919	1 015 977	6 193 288	16
	Mar	1 532 926	295 712	1 436 209	4 763 296	30
	April	2 449 370	414 310	2 177 857	3 213 487	68
	May	0	0	0	0	0
	June	0	0	0	0	0
	July	0	0	0	0	0
	Aug	0	0	0	0	0
	Sept	0	0	0	0	0
	Oct	304 491	51 723	278 264	148 787	187
	Nov	509 878	92 128	459 240	1 418 548	32
	Dec	867 469	171 045	816 442	5 362 468	15
Total		5 421 922	1 359 043	6 780 966	26 664 248	25

¹Energy = power (kW) times the number of hours in a day, times the number of days in the respective month.

²E_{heating} = E_{exchanger} + E_{heating}.

³Penetration level = percentage of the total energy demand that can be supplied by the designed GHPS system.

¹Economic Balance : Water Treatment Plant Entrance

Year	Month	² Costs incurred by a propane-based heating system	³ Costs generated by a GHPS	⁴ Costs incurred by a hybrid heating system	⁵ Net annual savings	Net annual savings
		(CAD)	(CAD)	(CAD)	(CAD)	(%)
2016	Jan	312 593	3 984	283 041	29 553	9
	Feb	390 179	6 909	333 081	57 098	15
	Mar	267 591	9 640	196 548	71 043	27
	April	162 987	13 507	66 033	96 953	59
	May	0	0	0	0	0
	June	0	0	0	0	0
	July	0	0	0	0	0
	Aug	0	0	0	0	0
	Sept	0	0	0	0	0
	Oct	8 155	1 686	1 686	6 469	79
	Nov	79 691	3 003	56 895	22 796	29
	Dec	337 837	5 576	291 977	45 860	14
Total		1 559 033	44 305	1 229 261	329 772	21

¹Energy production costs

²100 % of total heating energy demands

³Energy consumed by the compressor (E_{comp}) \times 3.26 ¢/kWh (Rate L, Hydro-Quebec) (personal communication, Newmont-Goldcorp, 2017)

⁴Cost of providing 100% of heating energy demand with a hybrid system = cost generated by a GHPS + cost incurred by the propane-based system once the penetration level of the GHPS has been deducted.

⁵Costs incurred by a propane burner system minus the costs incurred by a hybrid heating system.

Environmental Balance : Water Treatment Plant Entrance

Year Month	Propane-based system		Hybrid heating system		Propane savings	CO ₂ savings
	¹ Propane consumption (litres)	² CO ₂ emissions (tonnes)	³ Propane consumption (litres)	⁴ CO ₂ emissions (tonnes)		
2016	Jan	759 275	1 169	677 816	1 049	81 459
	Feb	845 092	1 301	706 459	1 097	138 633
	Mar	649 965	1 000	453 991	713	195 975
	April	438 489	675	141 315	239	297 175
	May	0	0	0	0	0
	June	0	0	0	0	0
	July	0	0	0	0	0
	Aug	0	0	0	0	0
	Sept	0	0	0	0	0
	Oct	20 302	31	0	2.8	20 302
	Nov	193 565	298	130 900	206	62 665
	Dec	731 724	1 126	620 318	963	111 406
Total		3 638 413	5 599	2 730 798	4 270	907 615
1 100% of heating needs provided by propane.						
2 kWh of energy produced by the propane heating system x [0.21 kgCO ₂ /kWh (Koufos, 2012)].						
3 Emissions generated by the propane heating system once the penetration level of the GHPs has been deducted.						
4 Emissions generated by the propane heating system once the penetration level of the GHPs has been deducted + emissions generated by the GHPs = kWh x [0.01 kgCO ₂ /kWh (Koufos, 2012)].						

Table V.2: Site 3 – Water Treatment Plant Exit

Energy Balance : Water Treatment Plant Exit						
Year	Month	¹ E _{exchanger}	E _{comp}	Total energy generated by the GHPS (² E _{heating})	Total heating energy demand of the underground workings	³ Penetration level
		(kWh)	(kWh)	(kWh)	(kWh)	(%)
2016	Jan	740 523	184 235	924 758	5 564 374	17
	Feb	877 382	222 031	1 099 413	6 193 288	18
	Mar	966 725	247 448	1 214 173	4 763 296	25
	April	1 078 508	273 577	1 352 085	3 213 487	42
	May	0	0	0	0	0
	June	0	0	0	0	0
	July	0	0	0	0	0
	Aug	0	0	0	0	0
	Sept	0	0	0	0	0
	Oct	768 333	203 377	971 711	148 787	653
	Nov	884 966	237 375	1 122 341	1 418 548	79
	Dec	1 092 369	289 402	1 381 771	5 362 468	26
Total		6 408 807	1 657 445	8 066 252	26 664 248	30

¹Energy = power (kW) times the number of hours in a day, times the number of days in the respective month.

²E_{heating} = E_{exchanger} + E_{heating}.

³Penetration level = percentage of the total energy demand that can be supplied by the designed GHPS system.

¹Economic Balance : Water Treatment Plant Exit

Year	Month	² Costs incurred by a propane-based heating system	³ Costs generated by a GHPS	⁴ Costs incurred by a hybrid heating system	⁵ Net annual savings	Net annual savings
		(CAD)	(CAD)	(CAD)	(CAD)	(%)
2016	Jan	312 593	6 006	266 649	45 945	15
	Feb	390 179	7 238	328 154	62 025	16
	Mar	267 591	8 067	207 448	60 143	22
	April	162 987	8 919	103 328	59 659	37
	May	0	0	0	0	0
	June	0	0	0	0	0
	July	0	0	0	0	0
	Aug	0	0	0	0	0
	Sept	0	0	0	0	0
	Oct	8 155	6 630	6 630	1 525	19
	Nov	79 691	7 738	24 379	55 312	69
	Dec	337 837	9 434	260 220	77 617	23
Total		1 559 033	54 033	1 196 807	362 226	23

¹Energy production costs

²100 % of total heating energy demands

³Energy consumed by the compressor (E_{comp}) \times 3.26 ¢/kWh (Rate L, Hydro-Quebec) (personal communication, Newmont-Goldcorp, 2017)

⁴Cost of providing 100% of heating energy demand with a hybrid system = cost generated by a GHPS + cost incurred by the propane-based system once the penetration level of the GHPS has been deducted.

⁵Costs incurred by a propane burner system minus the costs incurred by a hybrid heating system.

Environmental Balance : Water Treatment Plant Exit

Year Month	Propane-based system		Hybrid heating system		Propane savings (litres)	CO ₂ savings (tonnes)
	¹ Propane consumption (litres)	² CO ₂ emissions (tonnes)	³ Propane consumption (litres)	⁴ CO ₂ emissions (tonnes)		
2016	Jan	759 275	1 169	633 089	984	126 186
	Feb	845 092	1 301	695 074	1 081	150 018
	Mar	649 965	1 000	484 288	757	165 677
	April	438 489	675	253 994	404	184 496
	May	0	0	0	0	0
	June	0	0	0	0	0
	July	0	0	0	0	0
	Aug	0	0	0	0	0
	Sept	0	0	0	0	0
	Oct	20 302	31	0	9.7	20 302
	Nov	193 565	298	40 418	73	153 147
	Dec	731 724	1 126	543 178	850	188 547
Total		3 638 413	5 599	2 650 040	4 159	988 373
1 100% of heating needs provided by propane.						
2 kWh of energy produced by the propane heating system x [0.21 kgCO ₂ /kWh (Koufos, 2012)].						
3 Emissions generated by the propane heating system once the penetration level of the GHPs has been deducted.						
4 Emissions generated by the propane heating system once the penetration level of the GHPs has been deducted + emissions generated by the GHPs = kWh x [0.01 kgCO ₂ /kWh (Koufos, 2012)].						

Table V.3: Site 4 – Emissary

Energy Balance : Emissary						
Year	Month	¹ E _{exchanger}	E _{comp}	Total energy generated by the GHPs (² E _{heating})	Total heating energy demand of the underground workings	³ Penetration level
		(kWh)	(kWh)	(kWh)	(kWh)	(%)
2016	Jan	67 113	18 243	85 356	5 564 374	2
	Feb	598 872	170 982	769 855	6 193 288	12
	Mar	1 312 480	355 848	1 668 328	4 763 296	35
	April	1 092 234	290 639	1 382 873	3 213 487	43
	May	0	0	0	0	0
	June	0	0	0	0	0
	July	0	0	0	0	0
	Aug	0	0	0	0	0
	Sept	0	0	0	0	0
	Oct	364 349	82 346	446 695	148 787	300
	Nov	209 208	53 080	262 288	1 418 548	18
	Dec	339 756	94 888	434 644	5 362 468	8
Total		3 984 012	1 066 026	5 050 038	26 664 248	19

¹Energy = power (kW) times the number of hours in a day, times the number of days in the respective month.

²E_{heating} = E_{exchanger} + E_{heating}.

³Penetration level = percentage of the total energy demand that can be supplied by the designed GHPS system.

¹Economic Balance : Emissary

Year	Month	² Costs incurred by a propane-based heating system	³ Costs generated by a GHPS	⁴ Costs incurred by a hybrid heating system	⁵ Net annual savings	Net annual savings
		(CAD)	(CAD)	(CAD)	(CAD)	(%)
2016	Jan	312 593	595	308 393	4 200	1
	Feb	390 179	5 574	347 252	42 927	11
	Mar	267 591	11 601	185 469	82 122	31
	April	162 987	9 475	102 323	60 664	37
	May	0	0	0	0	0
	June	0	0	0	0	0
	July	0	0	0	0	0
	Aug	0	0	0	0	0
	Sept	0	0	0	0	0
	Oct	8 155	2 684	2 684	5 471	67
	Nov	79 691	1 730	66 686	13 004	16
	Dec	337 837	3 093	313 548	24 289	7
Total		1 559 033	34 752	1 326 355	232 678	15

¹Energy production costs

²100 % of total heating energy demands

³Energy consumed by the compressor (E_{comp}) \times 3.26 ¢/kWh (Rate L, Hydro-Quebec) (personal communication, Goldcorp, 2017)

⁴Cost of providing 100% of heating energy demand with a hybrid system = cost generated by a GHPS + cost incurred by the propane-based system once the penetration level of the GHPS has been deducted.

⁵Costs incurred by a propane burner system minus the costs incurred by a hybrid heating system.

Environmental Balance : Emissary

Year Month	Propane-based system		Hybrid heating system		Propane savings (litres)	CO ₂ savings (tonnes)
	¹ Propane consumption (litres)	² CO ₂ emissions (tonnes)	³ Propane consumption (litres)	⁴ CO ₂ emissions (tonnes)		
2016	Jan	759 275	1 169	747 628	1 151	11 647 17
	Feb	845 092	1 301	740 043	1 147	105 049 154
	Mar	649 965	1 000	422 317	667	227 648 334
	April	438 489	675	249 793	398	188 697 277
	May	0	0	0	0	0 0
	June	0	0	0	0	0 0
	July	0	0	0	0	0 0
	Aug	0	0	0	0	0 0
	Sept	0	0	0	0	0 0
	Oct	20 302	31	0	4.5	20 302 27
	Nov	193 565	298	157 775	245	35 790 52
	Dec	731 724	1 126	672 416	1 039	59 308 87
Total		3 638 413	5 599	2 989 971	4 652	648 442 947

¹100% of heating needs provided by propane.

²kWh of energy produced by the propane heating system x [0.21 kgCO₂/kWh (Koufos, 2012)].

³Emissions generated by the propane heating system once the penetration level of the GHPs has been deducted.

⁴Emissions generated by the propane heating system once the penetration level of the GHPs has been deducted + emissions generated by the GHPs = kWh x [0.01 kgCO₂/kWh (Koufos, 2012)].

13 APPENDIX VI GROK, MPROP, AND FPROP HGS FILES

FR : Fichiers d'entrée utilisée pour la simulation du modèle numérique hydrogéologique de la mine Éléonore. Voir les fichiers accompagnant le mémoire pour télécharger l'ensemble de fichiers.

EN: Input files used for the simulation of the hydrogeological model of the Éléonore mine. See the files accompanying the thesis to download the set of files.

14 APPENDIX VII ROCK SAMPLES THERMAL PROPERTIES

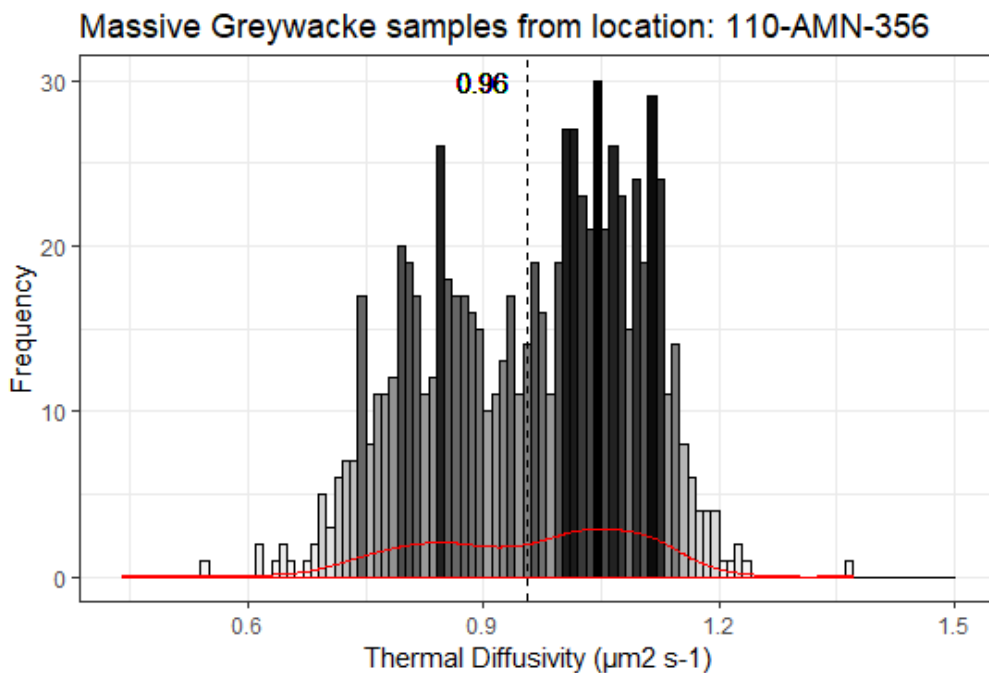
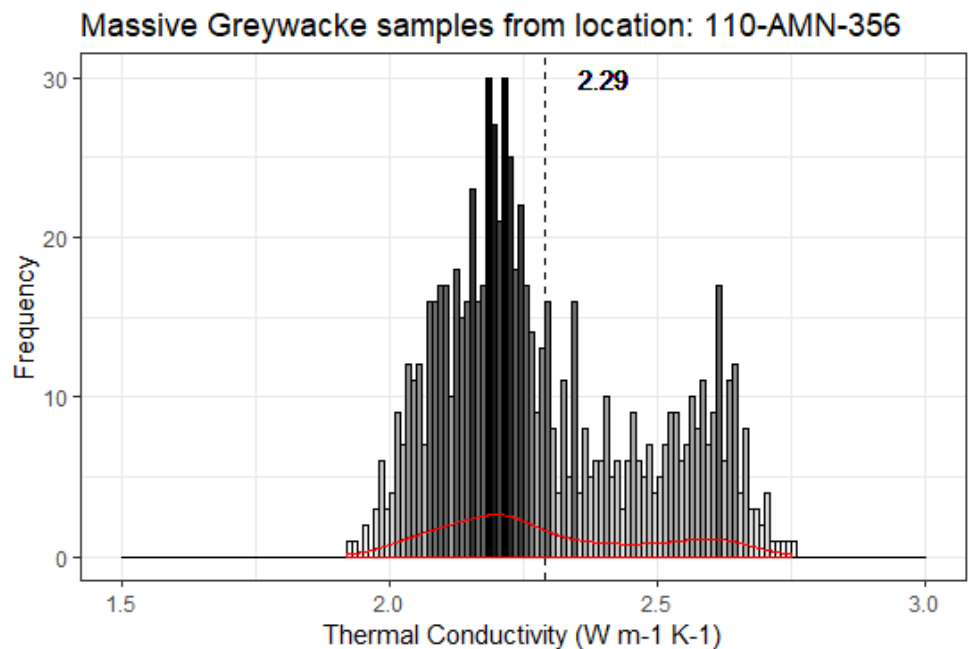
Table VII.1: Rock sampling locations and depths

Unit	Sample location ID	Number of samples	¹ Location	Depth (m)
Massive Greywacke	110-AMN-356	9	426 650; 5 839 524	110
	320-GRO-1N	10	426 550; 5 839 700	320
	770-AMN-507	9	426 500; 5 839 800	770
Aluminosilicate Greywacke	530-AMN-250	8	426 800; 5 839 200	530
	380-BRM-1N	6	426 550; 5 830 750	380
	740-GRO-1N	2	426 620; 5 839 750	740

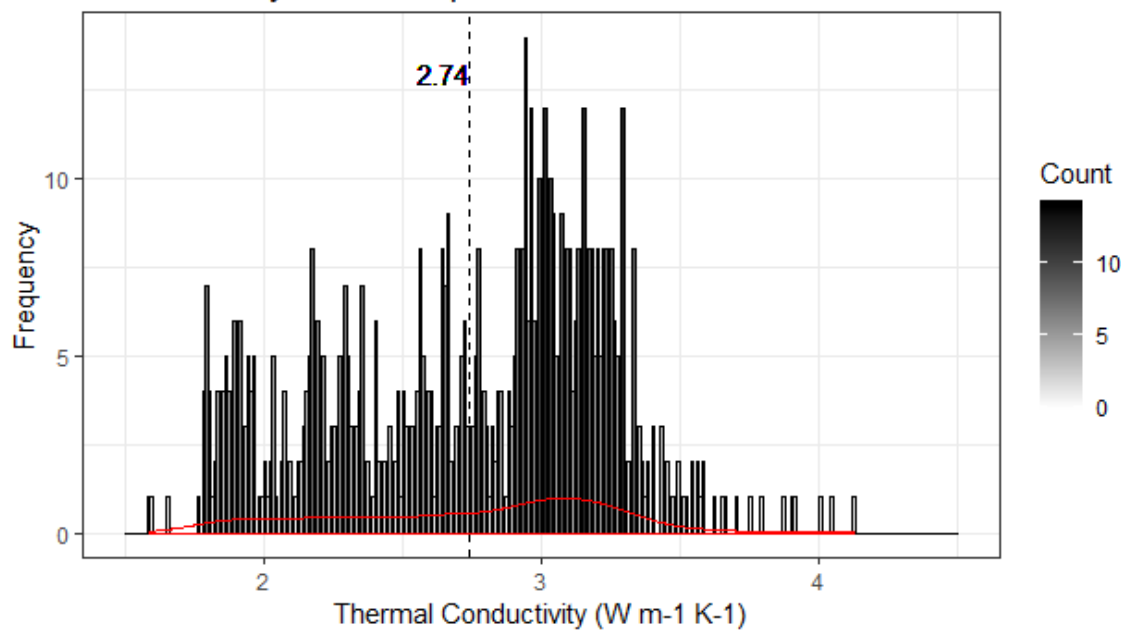
¹NAD 1983 UTM Zone 18N.

Statistical distribution of the thermal properties of rock samples from the Éléonore mine according to location

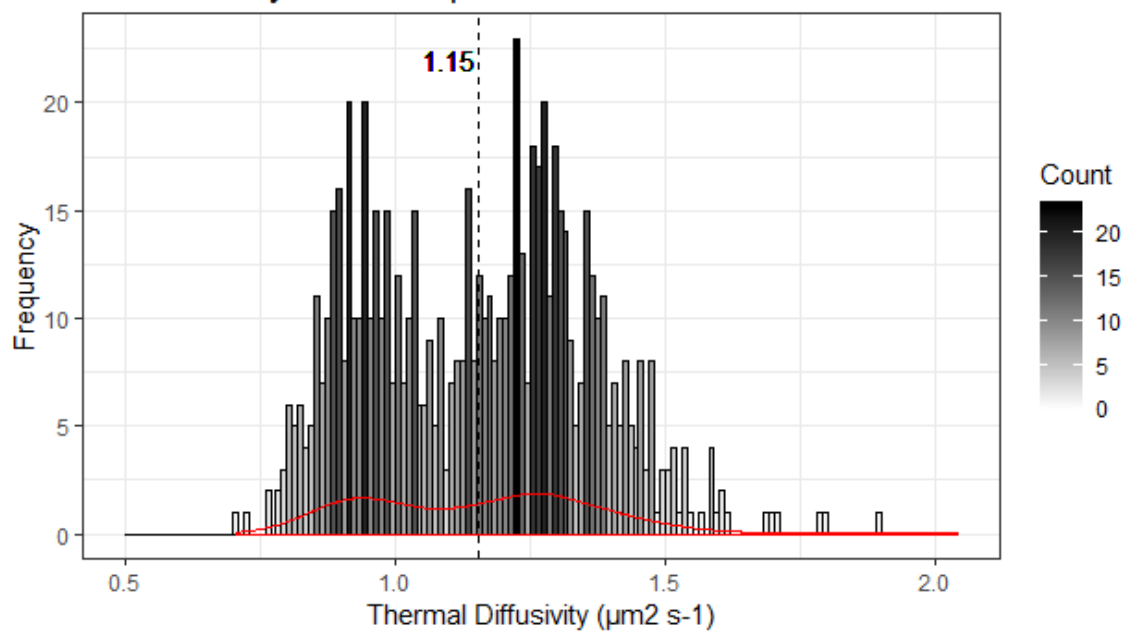
The thermal properties of samples from each one of the sampling locations are shown in the following histograms. The dashed line and the value that is displayed in each figure represents the mean value. The first graph on each page shows the thermal conductivity, and the second one corresponds to the thermal diffusivity data. Only these parameters are shown since the specific heat capacity is obtained by dividing the thermal conductivity by the thermal diffusivity.



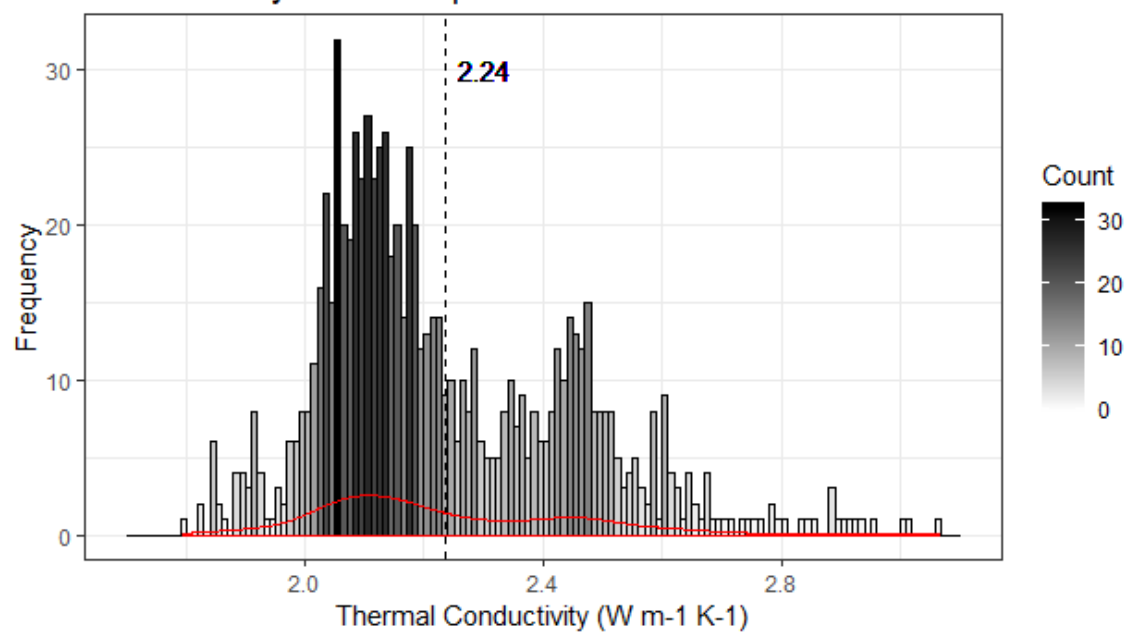
Massive Greywacke samples from location: 320-GRO-1N



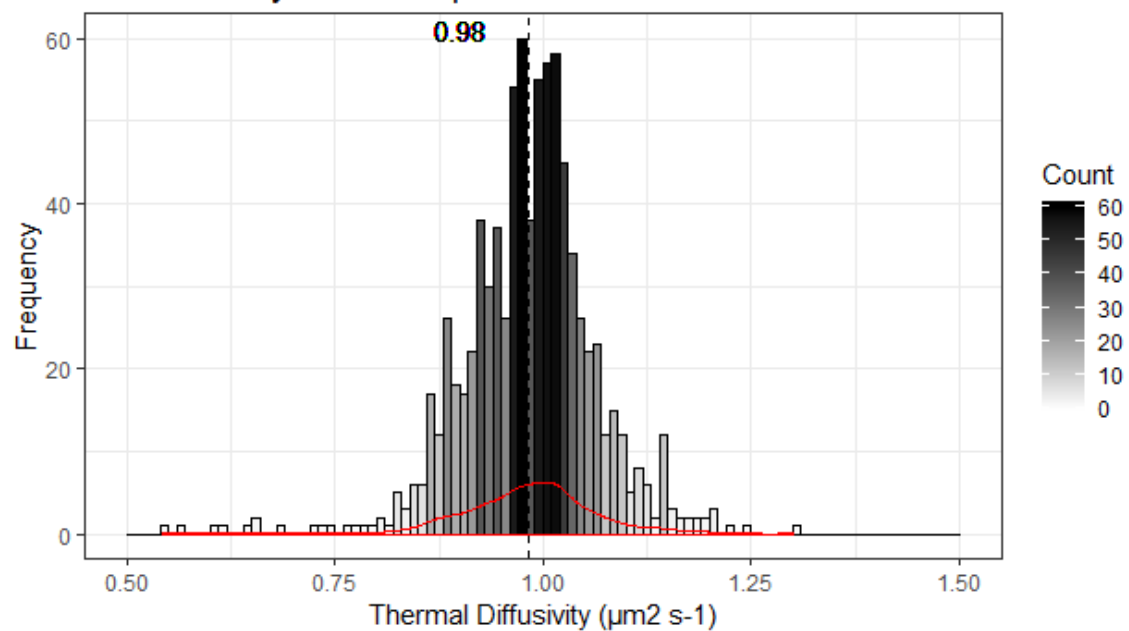
Massive Greywacke samples from location: 320-GRO-1N



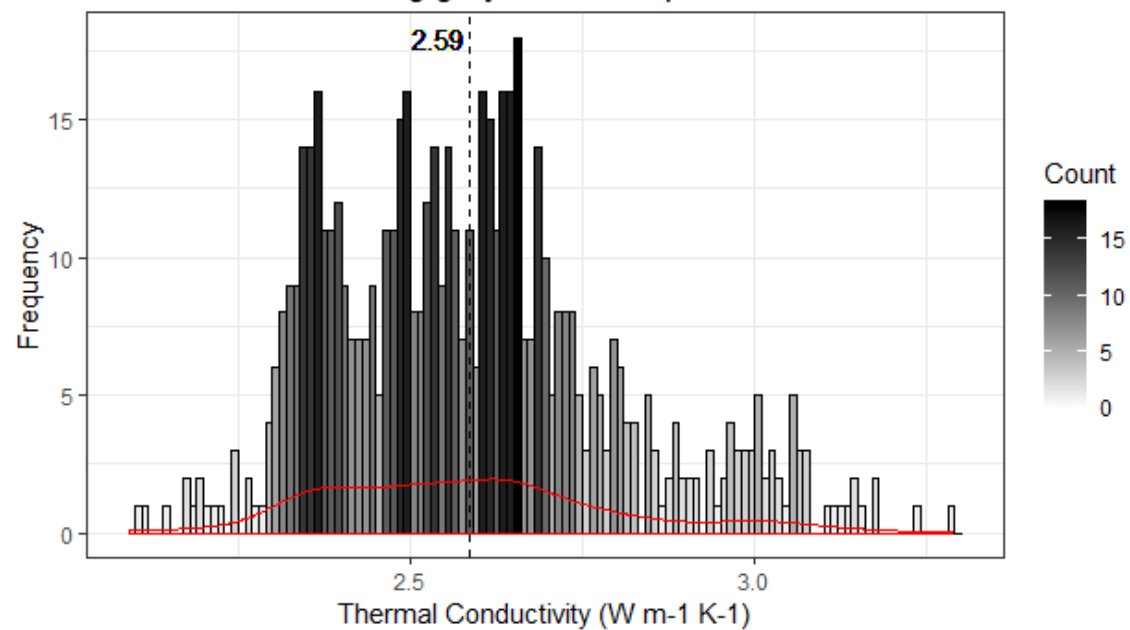
Massive Greywacke samples from location: 770-AMN-507



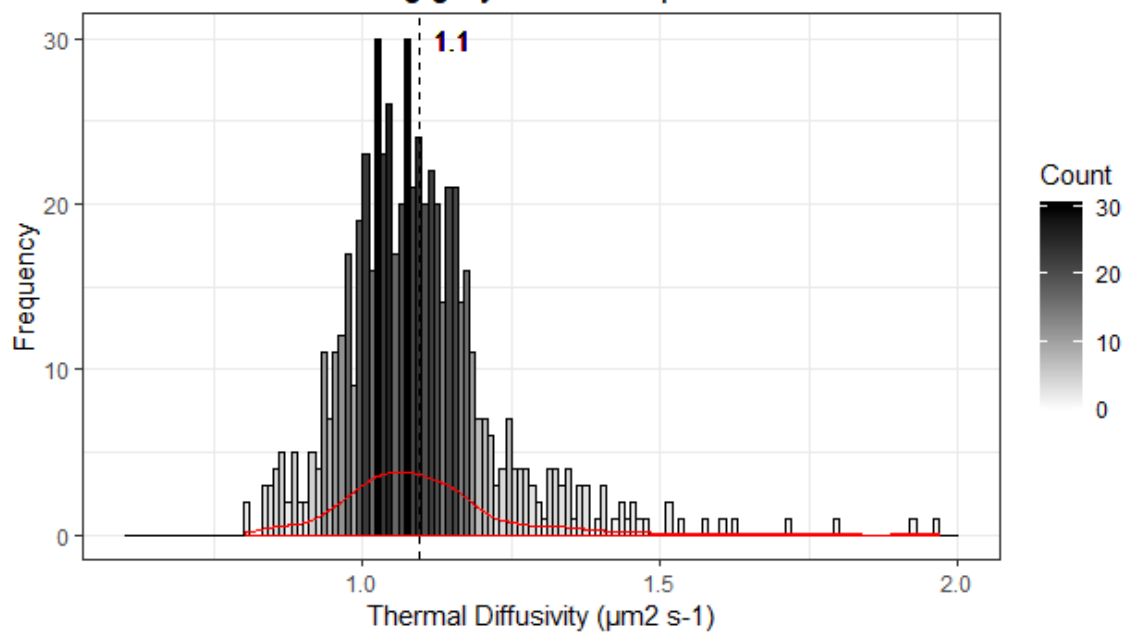
Massive Greywacke samples from location: 770-AMN-507



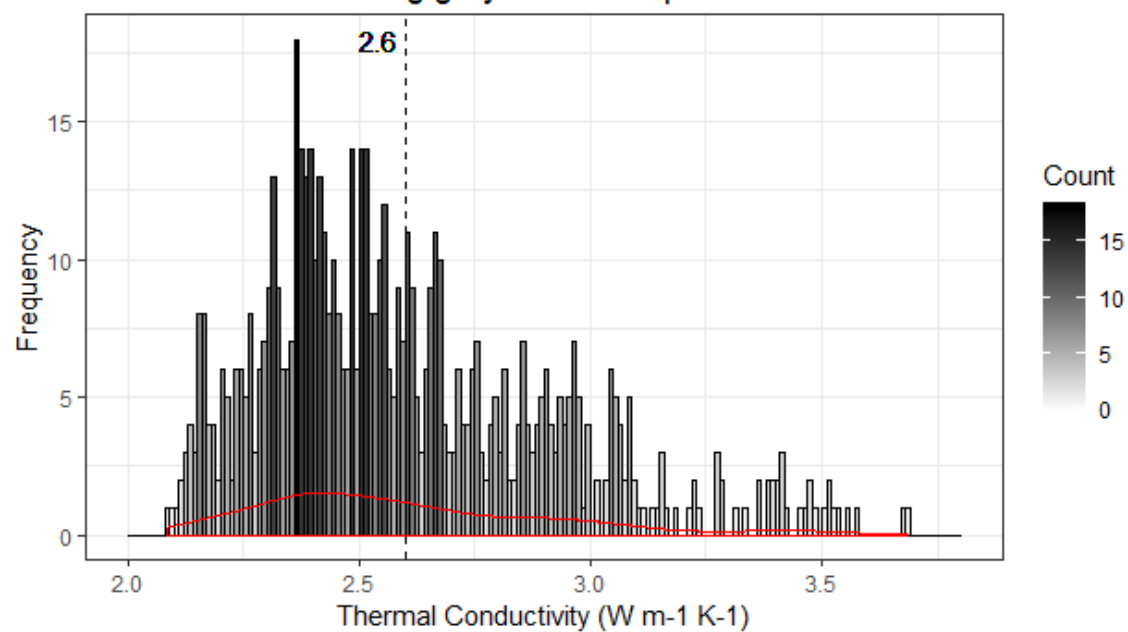
Aluminosilicate-bearing greywacke samples from location: 530-AMN-250



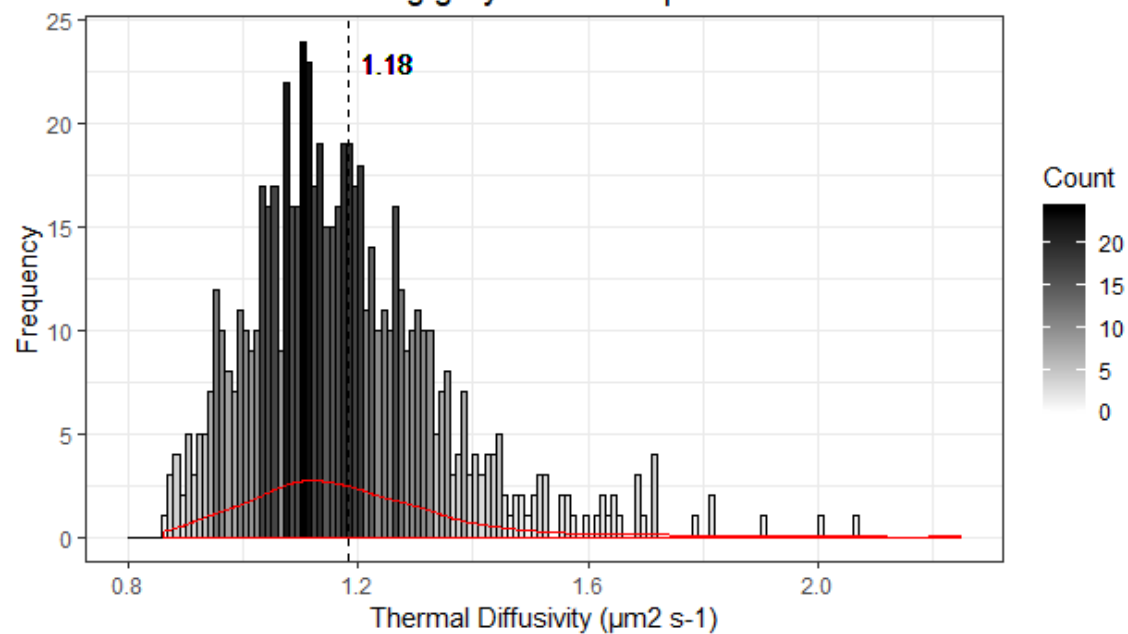
Aluminosilicate-bearing greywacke samples from location: 530-AMN-250



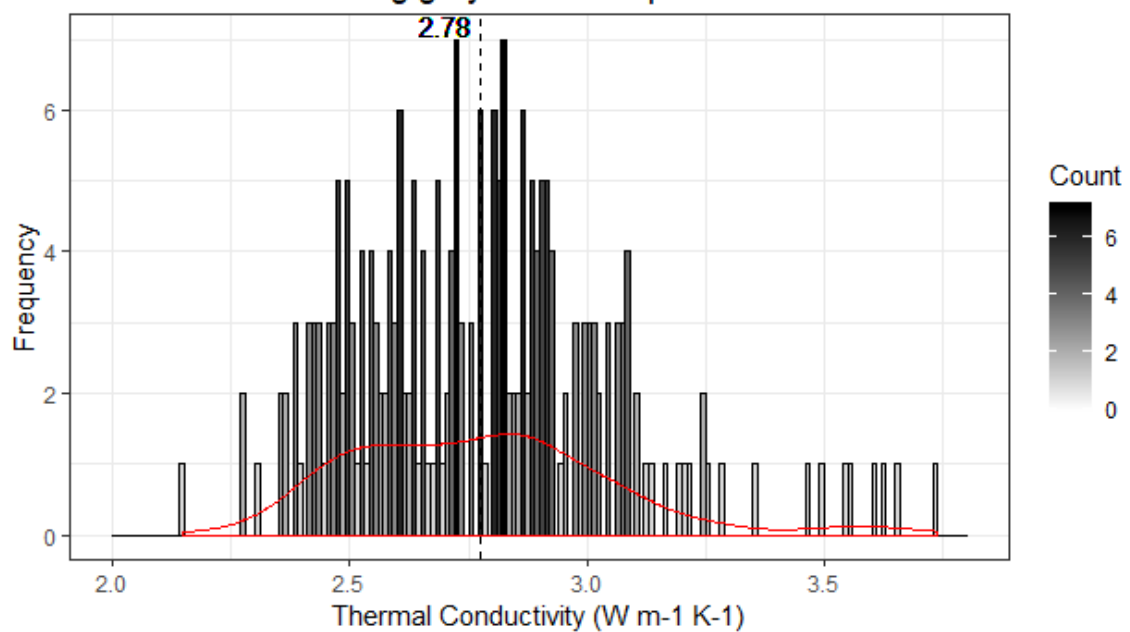
Aluminosilicate-bearing greywacke samples from location: 380-BRM-1N



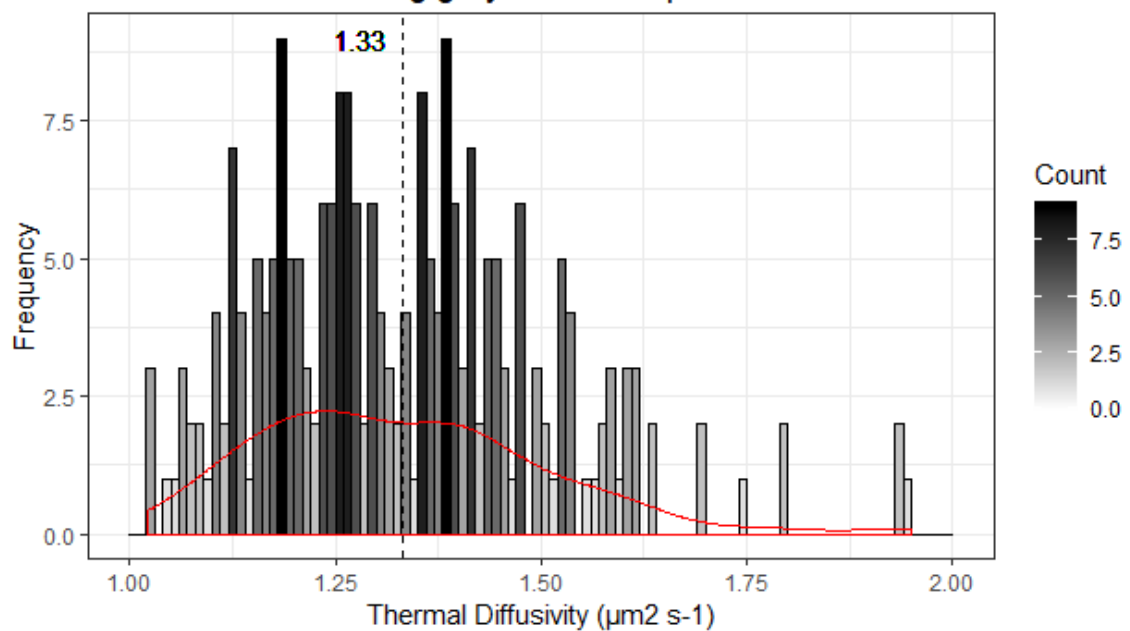
Aluminosilicate-bearing greywacke samples from location: 380-BRM-1N



Aluminosilicate-bearing greywacke samples from location: 740-GRO-1N

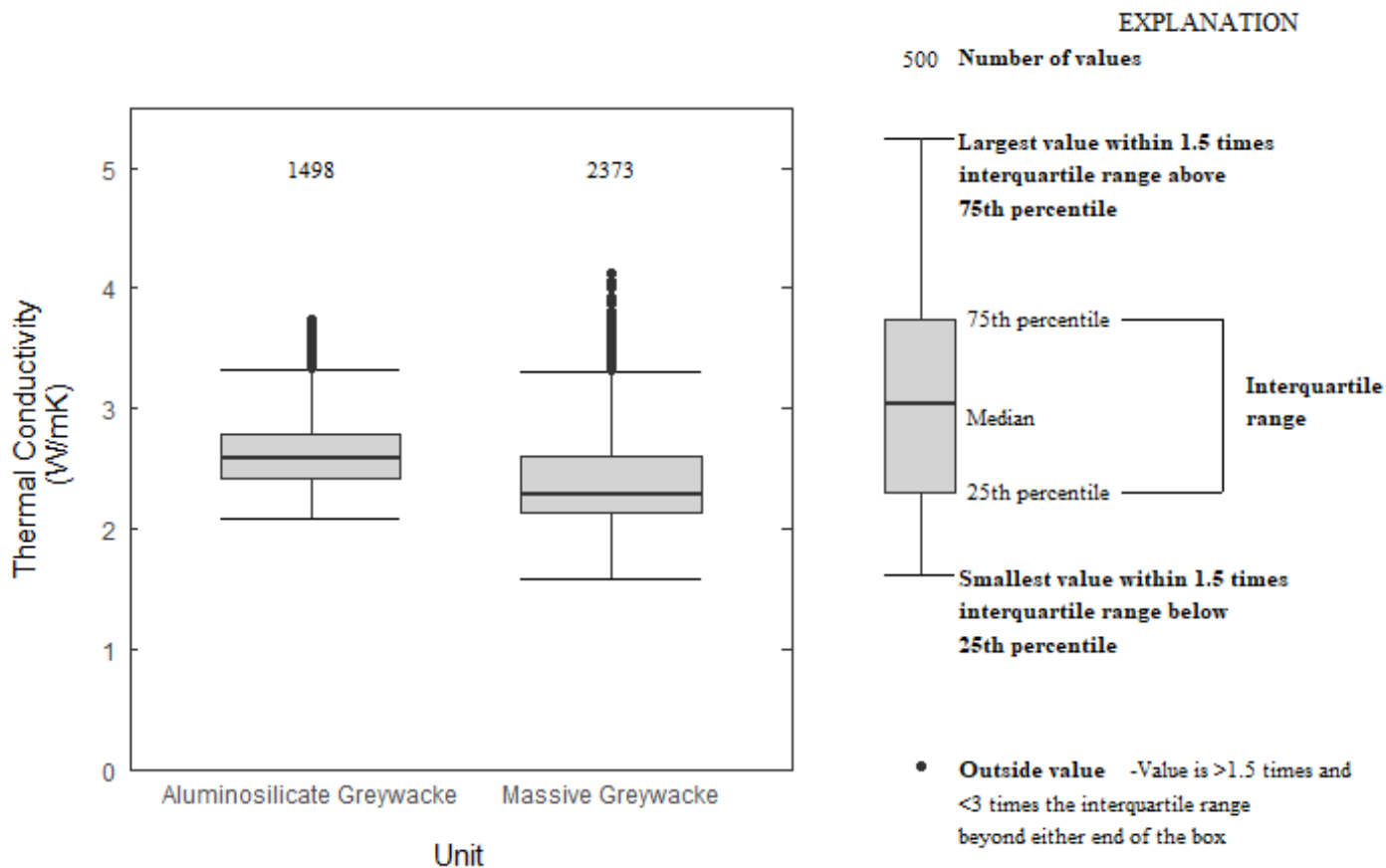


Aluminosilicate-bearing greywacke samples from location: 740-GRO-1N



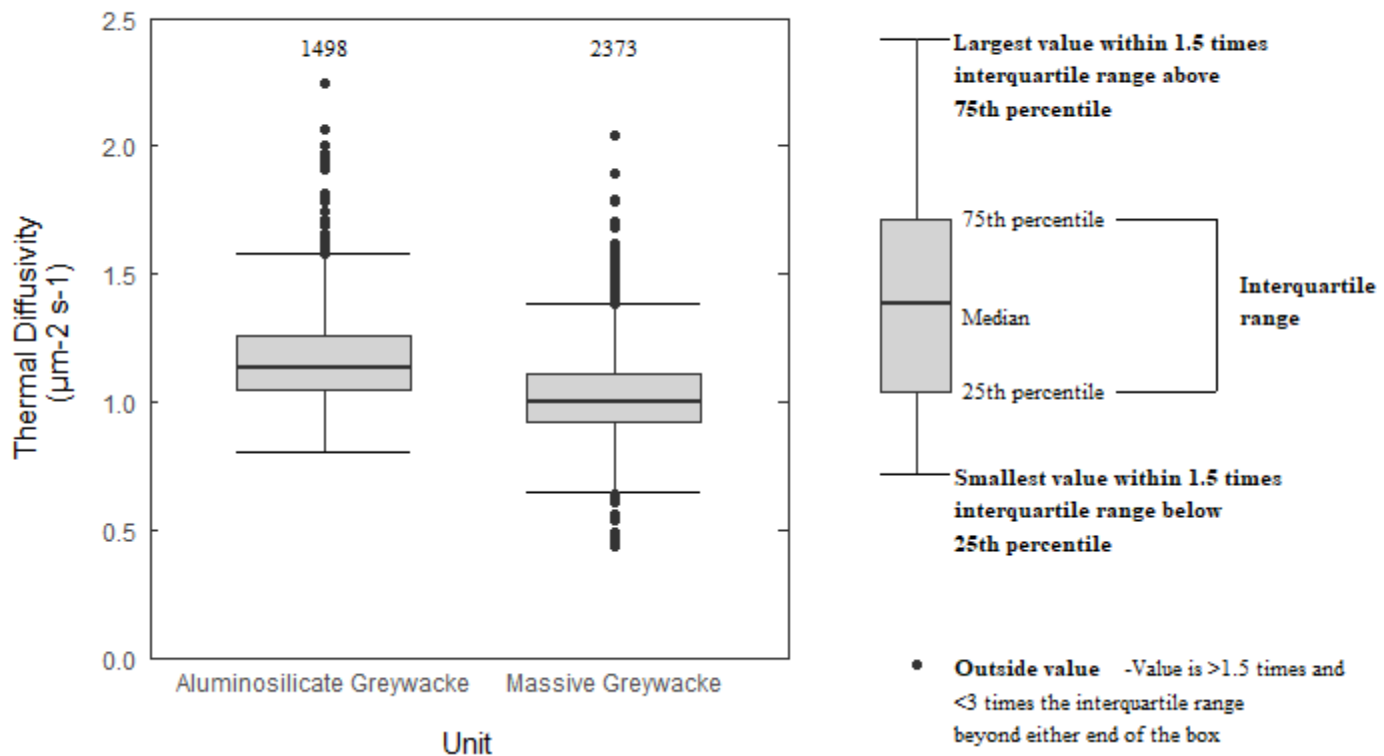
Statistical distribution of the thermal properties of rocks samples from the Éléonore mine according to geological unit

In the following boxplots, the number of values displayed for each unit corresponds to the total number of measuring points obtained from all the samples analyzed for that particular unit. In the case of the massive greywacke, a total of 2373 measure points were recorded from 28 different samples. The 1498 measure points shown for the aluminosilicate-bearing greywacke were obtained from 16 different samples.



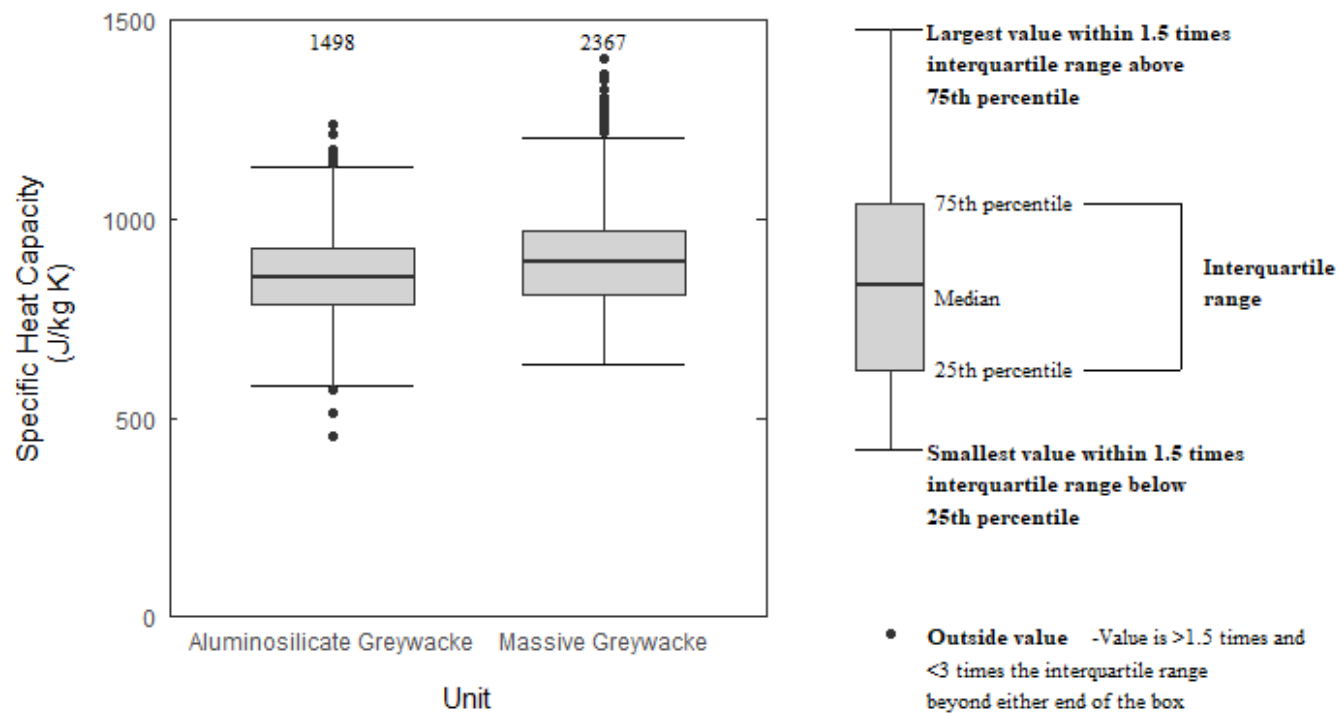
EXPLANATION

500 Number of values



EXPLANATION

500 Number of values



15 APPENDIX VIII DEWATERING GEOTHERMAL POTENTIAL OF THE ÉLÉONORE MINE RESEARCH REPORT (R1869)

FR : Rapport de travaux réalisés pour évaluer le potentiel géothermique de la mine Éléonore. Voir les fichiers accompagnant le mémoire pour télécharger le document.

EN: Report of the work carried out to evaluate the geothermal potential of the Éléonore mine. See the files accompanying the thesis to download the document.

Reference :

Alvarado, Edgardo Jose; Raymond, Jasmin; Therrien, René; Comeau, Félix-Antoine; Labrecque, David (2019). Évaluation du potentiel géothermique de la mine Éléonore: Rapport final Rapport de recherche (R1869). INRS, Centre Eau Terre Environnement, Québec.
<http://espace.inrs.ca/9664/>